

03092

2
24.

UNIVERSIDAD NACIONAL AUTONOMA DE MEXICO

Unidad Académica de los Ciclos Profesional y Posgrado
del Colegio de Ciencias y Humanidades
Instituto de Geofísica
Posgrado en Geofísica

**SISMOTECTONICA DEL OCCIDENTE DE
VENEZUELA**

TESIS

**PARA OPTAR AL GRADO DE DOCTOR EN GEOFISICA
(SISMOLOGIA Y FISICA DEL INTERIOR DE LA TIERRA)**

PRESENTA

GUSTAVO JOSE MALAVE BUCCE

Ciudad Universitaria Junio, 1997

**TESIS CON
FALLA DE ORIGEN**



Universidad Nacional
Autónoma de México



UNAM – Dirección General de Bibliotecas
Tesis Digitales
Restricciones de uso

DERECHOS RESERVADOS ©
PROHIBIDA SU REPRODUCCIÓN TOTAL O PARCIAL

Todo el material contenido en esta tesis esta protegido por la Ley Federal del Derecho de Autor (LFDA) de los Estados Unidos Mexicanos (México).

El uso de imágenes, fragmentos de videos, y demás material que sea objeto de protección de los derechos de autor, será exclusivamente para fines educativos e informativos y deberá citar la fuente donde la obtuvo mencionando el autor o autores. Cualquier uso distinto como el lucro, reproducción, edición o modificación, será perseguido y sancionado por el respectivo titular de los Derechos de Autor.

A Gladys y a mis dos chamos: Francisco Javier y Reinaldo Javier

RESUMEN

El análisis de la sismicidad superficial ($m_b \geq 5.4$) ocurrida en el occidente de Venezuela y de la sismicidad de profundidad intermedia ($m_b > 4.2$) generada al norte de Colombia y occidente de Venezuela durante el periodo 1964-94, permitió mejorar el conocimiento sobre el régimen tectónico de la región y proponer un modelo que explica el comportamiento de los diferentes fallamientos existentes en la zona. Primeramente, se evaluó la sismicidad de profundidad intermedia al norte de Colombia y occidente de Venezuela, lo cual permitió identificar la presencia de una placa litosférica subducida por más de 400 km de longitud por debajo de la costa suroeste del Caribe. La geometría de esta placa se definió en el rango de 60 a 180 km de profundidad, con una dirección aproximada *NNE-SSW* y un buzamiento hacia el este con una pendiente promedio de 25° - 32° , en ese rango de profundidades.

Luego, se evaluaron los parámetros focales de los sismos superficiales con magnitud $m_b \geq 5.4$ ocurridos en el occidente de Venezuela durante el periodo 1964-94. Los mecanismos focales obtenidos sugieren dos diferentes direcciones del campo de esfuerzos compresivo en el occidente de Venezuela: al suroeste, un campo de esfuerzos compresivo orientado *E-W* y en el noroeste de Venezuela, aproximadamente al norte de la latitud 10° N, una rotación de los ejes *P* desde el *NE-SE* hasta *NNE-SSW*. La correlación entre los mecanismos focales y las fallas activas muestran que la liberación de energía sísmica en el occidente de Venezuela no ocurre en un sistema de fallas único, sino que la sismicidad se genera en fallas con diferentes orientaciones, distribuidas sobre un gran volumen sismogénico. El cálculo de la deformación volumétrica de esta región muestra que en la parte norte, la tasa de deformación compresiva se orienta casi *N-S* y se debe a la subducción de la placa del Caribe por debajo de Sur América; mientras que la tasa de deformación compresiva en la parte sur se define en la dirección *E-W* y se asocia con la convergencia entre las placas Nazca y Sur América. En todo el volumen deformado, la tasa de deformación compresiva se orienta en la dirección *N-S*.

Otra evidencia que demuestra el carácter altamente deformado y fallado del occidente de Venezuela es la ocurrencia de eventos sísmicos complejos de magnitud moderada, originados por

fuentes múltiples. Además de la ocurrencia del sismo de El Tocuyo en 1812 y el de Caracas en 1967, existe la secuencia sísmica compleja de Boca del Tocuyo, noroccidente de Venezuela, en 1989. El evento principal del 30 de abril y la réplica mayor del 4 de mayo se generaron mediante fuente múltiples que indujeron la licuación de los suelos en el área epicentral.

La evaluación neotectónica de las fallas en el occidente de Venezuela, aunado a la determinación de los mecanismos focales y a la direcciones de los principales ejes de esfuerzos, permitieron proponer un modelo cinemático conocido con el nombre de "bookshelf". Al actuar los sistemas de fallas de Boconó y Oca-Ancón, en forma individual o como pareja de esfuerzos con desplazamiento lateral derecho, las fallas *NNE-SSW* que separan los bloques alargados en esa misma dirección, experimentan un deslizamiento lateral izquierdo y se produce una rotación de los bloques en sentido horario. Los resultados obtenidos también muestran evidencias que pudiesen relacionar la frontera entre las placas Caribe y Sur América con el sistema de fallas de Boconó y con el Cinturón Deformado del Caribe Sur. Por lo tanto, se pudiese estar presente ante una frontera de placas definida por toda una zona de deformación, comprendida entre los Andes Venezolanos y el Cinturón Deformado del Caribe Sur.

La presencia de una tectónica regional compleja en el occidente de Venezuela, motivó un intento de evaluar el comportamiento de la sismicidad superficial con magnitud $m_b < 5.4$ utilizando sismogramas regionales. Se analizaron dos metodologías para obtener los mecanismos focales de esos eventos menores y de esta manera recopilar mayor información para validar las conclusiones alcanzadas y los modelos propuestos. Lamentablemente la escasez de información en las estaciones sismológicas ubicadas a distancias regionales del occidente de Venezuela, no permitió cubrir ese objetivo. En su lugar se analizaron varios eventos ocurridos en el occidente de Estados Unidos, los cuales permitieron ensamblar un procedimiento que servirá en un futuro cercano cumplir con la meta propuesta, a raíz de la reciente instalación de nuevas estaciones banda-ancha a nivel regional. Los resultados obtenidos con los sismos analizados del occidente de Estados Unidos son satisfactorios, si se considera que el procedimiento utilizado se implantó para desarrollarse de una manera automática.

ABSTRACT

The analysis of the shallow, moderate-sized seismicity ($m_b \geq 5.4$) that have occurred in western Venezuela and the intermediate-depth seismicity ($m_b > 4.2$) originated in northern Colombia and western Venezuela during the 1964-1994 period, were evaluated to understand the complex tectonic environment in this region and its relationship to the interaction between the Caribbean and South American plates. Firstly, the recent intermediate-depth seismicity in northern Colombia and western Venezuela was analyzed to understand its origin, and its presumed relationship to a subducted lithospheric slab in northwestern South America. The isodepth curves reflect a slab striking in a *NNE-SSW* direction and dipping approximately at 25° - 32° to the southeast. This observation is corroborated by the direction and plunge of the *T*-axes of the focal mechanisms, which are generally parallel to the gradient of the slab defined by the spatial distribution of hypocenters.

Second, the shallow, moderate-sized seismicity occurred in western Venezuela was analyzed. The results indicate that most of the earthquakes nucleated on secondary fault systems, instead of on the major fault systems of Boconó and Oca-Ancón. The average direction of the *P*-axes clearly divides the region of western Venezuela into two zones: north and south of latitude 10°N . In the northern area, the *P*-axes rotate from a *NW-SE* to *NNE-SSW* direction; whereas in the southern zone, the *P*-axes are approximately oriented *E-W*. The determination of the compressional strain rate in the overall region over 30-years period of time is oriented almost *N-S*. According to the seismic activity on the secondary faults, the border between the Caribbean and South American plates may be distributed over a wide zone of deformation instead of a major single fault. The correlation between the left-lateral, strike-slip faults trending roughly *NNE-SSW*, the focal mechanisms and the Quaternary geological data suggest that the kinematics of the faulting pattern behave as a bookshelf faulting mechanism.

Another evidence of being in a high deformed and faulted region is the occurrence of earthquakes originated by multiple rupture processes. Besides the El Tocuyo 1812 and the Caracas 1967 earthquakes, there was the Boca del Tocuyo seismic sequence on April and May, 1989.

which had a special significance in assessing the seismic hazard of northern Venezuela. The mainshock and its largest aftershock induced intense liquefaction in most of the coastal towns near the epicentral area. Both earthquakes presented body-wave trains which are much longer than those expected for a single event of that magnitude.

The existence of a complex tectonics environment in western Venezuela motivated us to evaluate the behavior of the shallow seismicity with magnitude $m_b < 5.4$, using regional seismograms. We analyzed two methodologies to obtain the fault plane solution for those smaller events in order to compile more information to validate the conclusions and the models proposed in this study. Unfortunately, we could not reach that objective, since the information recorded at stations located at regional distances in western Venezuela was deficient. Instead, we analyzed several earthquakes that occurred in western United States, that permit us to assembly a methodology that it may be used in the near future, due to the deployment of new stations at regional distances from western Venezuela. The results obtained from the analysis of the western United States earthquakes can be considered as satisfactory, taking into account that the evaluation was made in an automatic way.

AGRADECIMIENTOS

A *INTEVEP, S.A.*, Centro de Investigación y Apoyo Tecnológico de Petróleos de Venezuela, S.A., por concederme el tiempo y el financiamiento necesario para realizar mis estudios de Doctorado en Geofísica. A Enrique Gajardo y Heriberto Echezuría del Departamento de Ingeniería General de *INTEVEP, S.A.*, quienes solicitaron la extensión de mi beca para la continuación de los estudios de posgrado. A Fermín Hernández, actual Gerente de ese Departamento, quien me apoyó en la última fase de mis estudios para la culminación y defensa de la Tesis Doctoral.

A la Universidad Nacional Autónoma de México (*UNAM*), en especial a la Unidad Académica de los Ciclos Profesional y de Posgrado (*UACPyP*) del Colegio de Ciencias y Humanidades (*CCH*), la cual me aceptó en sus instalaciones como un "paisano" más y me ofreció sus enseñanzas prácticamente de forma gratuita. Al Departamento de Sismología del Instituto de Geofísica (*IGF*) de la *UNAM*, sede del Posgrado, por el uso de sus instalaciones físicas y académicas. A la Dirección General de Apoyo para el Personal Académico (*DGAPA*) por su apoyo económico en la realización del proyecto de Tesis de Grado. Al Centro Sismológico Nacional de los Estados Unidos de América (*NEIC*), por permitirme realizar una estancia de un (1) año en sus instalaciones en Golden, Colorado, donde realicé parte de mi trabajo doctoral.

Sinceramente, mi más especial agradecimiento para Gerardo Suárez Reynoso, quien se desempeñó como Asesor de mis estudios y Tutor de la Tesis Doctoral: su amistad, apoyo y dirección fueron claves fundamentales para la culminación de mis estudios. A los miembros del Jurado de Tesis: Francisco Sánchez-Sesma, Gerardo Suárez Reynoso, Mario Chávez-García, Juan Manuel Espíndola, Vladimir Kostoglodov, Javier Pacheco y William Bandy, cuyos comentarios permitieron mejorar la calidad del presente trabajo.

A Carlos Mendoza, del *NEIC*, quien durante su visita al *IGF* se interesó en mi tema de trabajo y gestionó mi estancia en el *NEIC* por un año. Al grupo de investigadores del Departamento de Sismología del *IGF*: Sri K. Singh, Marco Guzman, Ramón Zúñiga, Luis

Quintanar, Javier Pacheco y Vladimir Kostoglodov, por sus excelentes enseñanzas en el transcurso de mi permanencia en ese Departamento.

A mis compañeros del posgrado: Jaime Domínguez, Diana Comte, Mario Pardo, Alexei Gorvatov, Adolfo Vázquez, David Escobedo, Carlos Ortiz y Mario Cruz, por todo el apoyo y aprecio recibido. A mis compañeritos de las pericias de Geotecnia y Mecánica Estructural de INTEVEP, S.A., quienes en todo momento me estuvieron apoyando para la realización de mis estudios y la culminación de mi Tesis Doctoral.

A Enedina Martínez, por toda su colaboración y apoyo durante la realización de mis estudios. A Norma Bravo, Asistente Administrativo del Posgrado en Geofísica, quien tuvo la paciencia de responder y apoyarme en todo momento. A Lilian González, por su ayuda en la preparación de las figuras sobre los sismogramas regionales.

INDICE

	<u>Página</u>
Resumen	iii
Abstract	v
I. Introducción	1
II. Sismicidad de profundidad intermedia al norte de Colombia y oeste de Venezuela y su relación con la subducción de la placa del Caribe (Intermediate-depth seismicity in northern Colombia and western Venezuela and its relationship to Caribbean plate subduction).	10
III. Características complejas de la fuente de los sismos de Boca del Tocuyo de 1989 en el noroeste de Venezuela (Complex source characteristics of the 1989 Boca del Tocuyo earthquakes in northwestern Venezuela).	47
IV. Deformación cortical y sismicidad superficial reciente en el oeste de Venezuela: implicaciones tectónicas regionales (Crustal deformation and recent shallow seismicity in western Venezuela: regional tectonic implications).	81
V. Determinación de mecanismos focales mediante sismogramas regionales de período largo. Factibilidad de aplicación de esta técnica al oeste de Venezuela (Determination of focal mechanisms using long-period regional seismograms. Feasibility to apply this technique in western Venezuela).	136
VI. Conclusiones	220

I. Introducción

El régimen tectónico del Occidente de Venezuela está íntimamente relacionado con la interacción de las placas Caribe y Sur América. El movimiento relativo entre estas dos placas es principalmente del tipo transcurrente dextral, y ocurre a una velocidad promedio aproximada de 2 cm/año (Fig. 1). Sin embargo, el movimiento promedio relativo medido en los sistemas principales de fallas transcurrentes dextrales de El Pilar y Boconó, postulados como frontera entre estas placas al este y occidente de Venezuela respectivamente, no exceden los 1.3 cm/año (Schubert, 1982; Soulas, 1986).

Con base en esta diferencia de velocidades y a la presencia de sistemas de fallas secundarios conjugados, se ha sugerido que este borde de placas parece no manifestarse a lo largo de un sistema simple de fallas, sino que se distribuye sobre una amplia zona de deformación. Todo esto ha traído como consecuencia, que el régimen tectónico de esta región haya sido un punto de controversia durante los últimos años, en los cuales, diferentes autores han sugerido al sistema de fallas de Boconó (e.g., Dewey, 1972; Soulas, 1986) y al Cinturón Deformado del Caribe Sur (e.g., Kellogg y Bonini, 1982; Ladd *et al.*, 1984; Freymueller *et al.* 1993), como la frontera actual entre las placas Caribe y Sur América (Fig. 1).

Esta discusión sobre el ambiente tectónico de la región motivó el desarrollo del presente estudio sobre la evaluación sismotectónica del occidente de Venezuela. Se planteó como objetivo principal el analizar con métodos robustos, los parámetros focales de los sismos ocurridos en la zona y correlacionarlos con los accidentes estructurales identificados a través de los estudios neotectónicos de campo. El hecho que la tasa de sismicidad del área de estudio sea relativamente baja y dispersa, se dispuso de diferentes metodologías para cumplir con los objetivos planteados.

Algunos estudios se han realizado previamente con este mismo propósito. Dewey (1972), mediante la instalación de una red sismológica local y utilizando datos telesísmicos, analizó la sismicidad del occidente de Venezuela y norte de Colombia, incluyendo el Nido de Bucaramanga. Además, determinó algunos mecanismos focales basados en las polaridades de las primeras llegadas y concluyó que la zona de fallas de Boconó es sísmicamente activa. Luego, Kafka y

Weidner (1981) evaluaron los mecanismos focales determinados por Dewey (1972), realizando una inversión del tensor de momento sísmico utilizando ondas Rayleigh. Sus mecanismos focales sugirieron un fallamiento transcurrente dextral paralelo a la falla de Boconó. Pennington (1981), tomando en cuenta los mecanismos focales determinados previamente y otros obtenidos por él con base en primeras llegadas, sugirió que el bloque norte de los Andes se mueve hacia el nor-noreste con respecto al resto de la placa de Sur América, a lo largo de un sistema de fallas ubicado al frente de la Cordillera Oriental de los Andes. Kellogg y Bonini (1982), Ladd et al. (1984) y Freymueller *et al.* (1993), utilizando diferentes metodologías propusieron al Cinturón Deformado del Caribe Sur como la frontera actual entre las placas Caribe y Sur América, y consideran la falla de Boconó como producto de la deformación intraplaca.

En los estudios de la sismotectónica del occidente de Venezuela, es indispensable considerar que la mayoría de los sismos se originan en la corteza terrestre ($h < 30$ km), como consecuencia de fallamientos superficiales. Sin embargo, existen también eventos de profundidad intermedia ($50 \leq h \leq 180$ km), que se han originado por la extensión de la placa litosférica subducida en el norte de Colombia y noroccidente de Venezuela hacia esta región. Es por ello que resulta necesario analizar ambos tipos de sismicidad, incluyendo la mayoría de los sismos ($m_b > 4.8$) de profundidad intermedia que ocurren en el norte de Colombia.

En el Capítulo 2 de este estudio, se determinó la orientación y geometría de la placa litosférica subducida al norte de Colombia y noroccidente de Venezuela, a través del análisis de los sismos de profundidad intermedia en esa región. Las profundidades focales de los eventos de menor magnitud ($m_b \leq 5.3$) se obtuvieron mediante la lectura de las diferencias de llegada de las ondas P y pP , en sismogramas de la World-Wide Standardized Seismograph Network (*WWSSN*), de la Global Digital Seismograph Network (*GDSN*), del Yellow Knife Array en Canadá (*YKA*) y del Norwegian Seismograph Array (*NORSAR*). Los mecanismos focales de estos sismos de menor magnitud, se determinaron mediante las polaridades de las primeras llegadas observadas en esos sismogramas. Para los eventos de mayor magnitud, las profundidades focales y los mecanismos de fallas se obtuvieron mediante la inversión del tensor de momento sísmico, utilizando sismogramas grabados a distancias telesísmicas (Nábelek, 1984).

Luego, para evaluar la sismicidad superficial del occidente de Venezuela, en los Capítulos 3 y 4 del presente trabajo se analizaron los parámetros de la fuente de los sismos superficiales de magnitud $m_b \geq 5.4$ ocurridos en la zona de estudio durante el período 1964-1994. Esta evaluación se efectuó mediante la inversión del tensor de momento sísmico utilizando ondas de volumen grabadas a distancias telesísmicas ($30 \leq \Delta \leq 90$) (Nábelek, 1984). En total, se estudiaron 16 sismos, los cuales permitieron proponer un modelo cinemático que explica la subsistencia de los diferentes sistemas de fallas principales y secundarios, en un régimen tectónico tan complejo. Igualmente, los resultados de este estudio permitieron definir el campo de esfuerzos compresivo existente en la región, y la tasa y orientación principal de la deformación compresiva promedio. Los sismos ocurridos durante 1989 en Boca del Tocuyo, noroccidente de Venezuela, se evaluaron detalladamente en el Capítulo 3, ya que se originaron mediante rupturas múltiples que produjeron trenes de ondas muy largos. Estas ondas indujeron la licuación de los suelos cercanos al área epicentral, ocasionando ligeros daños a las estructuras existentes.

Finalmente, en el Capítulo 5 se incluyeron dos metodologías para la modelación e inversión automática del tensor de momento sísmico, utilizando sismogramas grabados a distancias regionales ($\Delta < 12^\circ$). La idea original de llevar a cabo este estudio, con base en sismos con magnitud $m_b \leq 5.3$ ocurridos en el occidente de Venezuela, no pudo realizarse. Esto fue debido a la baja relación señal-ruido en los sismogramas de las estaciones ubicadas a distancias regionales. En su lugar, se analizaron siete (7) sismos ocurridos en el occidente de Estados Unidos de América, durante el período 1993-94, utilizando datos de la red sismológica de ese país y de otras estaciones ubicadas en la región. Sin embargo, con la implantación de nuevas estaciones sismológicas de banda ancha en la zona del Caribe, Centro América y Sur América, existe la posibilidad a corto plazo que puedan analizarse eventos futuros con estas metodologías.

El análisis de la sismicidad con magnitud $m_b \leq 5.3$ de la zona tiene un valor agregado muy importante en la validación del modelo tectónico propuesto para la región, ya que algunos de ellos se han generado posiblemente en fallas donde no han ocurrido sismos de mayor magnitud. De todas formas, los sismos con magnitud $m_b \geq 5.4$ generados en el período 1995-96 y no incluidos en el presente estudio, avalan el modelo sugerido.

Referencias

- Beltrán, C. (1993). Mapa Neotectónico de Venezuela. Escala 1:2.000.000. *FUNVISIS*, Departamento de Ciencias de la Tierra, Caracas, Venezuela.
- Dewey, J. (1972). Seismicity and tectonics of western Venezuela, *Bull. Seismol. Soc. Am.* **62**, 1711-1751.
- Freymueller, J., J. Kellogg y V. Vega (1993). Plate motions in the North Andean region. *J. Geophys. Res.* **98**, 21853-21893.
- Kafka A. y D. Weidner (1981). Earthquake focal mechanisms and tectonics processes along the southern boundary of the Caribbean plate, *J. Geophys. Res.* **86**, 2877-2888.
- Kellogg, J. y W. Bonini (1982). Subduction of the Caribbean plate and basement uplifts in the overriding South American plate, *Tectonics* **4**, 785-790.
- Ladd, J., M. Truchan, M. Talwani, P. Stoffa, P. Buhl, R. Houtz, A. Manfrett y G. Westbrook (1984). Seismic reflection profiles across the southern margin of the Caribbean, in Bonini *et al.*, eds. The Caribbean-South América Plate Boundary and Regional Tectonics, *Geol. Soc. Am. Mem.* **162**, 239-261.
- Nábelek, J. L. (1984). Determination of earthquakes source parameters from inversion of body waves, Ph.D. Thesis, Massachusetts Institute of Technology, Cambridge. 361 pp.
- Pennington, W. (1981). Subduction of the Eastern Panama Basin and Seismotectonics of Northwestern South America, *J. Geophys. Res.* **86**, 10753-10770.
- Schubert, C. (1982). Neotectonics of Boconó fault. western Venezuela, *Tectonophysics* **85**, 205-220.
- Singer, A., F. Audemard, C. Beltrán, J. A. Rodríguez, F. De Santis, A. Adrianza, C. Chacín, M. Lugo, J. Mendoza, y C. Ramos (1992). Actividad tectónica cuaternaria y características sismogénicas de los sistemas de fallas de Oca-Ancón (tramo oriental). de la península de Paraguaná y región de Coro y de la costa nororiental de Falcón. *FUNVISIS*, Caracas, Venezuela.

- Soulas, J. P. (1986). Neotectónica y tectónica activa en Venezuela y regiones vecinas. *Memorias VI Congreso Geológico Venezolano*, Caracas, X, 6639-6656.
- Soulas, J. P., C. Giraldo, D. Bonnot y M. Lugo (1987). Actividad cuaternaria y características sismogénicas del sistema de fallas Oca-Ancón y de las fallas de Lagarto, Urumaco, Río Seco y Pedregal. *FUNVISIS*, Caracas, Venezuela.

Descripción de Figuras

Figura 1. Sismicidad ($m_b \geq 5.0$) relacionada con la interacción de la placa del Caribe con sus placas vecinas (Atlántico, Cocos, Nazca, Norte América y Sur América). Las flechas indican las direcciones de los movimientos relativos de las placas. La sismicidad se muestra como círculos abiertos; por lo que las áreas oscuras reflejan una alta concentración de sismos.

Figura 2. Sistemas mayores de fallas activas en Venezuela (Beltrán, 1993; Singer *et al.*, 1992; Soulas, 1986; Soulas *et al.*, 1987). Las flechas indican las direcciones de movimientos relativos de las fallas.

Figura 3. Sistemas mayores de fallas activas en el occidente de Venezuela (Beltrán, 1993; Singer *et al.*, 1992; Soulas, 1986; Soulas *et al.*, 1987). Se muestra la sismicidad ($m_b \geq 5.0$) ocurrida durante los últimos 30 años en la región, reportada por el Centro Sismológico de los Estados Unidos de América (NEIC). Los círculos corresponden a sismos con magnitud $m_b \leq 5.3$; los cuadrados, con magnitud $m_b \geq 5.3$. Los símbolos claros representan la sismicidad superficial ($h < 70$ km), mientras que los símbolos oscuros indican los eventos de profundidad intermedia ($h \geq 70$ km). Las flechas denotan las direcciones de los movimientos relativos de las fallas.

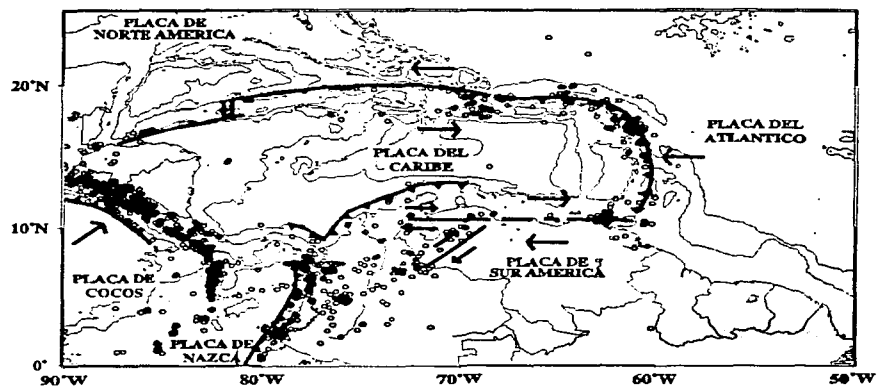


Figura 1

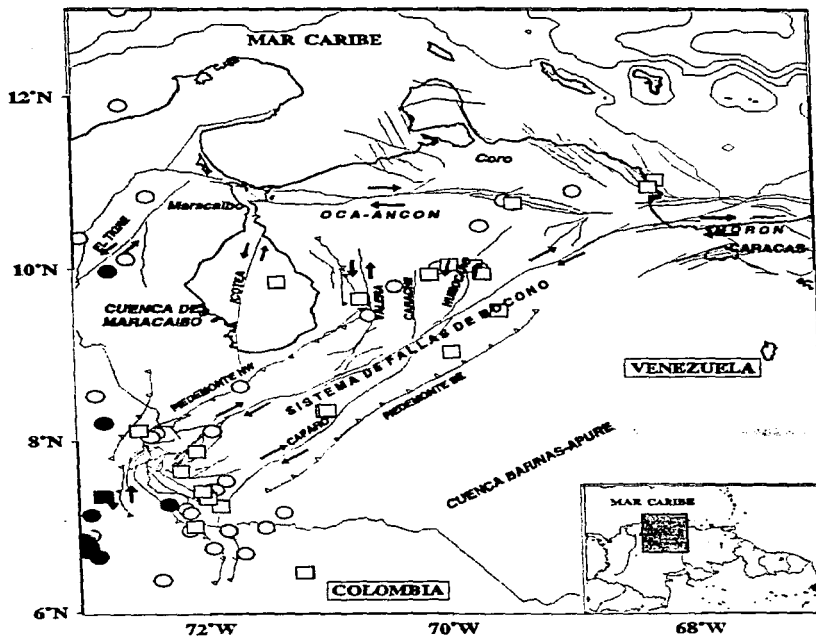


Figura 3

II. Sismicidad de profundidad intermedia al norte de Colombia y oeste de Venezuela y su relación con la subducción de la placa del Caribe

Intermediate-depth seismicity in northern Colombia and western Venezuela and its relationship to Caribbean plate subduction

Gustavo Malavé¹ and Gerardo Suárez

Instituto de Geofísica, Universidad Nacional Autónoma de México, Mexico City, Mexico

¹ Also at: INTEVEP, S.A., Apartado Postal 76343, Caracas 1070A

Abstract. The recent intermediate-depth seismicity in northern Colombia and western Venezuela was analyzed to understand its origin, and its presumed relationship to a subducted lithospheric slab in northwestern South America. The area included in this study is located to the north and east of the Bucaramanga Nest, which is a particular region beneath Bucaramanga, northern Colombia, that presents a high concentration of intermediate-depth earthquakes. To the north of the nest, the seismicity of the area is sparse and most of the events are of low magnitude ($m_b \leq 5.1$). Thus, only twenty-three earthquakes were large enough to be investigated using teleseismic data. The focal parameters of the two largest events ($m_b \geq 5.4$) were obtained from the formal inversion of long-period bodywaves recorded at teleseismic distances. The focal mechanisms of ten more events were determined from first-motion data. In total, the focal mechanisms of twelve events were determined from both the inversion of P and SH waveforms and from the polarities of first arrivals. For the smaller earthquakes, the focal depths were calculated by

measuring the observed pP - P interval time and comparing it to the theoretical travel-time tables. The isodepth curves reflect a slab striking in a NNE-SSW direction and dipping approximately at 25° - 32° to the southeast. This observation is corroborated by the direction and plunge of the T -axes of the focal mechanisms, which are generally parallel to the gradient of the slab defined by the spatial distribution of hypocenters. These results indicate that the intermediate-depth earthquakes in western Venezuela and northern Colombia are apparently related to the presence of a continuous lithospheric slab subducted near the northern coast of Colombia. The two largest earthquakes, located at a significant distance from the Bucaramanga nest, present similar fault plane solutions. Moreover, they also agree with those of the two largest earthquakes reported inside the nest. This similarity suggests that the Bucaramanga nest lies on the same subducted slab where the other earthquakes occur. There is not enough shallow seismicity to define the location where the Caribbean lithosphere subducted beneath the South American plate. However, the extension of the slab towards the surface, inferred from the intermediate-depth seismicity, suggests that the subducted lithosphere may still be attached to the Caribbean plate.

Introduction

The seismicity in western Venezuela is characterized mainly by the occurrence of shallow earthquakes ($h < 30$ km) of moderate magnitude ($m_b < 5.4$), associated with a wide zone of deformation dominated by the right-lateral, strike-slip motion on the Boconó and Oca-Ancón fault systems. However, several earthquakes with depths ranging from 140 to 190 km have occurred in the region since 1964. They are located near the Venezuela-Colombia border, beneath the Sierra de Perijá and to the north and east of the Bucaramanga nest (Figure 1).

The seismicity ($m_b \geq 4.0$) of northern Colombia and western Venezuela reported by the National Earthquake Information Center (NEIC) since 1963, shows that the seismic activity to the north of latitude 8°N is sparse (Figure 1). To the south of that latitude, two clusters of seismicity may be identified: the Bucaramanga nest composed of intermediate-depth events, and a cluster of shallow earthquakes located near the Colombia-Panama border near 76°W . In this latter area, two large earthquakes occurred on October 17 and 18, 1992 ($M_S = 6.7$ and 7.3 , respectively), associated probably with the east-west convergence of the Nazca plate beneath South American plate.

The Bucaramanga nest has been a point of interest and intense study for several years. The origin of this highly concentrated, intermediate-depth seismic source and its relationship to a presumably subducted lithosphere in northern Colombia have motivated several authors to analyze the seismicity of the area [e.g., Dewey, 1972; Pennington, 1981; Schneider *et al.*, 1987; Rivera, 1989; Shih *et al.*, 1991]. According to these authors, the Bucaramanga seismicity occurs within a limited volume (radius less than 10 km). The mislocation of the hypocenters obtained by the international seismological agencies (ISC: International Seismological Centre; NEIC) seems to define a larger volume for the Bucaramanga Nest (Figure 1). However, hypocenters determined by local, temporary seismological networks and by the relocation of data collected by those agencies delineate a volume of ~ 10 km in diameter of the Bucaramanga Nest.

Dewey [1972] investigated several intermediate-depth earthquakes beneath the Cordillera Oriental and Sierra de Perijá, and concluded that if those events occurred in the same lithospheric

slab as that containing the Bucaramanga source, the slab must have a strike of N10E and dip towards the east. His dataset, however, was insufficient to accurately map the supposed subducted lithosphere. Later, *Pennington* [1981] studied other intermediate-depth earthquakes and defined a Bucaramanga segment dipping to the N109E at $\sim 20^{\circ}$ - 25° . *Kellogg and Bonini* [1982; 1985] suggested that the Caribbean oceanic lithosphere is actively underthrusting beneath South America in northern Colombia and northwestern Venezuela. They postulated that the resulting seismic zone dips at $\sim 30^{\circ}$ towards the southeast and ends at a depth of 200 km beneath the Maracaibo Basin. More recently, *Schneider et al.* [1987] analyzed several intermediate-depth microearthquakes near the Bucaramanga nest and defined a Wadati-Benioff zone, spanning depths from 110 to 190 km, striking N10E, and a dip increasing from 30° E at shallower depths to near-vertical beneath the nest.

In this study, the hypocentral location and the focal mechanisms of several intermediate-depth earthquakes in western Venezuela and northern Colombia are analyzed to understand their presumed relationship to Caribbean plate subduction. Since most of the events included here occurred in the last two decades, only a few of them have been considered in previous studies. As mentioned above, the seismicity in this area is sparse and most of the events are of magnitude $m_b \leq 5.1$. As a consequence of that low magnitude, the signal to noise ratio of the available teleseismic data was relatively low, but still good enough for hypocentral and focal mechanism analysis.

The only two earthquakes of magnitude $m_b > 5.4$ were evaluated through the formal inversion of long-period bodywaves recorded at teleseismic stations [*Nábelek*, 1984]. The earthquakes of smaller magnitudes were investigated by reading the arrival time difference between the P and pP phases to calculate the focal depths; the polarities of the P -waves were used to determine the fault plane solutions. In total, the focal depths of twenty-three earthquakes were estimated, and the focal mechanisms of twelve events were constructed (Table 1). In addition to these, the focal mechanisms of three events determined by *Dziwowski et al.* [1987a; 1987b; 1988] are included in the study.

Although the Bucaramanga nest is located within the area studied here, the earthquakes that have occurred inside this zone were not analyzed in detail, because they have been well studied by the authors mentioned above. The earthquake of August 30, 1973 ($m_b=5.7$), that occurred near the nest [Pennington, 1981] and the event of November 17, 1968 ($m_b=5.8$), located ~200 km to the north of the first one were the two earthquakes for which a formal inversion was performed. Their source parameters were compared with those of other events reported inside the Bucaramanga source, and with those of other intermediate-depth earthquakes that are located far from the nest.

Data

Different datasets were used to evaluate the source parameters of the earthquakes studied, according to their range of magnitude, the data available, and the date when they occurred. Short and long-period analog seismograms from the World-Wide Standardized Seismograph Network (*WWSSN*), and short-period digital records from the Global Digital Seismograph Network (*GDSN*), the Yellow Knife Array in Canada (*YKA*), and the Norwegian Seismograph Array (*NORSAR*) were collected. For earthquakes that occurred before 1978, analog seismograms from the *WWSSN* were used. However, for events occurring after 1978, digital data available from the *GDSN* and from regional digital networks were analyzed in addition to the *WWSSN* analog seismograms. The *ISC* earthquake database was utilized for recalculating the hypocenters of most of the earthquakes, except for an event that occurred in 1992, for which the *NEIC* database was used.

Analog data

The analog seismograms were copied and amplified from microfilms to facilitate the digitization of the waveforms for the inversion, the readings of polarities and the measurement of *pP-P* interval times. Due to the large number of those analog stations installed worldwide, sufficient information was obtained to constrain the source parameters. Since 1978, the format to record the *WWSSN* seismograms in microfilms was changed to a compressed one. Consequently, it was difficult to identify the smaller events that occurred after 1978 on the *WWSSN* seismograms. Fortunately, the number of digital stations of the *GDSN* increased worldwide since that time, which permitted to complement this study by using those stations and data recorded at the *YKA* and the *NORSAR* seismic arrays.

Digital data

The digital data was the most useful type of information for earthquakes that occurred after 1978. Broad-band and long-period instrumental records were examined whenever available. The short-period seismograms were used generally due to the low magnitude of the events. All digital seismograms were high-pass filtered to eliminate long-period noise. The cut-off frequency varied in according to the level of the noise on the seismograms.

Local seismic arrays

The *YKA* and *NORSAR* seismic arrays are located at teleseismic distances of approximately 60° and 80° from the area studied, respectively. Thus the individual stations in each array were considered as a single point on the focal sphere. In spite of the low magnitude of the events, the quality of the *YKA* data was excellent. The readings of the *pp-P* time difference were made accurately at all the stations of the array and then averaged. In the case of the *NORSAR* array, as a result of the larger epicentral distance, a stacking (plain sum) of the seismograms of the array was used to improve the signal to noise ratio.

Methodology

The determination of the reliable focal depths and source mechanisms of the earthquakes in this area is a crucial factor in the aim of this study. First, we collected the focal depths obtained by *ISC*, including its *pP-P* depth determination when available, and those reported by *NEIC* (Table 1). Next, the hypocenters were relocated using the single-event location program (SE89) of Dewey [1971] with both the *ISC* and *NEIC* earthquake databases (Table 1). This was done as an effort to reduce the errors in the hypocentral locations determined by *ISC* and *NEIC*, since this method permits a better constrained estimate of the focal depth when a considerable number of *pP* phases are included. In addition to this, we analyzed the source parameters of the two larger earthquakes ($m_b \geq 5.4$) by using a formal inversion of bodywaves. In the case of the smaller events ($m_b \leq 5.1$), the *pP-P* interval times were read directly from the seismograms to estimate the focal depths, as were the polarities of first arrivals to obtain the focal mechanisms. A more detail explanation of the procedures used in this study is presented in the following sections.

Bodywave inversion

The source parameters of the earthquakes that occurred on November 17, 1968 ($m_b=5.8$), and August 30, 1973 ($m_b=5.7$) (events 2 and 4 on Table 1), were analyzed through the inversion of long-period *P* and *SH* waves recorded at teleseismic distances by stations of the *WWSSN* (Figures 2 and 3). These events are two of the largest intermediate-depth earthquakes recorded in western Venezuela and northern Colombia.

Only seismograms of stations within an epicentral distance range of 25° to 90° were included in the study; within this distance range, the Green's functions for a source embedded in a layered earth are simple to calculate and can be accurately estimated [e.g., Nabelek, 1984]. The analog records were hand-digitized with a sampling rate of 0.5 s. All seismograms were high-pass filtered with a cut-off period of 60 s in order to remove very long-period noise. The crustal and mantle structure beneath the recording stations was assumed to be a half-space with a

compressional wave velocity of 6 km/s; a Poisson ratio of 0.25, and a density of 2.6 g/cm³. The crustal and mantle structure at the source region is shown on Table 2. The anelastic attenuation along the propagation path was parameterized using a $t^* = 1$ s for *P* waves and a $t^* = 4$ s for *SH* waves. A priori single point source with a source time function duration of 4 s was used for both events.

The inversion procedure is discussed in detail by *Nábelek* [1984]. Briefly, the method may be explained as follows. According to the size of the earthquake, the source time function is parameterized as a single point source or as an event composed of several point sources (subevents) separated in time and space. For each subevent, the model parameters include the focal mechanism (strike, dip, and rake), centroidal depth, seismic moment, source time function, and the relative location and time delay of each subevent with respect to the first one. The source time function is allowed to take an arbitrary shape. Theoretical seismograms are iteratively matched to the observed seismograms using a least squares criterion until a prescribed variance reduction is achieved.

Focal depths and fault plane solutions for earthquakes of small magnitude ($m_b \leq 5.1$)

As mentioned above, the hypocenters of all the events included in this study were estimated using a single-event method (*SE89*) [*Dewey*, 1971]. In general, the hypocentral locations determined using *SE89* are similar to those obtained by the *ISC* (Table 1). In addition, the focal depths of earthquakes with magnitude $m_b \leq 5.1$, for which a formal inversion was not possible, were calculated comparing the observed *pP-P* interval times read from the seismograms with the theoretical travel-time tables published by the International Association of Seismology and Physics of the Earth's Interior (*IASPEI*) [*Kennett*, 1991]. In order to evaluate with more confidence and precision the estimations of the focal depth, the readings of *pP-P* versus the epicentral distance of the stations used in the calculation were plotted. A linear, least-squares fit of the data was then made and compared with theoretical travel-times [*Kennett*, 1991] for a similar range of depths (Figure 4).

On the other hand, ten focal mechanisms of these earthquakes were determined by plotting the polarities of the first motions in a lower-hemisphere projection (Figure 5). The readings of pP - P times and polarities of the first arrivals were made mostly on short-period seismograms recorded by the *WWSSN* and the *GDSN* networks, and *YKA* and *NORSAR* arrays. The velocity model utilized to calculate the take off angle corresponding to each station is the same that used in the inversion scheme. In general, the focal mechanisms are well constrained because they show opposite polarities separating the nodal planes. However, the nodal planes of some of those mechanisms could vary but without interfering the conclusions.

To validate the results obtained using the methods described above, synthetic short-period seismograms were generated and then visually compared with the observed data. The synthetic waveforms were generated with the depth and focal mechanism determined in this study as input parameters for each event, and using the same source structure as that used in the inversion procedure described before. A source time function of 1 s was used in all cases. As an example, the synthetic and observed filtered-seismograms recorded at the *GDSN* stations *BCAO* and *ANMO* for the earthquake of October 28, 1980 are shown on Figure 6. In general, the comparison of the waveforms and of the arrival time of the phases P , pP , and sP in both stations coincide and corroborate the results obtained.

Results of the Analysis

The results obtained from the bodywave inversion of the earthquakes that occurred on November 17, 1968, and August 30, 1973, are shown on Figures 2 and 3. In both cases, the fit between the synthetic seismograms and the observed data is good. Although most of the stations used in the inversion are located to the north and to the northeast of the epicenter, the fault plane solutions of these two earthquakes are well constrained. There are stations in opposite quadrants controlling the position of the nodal planes in either the P and SH mechanisms for both earthquakes.

The fault plane solution determined in this study for the event of November 17, 1968, shows a T -axis dipping to the N140E at 44° . This mechanism agrees well with that reported by Kellogg and Bonini [1982], which was calculated by O. Pérez, W. R. McCann, and A. J. Murphy [Lamont-Doherty Geological Observatory, Palisades, New York, unpublished data, 1978] using first arrivals. It differs, however, from the focal mechanisms obtained by Dewey [1972] and Pennington [1981] using first-motion polarities (Figure 7). That difference is basically indicated by the presence of a strike-slip component in the fault plane solution reported by these latter authors. On the other hand, the focal mechanisms of the earthquake of August 30, 1973, reported here and by Pennington [1981] are very similar. Furthermore, this mechanism agrees with the fault plane solutions obtained by Molnar and Sykes [1969] and by Dewey [1972] for an event that occurred in the Bucaramanga nest on July 29, 1967 (Figure 7). The focal mechanism of the event of August 30, 1973 shows a T -axis oriented N110E and dipping 46° .

The seismic moment resulting from the bodywave inversion for the events of November 17, 1968, and August 30, 1973, are 8.1×10^{17} Nm and 2.8×10^{18} Nm, respectively, and correspond to moment-magnitude estimations of $M_w = 5.9$ and 6.2 [Hanks and Kanamori, 1979]. Their focal depths are 166 ± 1 and 175 ± 1 km, respectively (Table 3).

Most of the focal mechanisms of the events obtained from first motion data, similarly to those determined by the inversion, show predominantly T -axes oriented to the southeast (Figure 8 and Table 3). Only three of the earthquakes considered in this study (events 1, 5, and 18 on

Figure 8 and Table 3) show T -axes striking in a different direction. Coincidentally, they are three of the shallower events. The fault plane solutions obtained here for the events of October 28, 1980, and August 13, 1986 (events 8 and 15 on Figure 8), are similar to those determined by *Dziewonski et al.* [1987a; 1988]. *Dziewonski et al.* [1987b] also examined the focal mechanism of an earthquake that occurred offshore Colombia, on April 28, 1978 (Event 24 on Figure 8), that presents a T -axis trending practically north-south.

In general, the focal depths estimated in this study by bodywave inversion, single-event method, and readings of pP - P are similar to those calculated by *ISC* (Tables 1 and 3). All of them are in the range of errors that have been implicitly introduced by the velocity models utilized, errors in reading seismograms, and in the computation. Our conclusions, however, are not sensitive to these small differences in focal depth. For the analysis, we selected the focal depths obtained in this study from the inversion of bodywaves and readings of pP - P (Figure 9 and Table 3). We do not include our epicentral relocations on Table 3 because, as mentioned before, they are very similar to those calculated by *ISC* (Table 1).

Discussion

Geometry of the sinking slab based on the focal depth of the earthquakes

The results obtained in this study show that there is a close spatial and tectonic relationship between the intermediate-depth earthquakes in western Venezuela and those in northern Colombia. Apparently, all of these events lie within a lithosphere slab which presumably subducted beneath the southern Caribbean coast. The geometry of this slab was determined from the analysis of twenty-three earthquakes with depths ranging from 49 km to 189 km (Figure 9).

The isodepth lines reflect the presence of a lithospheric plate subducted along the northern Colombia coastline, which strikes roughly in a NNE-SSW direction and dips toward the southeast. Three cross-sections were made to estimate the dip of the slab; two on a plane trending 118° that include the events that occurred in the northern zone (A-A'; B-B') and another profile in an E-W direction that includes the events located in the southern part of the study area (C-C') (Figure 9).

The orientation of the cross-sections was selected based on the hypothesis that the slab subducted initially from the suture zone between South America and Panama. This plate boundary between the Caribbean and South American plates is probably the Southern Caribbean Deformed Belt [Ladd *et al.*, 1984; Freymueller *et al.*, 1993]. The three cross-sections show seismic zones dipping approximately 25° - 32° to the ESE, down to a maximum depth of about 200 km. The profiles also reflect an increase in the dip of the slab from south to north. The dispersion of hypocenters observed in cross-section A-A' may be the result of the curvature of the subducted slab when projected onto the profile.

Focal mechanisms and the geometry of the subducted slab

Most of the fault plane solutions determined in this study (Figure 5) and those calculated by Dziewonski *et al.* [1987a; 1987b; 1988] consistently show tensional faulting with *T*-axes oriented

in the downdip direction of the presumed slab (Table 3). The focal mechanisms were projected onto the two cross-sections mentioned above, on side-looking lower hemispheric projections (Figure 9). This shows the trend of the T -axes as a function of depth. In general, the plunge of the T -axes increases consistently with depth, ranging from 22° to 46° . The plunge of the T -axes coincides with the gradient of the subducted slab defined by the relocated earthquakes. The coincidence between the dip of the slab and the orientation of the T -axes has been reported also at intermediate depths in others slabs [Isacks and Molnar, 1971; Apperson and Frohlich, 1987; Araujo and Suárez, 1994].

The Bucaramanga source and the intermediate-depth seismicity outside the nest

The intermediate-depth seismicity outside of the Bucaramanga source takes place as isolated earthquakes, rather than occurring in a tight cluster as it does in the Bucaramanga nest (Figure 1). Consequently, it is important to understand whether there is a correlation between the focal mechanisms of earthquakes located within the nest with those of events outside the nest [e.g. Dewey, 1972; Schneider et al., 1987; Rivera, 1989].

Schneider et al. [1987] obtained the focal mechanisms of fifty-nine microearthquakes occurring within the Bucaramanga nest; they did not identify, however, any dominant trend in them. Furthermore, their efforts to correlate those fault plane solutions with a regional stress pattern or with previously determined mechanisms from teleseismic data were unsuccessful.

The comparison between the results obtained in this study and those of previous workers shows interesting aspects. The inversion results of the P and SH waves of the November 17, 1968, earthquake, located approximately 250 km to the north of the Bucaramanga nest, and of the August 30, 1973, event, located very close to the nest, present a very similar focal mechanism and orientation of the T -axes (events 2 and 4 on Figure 8). In both cases, the T -axes are oriented northwest-southeast and dip towards the southeast.

The focal mechanisms of these two earthquakes agree with the fault plane solutions reported for two of the largest events that occurred inside or near the nest on February 26, 1965

($m_b=5.7$), and July 29, 1967 ($m_b=6.0$) [Molnar and Sykes, 1969; Isacks and Molnar, 1971; Dewey, 1972]. However, they differ from the mechanisms of the events that occurred on September 11, 1966 ($m_b=5.9$), and on July 8, 1973 ($m_b=5.4$) [Dewey, 1972; Pennington, 1981] (Figure 7).

Those four earthquakes have been reported to occur presumably inside the nest [e.g. Molnar and Sykes, 1969; Dewey, 1972; Pennington, 1981]. However, according to Schneider et al. [1987], the last two events mentioned above are the only earthquakes that are really within the nest itself. This conjecture is based on the fact that the focal mechanisms of these two latter earthquakes have a NW-SE striking nodal plane that is parallel to the alignment of the nest. Nevertheless, due to the small and limited volume of the Bucaramanga source and considering the errors present in the hypocentral determination, it is difficult to affirm whether an earthquake close to this area is within the nest or not.

In summary, the fact that the largest earthquakes reported inside or near the nest present a similar focal mechanism and orientation of the T -axes to that of the largest events occurring outside of the nest suggests that the Bucaramanga nest lies on the same subducted slab where the other intermediate-depth events in northern Colombia and western Venezuela occur.

The subducted slab

The distribution of the relocated hypocenters in northern Colombia and western Venezuela clearly suggest the presence of a subducted lithosphere in the region. This slab, oriented in a NNE-SSW direction, extends for a distance of over 400 km and dips to the southeast. The orientation and geometry of the slab strongly suggest that its presence is due to the subduction of the Caribbean plate beneath northern Colombia. Furthermore, the inferred isodepth curves and the orientation of the T -axes of the focal mechanisms, suggest that the Bucaramanga nest occurs within the same slab. However, considering the existence of focal mechanisms in the Bucaramanga nest that differ from those of the rest of the slab and the remarkable high

concentration of seismicity, evidently something unusual and not yet determined is occurring in this part of the slab.

The timing and combination of relative plate motions that produced the subduction which now is responsible for the slab present in northern Colombia and western Venezuela are not fully understood. However, the slab appears to be the product of the same type of relative plate motion that resulted from the collision of the Panamanian arc with South America. Although it can not be unequivocally stated with the data on hand, the low rate of shallow seismicity and the absence of underthrusting earthquakes along the coast of northwestern Colombia, suggest that subduction is not occurring today; however, if subduction takes place today, it probably occurs at a very low rate (<1 cm/yr), reflected by the low seismicity of the area.

Undoubtedly, the neotectonic regime in northern Colombia and western Venezuela has changed since the collision between the Panamanian arc and South America took place [Freymueller *et al.*, 1993]. Apparently, the subduction of the Nazca and Caribbean plates beneath the Northern Andes block continued after the initial collision took place [Kellogg and Bonini, 1985]. According to Wadge and Burke [1983], the deformation, uplift, and suturing of the Panamanian arc onto Colombia began between 15 and 10 m.y.a. Mann and Burke [1984], and more recently Mann and Corrigan [1990], suggested that the best estimate of the age of the collision appeared to be latest Miocene to early Pliocene.

Silver *et al.* [1990] suggested that the collision occurred in the middle to late Miocene, when the Panama block was apparently oroclinally bent, with free boundaries along both the northern and southern margins. Nonetheless, if we assume a rate of subduction of 2 cm/yr, the occurrence of intermediate-depth earthquakes at a depth of approximately 200 km in this region, suggests that underthrusting of the Caribbean lithosphere beneath South American plate may have taken place as recently as 10 m.y.a.

The geometry of the slab can be inferred based on the seismicity from a depth of ~50 km (Figure 9). The slab dips at an angle of ~25° at depths of less than 100 km. At that depth, the dip increases to about 30° to 35°. The angle of subduction inferred from the distribution of seismicity is steeper than the one dipping at ~17° determined by van der Hilst and Mann [1994] based on

seismic tomography. The steeper dip angle of the subducted slab observed here does not support the hypothesis that the shallow subduction angle of the Caribbean plate beneath South America results in "Laramide-style" deformation on vertical block uplifts in the overriding plate [Kellogg and Bonini, 1982; Kellogg, 1984; van der Hilst and Mann, 1994].

van der Hilst and Mann (1994) identified a shallow velocity anomaly that together with the extension of the seismicity towards the surface, in the NW direction (cross-sections A-A' and B-B'), suggests that the location of the trench or paleotrench coincides with the location of the Southern Caribbean Deformed Belt, considered by Freymueller *et al.* [1993] as a major plate boundary. This is also corroborated by the occurrence of events 10, 11, 13, and 18, which clearly are not located within the South American plate (Figures 8 and 9). The location and focal mechanisms of these intermediate-depth earthquakes suggest that the subducted slab is still attached to the Caribbean lithosphere.

Towards the southwestern part of the study area, understanding the geometry of the slab is more complicated. The dip of the slab appears to change near the suture zone due to the collision of the Panamanian arc. In this region it is more difficult to assert whether the slab is still attached to the Caribbean plate, since it can not be established with certainty to which tectonic plate the earthquakes are related to: the Caribbean or Nazca plates.

The lack of intermediate-depth earthquakes north of approximately 11.5°N suggests that the subduction zone terminated near this latitude [Dewey, 1972]. Nevertheless, an earthquake ($m_b=4.8$) with a reverse-faulting source mechanism occurred on June 11, 1984 (event 12 on Figure 8 and Table 3), at a latitude of approximately 10.8°N, and at a depth of 61 km. Another earthquake with similar fault plane solution and depth was reported by Vierbuchen [1978] (event 25 on Figure 8). This event occurred on March 12, 1968, and is located offshore northern Colombia (13.2°N; 72.3°W) at a depth of 58 km. The depths of these earthquakes seem to indicate the shallowest and northernmost portion of the slab.

Summary and Conclusions

The analysis of intermediate-depth earthquakes in western Venezuela and northern Colombia shows the presence of a continuous lithospheric slab over 400 km long, subducted beneath the southern Caribbean coast. The geometry and maximum depth extent of the slab were obtained from the focal parameters of twenty-three low to moderate-magnitude events ($4.2 \leq m_b \leq 5.8$). The long-period bodywaves of the two largest earthquakes ($m_b > 5.4$) were formally inverted, whereas the focal depths for the smaller events ($m_b \leq 5.1$) were determined by comparing the observed data with the theoretical travel times. The fault plane solutions of the smaller earthquakes were obtained by plotting the polarities of the first motions on a lower-hemisphere projection.

Based on the examination of the focal depths, the geometry of the slab was defined at depths ranging from 60 km to 180 km. The isodepth lines show a slab striking in a NNE-SSW direction and dipping approximately 25° - 32° to the east. The orientations of the T -axes indicate tensional faulting and are generally aligned parallel to the gradient of the slab inferred from the seismicity. The results obtained from the analysis of the earthquakes that occurred on November 17, 1968 (approximately 250 km to the north of the Bucaramanga nest), and on August 30, 1973 (near the nest), show similar focal mechanisms and they agree with other fault plane solutions of two moderate-magnitude events reported inside the nest. Thus it appears that the seismicity in the Bucaramanga nest is part of a seismic zone reflecting the presence of a subducted portion of the Caribbean plate beneath the overriding South American plate.

Acknowledgments. The authors thank J. Dewey and C. Mendoza for their comments and discussions. The manuscript benefited from thoughtful and thorough reviews by C. Frohlich and J. Kellogg. T. Aherns, C. Lindholm, R. G. North, and M. Zirbes made available copies of the *IRIS*, *NORSAR*, *YKA*, and *GDSN* digital seismograms, respectively. M. Benites and J. Taggart helped us to make copies of the *WISSN* analog seismograms. This paper was partially written while one of the authors (G.M.), as a graduate student of the Universidad Nacional Autónoma de México, was visiting the U. S. Geological Survey in Golden, Colorado. The use of facilities is greatly appreciated. G.M. received financial aid in the form of an INTEVEP, S.A. Fellowship.

References

- Apperson, K. D. and C. Frohlich, The relationship between Wadati-Benioff zone geometry and P , T , and B axes of intermediate and deep focus earthquakes, *J. Geophys. Res.*, 92 (B13), 13821-13831, 1987.
- Araujo, M. and G. Suárez, Geometry and state of stress of the subducted Nazca plate beneath central Chile and Argentina: Evidence from teleseismic data, *Geophys. J. Int.*, 116, 283-303, 1994.
- Dewey, J. W., Seismicity studies with the method of joint hypocenter determination, Ph. D. Dissertation, University of California, Berkeley, 1971.
- Dewey, J. W., Seismicity and tectonics of western Venezuela, *Bull. Seism. Soc. Am.*, 62, 1711-1751, 1972.
- Dziewonski, A. M., G. Ekstrom, J. E. Franzen, and J. H. Woodhouse, Centroid-moment tensor solutions for July-September 1986, *Phys. Earth Planet. Int.*, 46 (4), 305-315, 1987.
- Dziewonski, A. M., G. Ekstrom, J. E. Franzen, and J. H. Woodhouse, Global seismicity of 1978: centroid-moment tensor solutions for 512 earthquakes, *Phys. Earth Planet. Int.*, 46 (4), 316-342, 1987.
- Dziewonski, A. M., G. Ekstrom, J. E. Franzen, and J. H. Woodhouse, Global seismicity of 1980: centroid-moment tensor solutions for 515 earthquakes, *Phys. Earth Planet. Int.*, 50 (2), 127-154, 1988.
- Freymueller, J. T., J. N. Kellogg, and V. Vega, Plate motions in the North Andean region, *J. Geophys. Res.*, 98, 21853-21893, 1993.
- Hanks, T. and H. Kanamori, A moment magnitude scale, *J. Geophys. Res.*, 84 (B5), 2348-2350, 1979.
- Isacks, B. and P. Molnar, Mantle earthquake mechanisms and the sinking of the lithosphere, *Nature*, 223, 1121-1124, 1969.

- Isacks, B. and P. Molnar, Distribution of stresses in the descending lithosphere from a global survey of focal-mechanism solutions of mantle earthquakes, *Rev. Geophys. Space Phys.*, 9, 103-174, 1971.
- Kellogg, J. N., Cenozoic tectonic history of the Sierra de Perijá, Venezuela-Colombia, and adjacent basins, in Bonini, W. E. *et al.*, eds., The Caribbean South American plate boundary and regional tectonics, *Geol. Soc. Am. Mem.*, 162, 239-261, 1984.
- Kellogg, J. N. and W. E. Bonini, Subduction of the Caribbean plate and basement uplifts in the overriding South American plate. *Tectonics*, 1 (3), 251-276, 1982.
- Kellogg, J. N. and W. E. Bonini, Reply. *Tectonics*, 4 (7), 785-790, 1985.
- Kennett, B., ed., IASPEI 1991 Seismological Tables, Research School of Earth Sciences, Australian National University, 167 pp, 1991.
- Ladd, J. W., M. Truchan, M. Talwani, P. L. Stoffa, P. Buhl, R. Houtz, A. Manfrett, and G. Westbrook, Seismic reflection profiles across the southern margin of the Caribbean, in Bonini, W. E. *et al.*, eds., The Caribbean-South America plate boundary and regional tectonics, *Geol. Soc. Am. Mem.*, 162, 239-261, 1984.
- Mann, P. and K. Burke, Neotectonics of the Caribbean, *Review of Geophysics and Space Physics*, 22 (4), 309-362, 1984.
- Mann, P. and J. Corrigan, Model for late Neogene deformation in Panama, *Geology*, 18, 558-562, 1990.
- Molnar, P. and L. R. Sykes, Tectonics of the Caribbean and middle America regions from focal mechanisms and seismicity, *Bull. Seism. Soc. Am.*, 80, 1639-1684, 1969.
- Nábelek, J. L., Determination of earthquakes source parameters from inversion of body waves, [Ph.D. thesis]: Massachusetts Institute of Technology, Cambridge, 361 pp, 1984.
- Pennington, W. D., Subduction of the Eastern Panama Basin and Seismotectonics of Northwestern South America, *J. Geophys. Res.*, 86 (B11), 10753-10770, 1981.
- Rivera, L., Inversion du Tenseur des Contraintes et des Mécanismes au Foyer à partir des Données de Polarité pour une Population de Séismes. Application à l'Etude du Foyer de

- Sismicité Intermédiaire de Bucaramanga (Colombie), [These de Doctorat]: Université Louis-Pasteur de Strasbourg, 266 pp, 1989.
- Schneider, J. F., W. D. Pennington, and R. P. Meyer, Microseismicity and Focal Mechanism of the Intermediate-Depth Bucaramanga Nest, Colombia, *J. Geophys. Res.*, 92 (B13), 13913-13926, 1987.
- Shih, X. R., R. P. Meyer, and J. F. Schneider, Seismic anisotropy above a subducted plate, *Geology*, 19, 807-810, 1991.
- Silver, E., D. Reed, J. Tagudin, and D. Heil, Implications of the North and South Panama thrust belts for the origin of the Panama orocline, *Tectonics*, 9 (2), 261-281, 1990.
- van der Hilst, R. and P. Mann, Tectonic implications of tomographic images of subducted lithosphere beneath northwestern South America, *Geology*, 22, 451-454, 1994.
- Vierbuchen, R. C., Jr., The tectonics of northeastern Venezuela and the southeastern Caribbean Sea, Ph. D. thesis, Princeton University, N. J, 1978.
- Wadge, G. and K. Burke, Neogene Caribbean plate rotation and associated Central American tectonic evolution, *Tectonics*, 2 (6), 633-643, 1983.

Figure Captions

- Figure 1.** Seismicity ($m_b \geq 4.0$) of northern Colombia and western Venezuela reported by the National Earthquake Information Center (NEIC) since 1963. The thick solid lines on the map indicate the direction of the three cross-sections shown: A-A', B-B', and C-C'. The contour lines are bathymetric curves in meters. The seismicity is shown as crosses ($0 < h \leq 70$ km.) and shaded circles ($h > 70$ km.).
- Figure 2.** Results of the simultaneous inversion of the (top) P and (bottom) SH waves of the November 17, 1968, earthquake, using a point source with a source time function duration of 4 s. The theoretical seismograms (dashed lines) and observed waves (solid lines) match very well the waveforms in all the stations considered. The focal mechanisms are shown in a lower hemisphere projection. The shaded areas in the P waves fault plane solution represent compressional first motion. Amplitudes of the waveforms are normalized to an instrumental magnification of 1500 and a geometrical spreading corresponding to an epicentral distance of 40° . Abbreviations are the names of the seismological stations.
- Figure 3.** Comparison between the theoretical seismograms (dashed lines) and observed (top) P and (bottom) SH waves (solid lines) of the August 30, 1973, earthquake using a point source with a source time function duration of 4 s. The symbols, abbreviations, and amplitude normalization are the same as in Figure 2.
- Figure 4.** An example of the method used in this study to determine the value of the focal depth using the difference between the arrival times of the P and pP phases (stars). This chart correspond to the May 12, 1976, earthquake which occurred in northern Colombia. The solid line represents the linear least square fit obtained from the observed data. The dashed lines indicate the linear least square fit from the theoretical data for specific depths.
- Figure 5.** Focal mechanisms determined in this study ($m_b \leq 5.1$). The polarities of the first arrivals used to constrain the fault plane solutions are shown as open circles for dilatational arrivals and solid circles for compressional arrivals. The focal mechanisms are shown in a lower hemisphere projection. The event numbers are the same those in Table 1.

Figure 6. Observed and synthetic short-period seismograms for the event on October 28, 1980 in northern Colombia, recorded at the Global Digital Seismograph Network (*GDSN*) stations: *BCAO* (Bangui, Central Africa; epicentral distance 93°) and *ANMO* (Albuquerque, New Mexico; epicentral distance 40°). The first and third seismograms are observed and the second and fourth are synthetic waveforms. The seismograms are normalized to the maximum amplitude. The approximate arrival times of the *P*, *pP*, and *sP* phases in each station are shown on the seismograms.

Figure 7. Focal mechanisms of several intermediate-depth earthquakes that occurred in northern Colombia and western Venezuela determined in this study and by previous workers. The fault plane solutions are shown in a lower hemisphere projection. The solid quadrants indicate compressional arrivals. The solid and open circles correspond to the position of the *P* and *T* axes, respectively, in the focal sphere. The focal mechanism of the earthquake that occurred on November 17, 1968, reported by *Kellogg and Bonini* [1982] was taken from their Figure 11.

Figure 8. Fault plane solutions determined in this study for 12 intermediate-depth events which occurred in northern Colombia and western Venezuela. The centroidal moment tensor solution of the April 24, 1978, earthquake (event 24) [*Dziewonski et al.*, 1987b] and the mechanism of the March 12, 1968, event (number 25) [*Vierbuchen*, 1978] were also included. The focal mechanisms are shown in a lower hemisphere projection. The size of the focal mechanism is proportional to the magnitude (m_b) of the events (Table 3). The solid quadrants indicate compressional arrivals. The solid and open circles correspond to the position of the *P* and *T* axes, respectively, on the focal sphere. The numbers are the same as those in Tables 1 and 3.

Figure 9. Intermediate-depth seismicity of northern Colombia and western Venezuela analyzed in this study. The dashed lines show the isodepth curves of the subducted lithospheric slab. The solid circles in the map indicate the epicentral location of the events. The numbers are the same as those in Tables 1 and 3, with depths in parentheses. The thick solid lines on the map show the direction of the three cross sections: A-A', B-B', and C-C'. The contour lines

in the map are bathymetric curves in meters. The solid lines in the profiles indicate the position of the slab inferred from the relocated seismicity. The focal mechanisms in the cross sections are projected onto the profiles on side-looking hemispheric projections. The solid quadrants indicate compressional arrivals. The solid and open circles correspond to the P and T axes, respectively, on the focal spheres.

MALAVE AND SUAREZ: SUBDUCTION IN THE NORTHERN ANDES

Table 1. Focal Parameters of the Events Reported by *ISC* and Calculated by the Program *SE89*

Event	Date	Latitude,*	Longitude,*	Depth,*	Depth (<i>pP-P</i>),*	Depth (<i>SE89</i>),	Magnitude,*
		° N	° W	km	km	km	<i>m_b</i>
1	March 25, 1964	7.62	75.39	47±7.0	60±3.0	59	5.0
2	Nov. 17, 1968	9.57	72.63	150±3.4	174±1.0	176	5.8
3	Dec. 14, 1970	9.99	72.68	165±3.5	160±1.0	167	5.1
4	Aug. 30, 1973	7.24	72.85	179±2.3	182±1.0	187	5.7
5	May 12, 1976	7.43	74.95	61±3.7	47±3.8	56	5.1
6	Oct. 31, 1979	8.00	74.10	123±14.0	---	---	4.9
7	March 9, 1980	7.48	73.94	101±2.3	94±1.4	101	4.9
8	Oct. 28, 1980	7.26	74.76	69±2.5	60±1.1	68	5.0
9	Aug. 23, 1981	8.65	74.16	129±13.0	---	---	4.2
10	Jan. 13, 1983	11.90	73.59	20±4.8	26±8.0	---	5.1
11	Aug. 14, 1983	9.13	73.90	86±3.7	76±1.4	88	4.9
12	June 11, 1984	10.82	74.20	69±3.0	62±6.0	70	4.8
13	Oct. 27, 1984	9.82	74.73	61±9.7	---	57	5.0
14	Nov. 18, 1984	8.82	73.18	146±2.2	143±1.8	146	4.9
15	Aug. 13, 1986	7.70	74.71	50±6.9	54±9.0	60	5.1
16	Sep. 15, 1986	7.46	74.96	68±7.4	54±1.1	64	4.8
17	April 12, 1987	7.86	73.18	152±7.2	---	158	4.5
18	Aug. 9, 1987	10.09	74.27	43±6.6	28±4.0	34	5.1
19	April 15, 1988	8.47	73.20	140±25.0	---	136	4.3
20	Nov. 6, 1988	8.26	73.10	182	---	---	4.2
21	Jan. 12, 1990	8.50	72.40	202±26.0	---	---	4.3
22	Dec. 19, 1990	8.09	73.91	94±12.0	---	---	4.6
23 [†]	Feb. 6, 1992	8.21	72.80	172±3.6	---	167	4.5 [†]

ISC is the International Seismological Centre, and *SE89* is the single event location program of Dewey [1971].

* Information reported by *ISC*.

[†] Information reported by National Earthquake Information Center (*NEIC*).

Table 2. Crustal and Mantle Structure at the Source Region for the Inversion of the Events of November 17, 1968 and August 30, 1973

Layer	Thickness, km	V_P , km/s	V_S , km/s	Density, g/cm ³
1	40	6.00	3.46	2.6
2	160	8.00	4.62	2.7
3	Half-space	8.20	4.73	2.8

V_P and V_S are the compressional and shear velocities respectively.

MALAVE AND SUAREZ: SUBDUCTION IN THE NORTHERN ANDES

Table 3. Focal Mechanisms and Depths Determined in This Study

Event	Date	Strike, deg	Dip, deg	Rake, deg	<i>P</i> axis Tr°/Pl°	<i>T</i> axis Tr°/Pl°	Depth, km	Method/Data for Focal Depth*
1	March 25, 1964	331	48	-72	312/77	48/2	65±3	<i>pP-P</i> (W)
2	Nov. 17, 1968	149±4	8±2	-179±4	336/45	140/44	166±1	<i>P, SH</i> Inversion (G)
3	Dec. 14, 1970	159	14	-122	291/56	96/33	158±2	<i>pP-P</i> (W)
4	Aug. 30, 1973	183±1	86±1	107±1	258/39	110/46	175±1	<i>P, SH</i> Inversion (G)
5	May 12, 1976	323	42	-89	220/87	52/3	49±2	<i>pP-P</i> (G, W)
6	Oct. 31, 1979	---	---	---	---	---	137±5	<i>pP-P</i> (G)
7	March 9, 1980	114	12	173	312/42	109/45	95±3	<i>pP-P</i> (G, W)
8	Oct. 28, 1980	215	32	-91	308/77	126/13	62±3	<i>pP-P</i> (G, W)
---	Oct. 28, 1980	36	58	-55	0/60	102/7	72	CMTS
9	Aug. 23, 1981	---	---	---	---	---	126±5	<i>pP-P</i> (G, Y)
10	Jan. 13, 1983	---	---	---	---	---	28±4	<i>pP-P</i> (G, Y)
11	Aug. 14, 1983	321	12	23	288/39	130/46	118±4	<i>pP-P</i> (G, N, W)
12	June 11, 1984	88	46	80	5/1	100/83	61±1	<i>pP-P</i> (G, N, W, Y)
13	Oct. 27, 1984	---	---	---	---	---	49±1	<i>pP-P</i> (G, W, Y)
14	Nov. 18, 1984	228	27	-53	251/62	111/22	136±5	<i>pP-P</i> (G, N, W, Y)
15	Aug. 13, 1986	307	32	-1	280/37	156/36	63±1	<i>pP-P</i> (G, W)
---	Aug. 13, 1986	16	76	-140	243/38	140/16	91	CMTS
16	Sep. 15, 1986	---	---	---	---	---	59±3	<i>pP-P</i> (G, W)
17	April 12, 1987	---	---	---	---	---	144±2	<i>pP-P</i> (Y)
18	Aug. 9, 1987	259	85	-146	308/27	207/19	50±1	<i>pP-P</i> (G, W, Y)
19	April 15, 1988	---	---	---	---	---	144±2	<i>pP-P</i> (G, Y)
20	Nov. 6, 1988	---	---	---	---	---	179±3	<i>pP-P</i> (Y)
21	Jan. 12, 1990	---	---	---	---	---	189±5	<i>pP-P</i> (G, N, Y)
22	Dec. 19, 1990	---	---	---	---	---	122±3	<i>pP-P</i> (G, Y)
23	Feb. 6, 1992	---	---	---	---	---	168±5	<i>pP-P</i> (G)
24	April 28, 1978	70	84	-112	317/47	179/35	62	CMTS

Abbreviations are Tr, trend and P, plunge.

*G is the Global Digital Seismograph Network (GDSN); N is the Norwegian Seismograph Array (NORSAR); W is the World-Wide Standardized Seismograph Network (WWSSN); Y is the Yellow Knife Array (YKA); CMTS is the centroidal moment tensor solution.

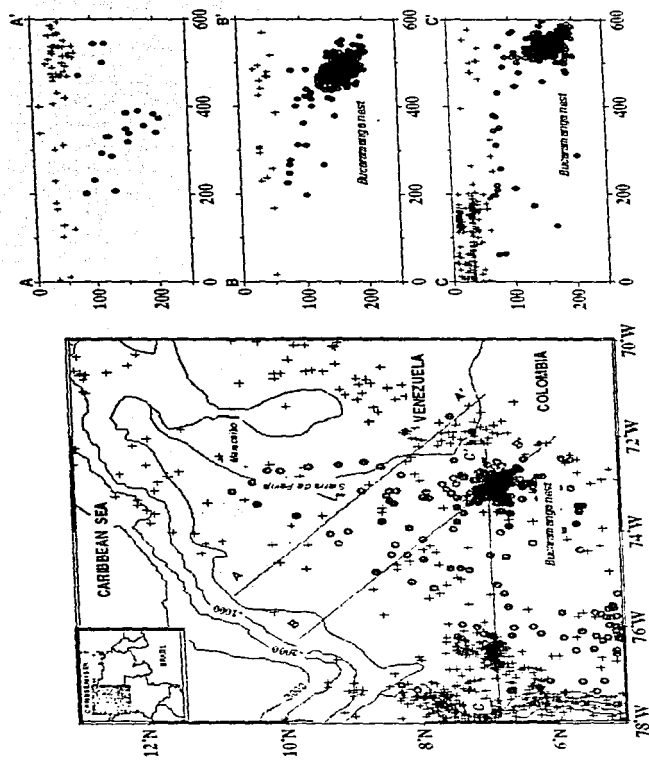


Figure 1

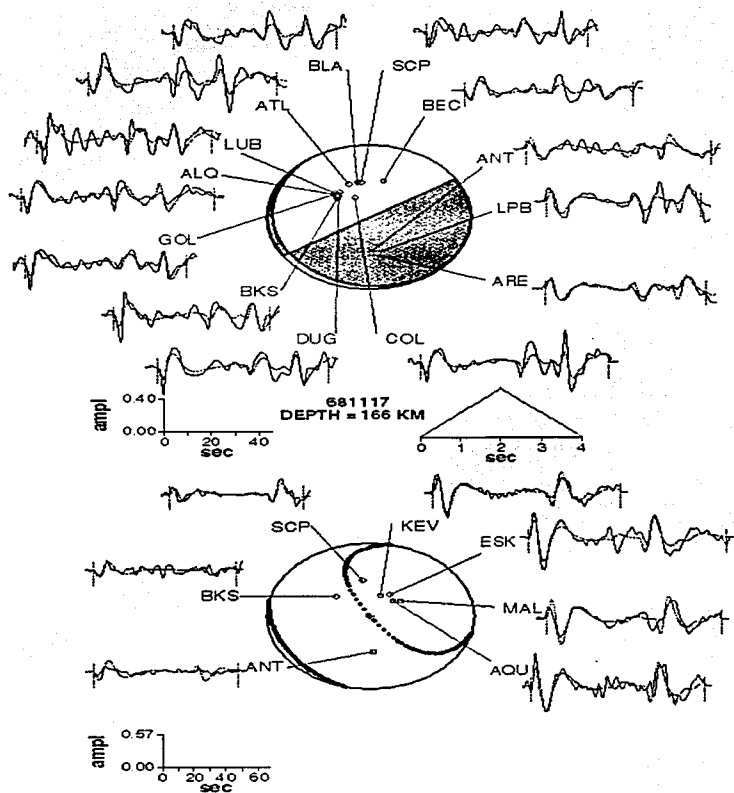


Figure 2

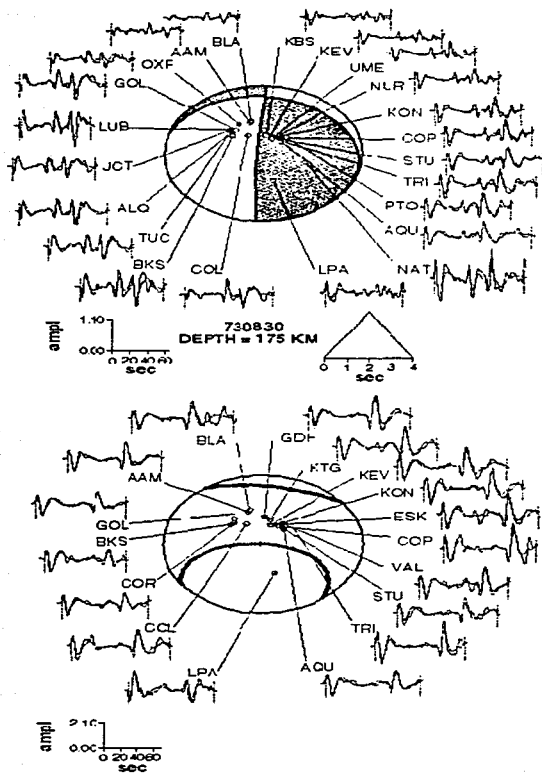


Figure 3

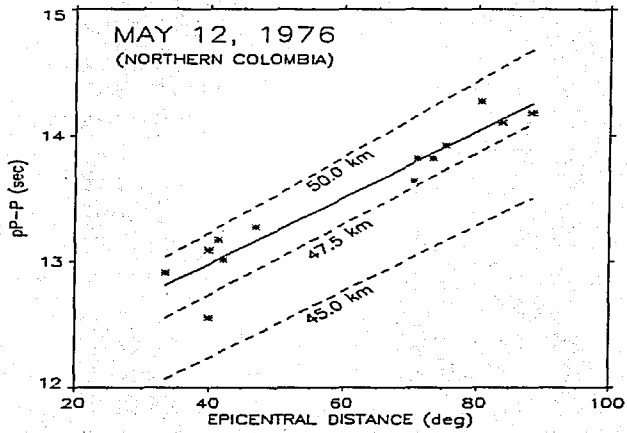


Figure 4

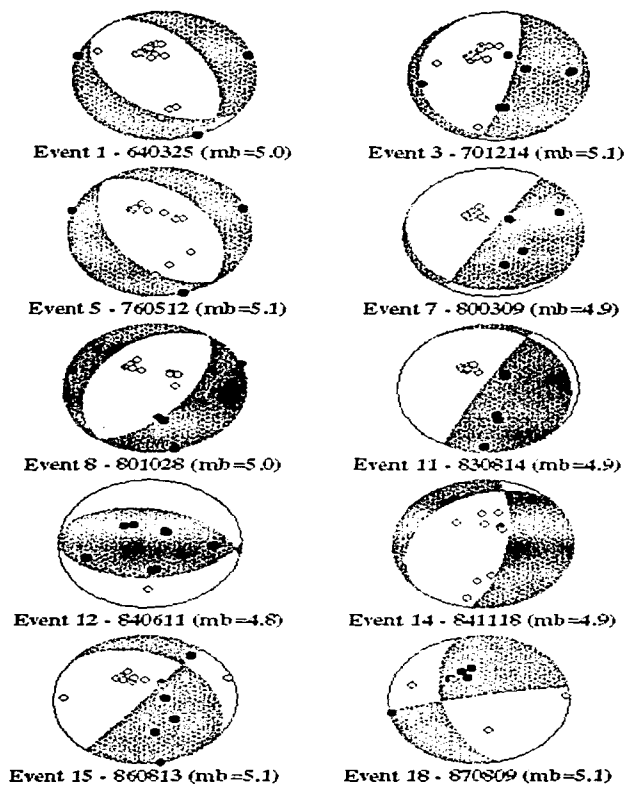


Figure 5

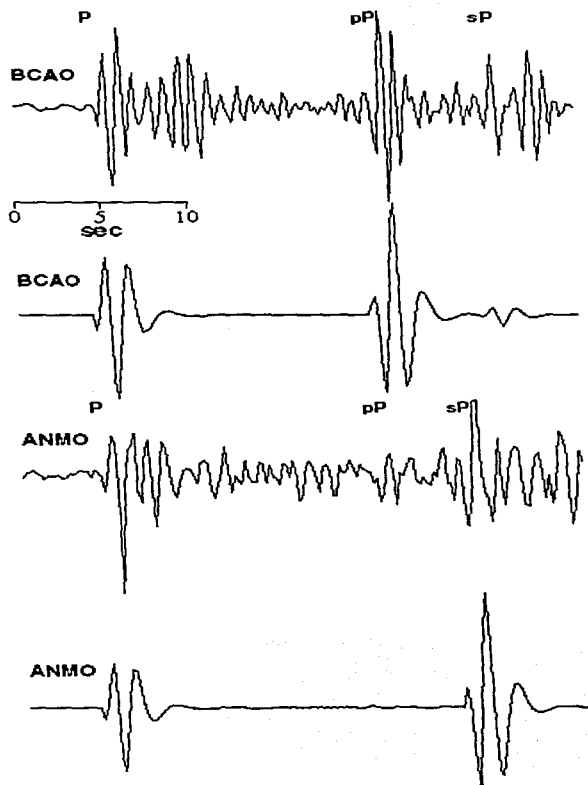


Figure 6

MALAVE AND SUAREZ: SUBDUCTION IN THE NORTHERN ANDES

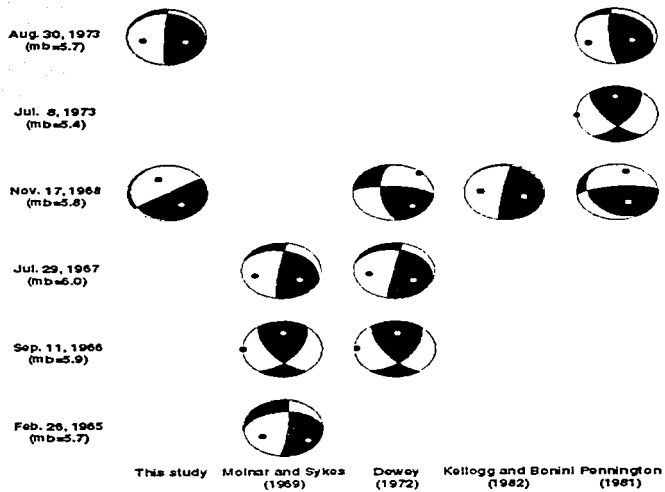


Figure 7

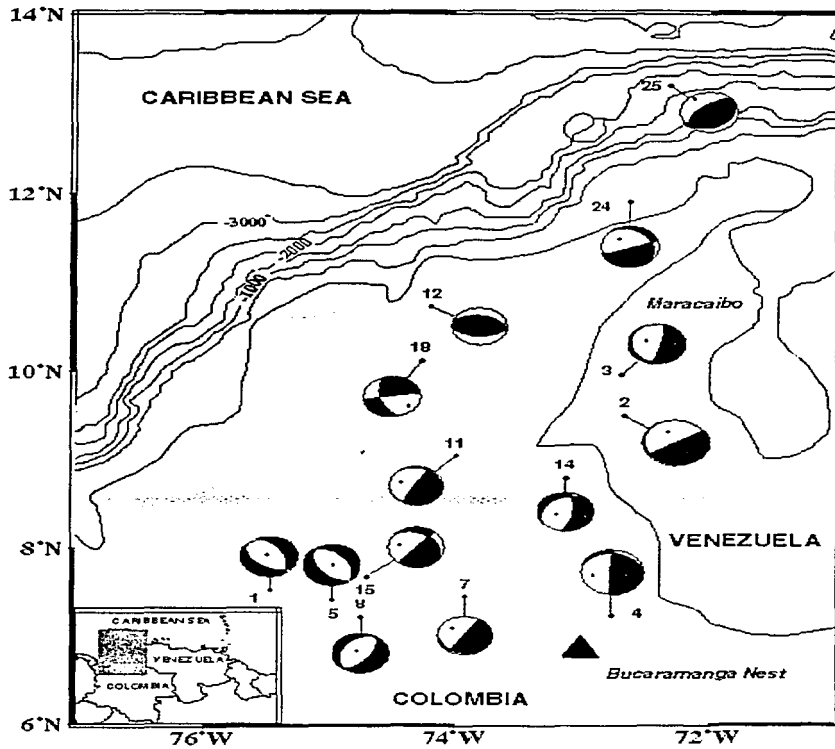


Figure 8

**III. Características complejas de la fuente de los sismos de
Boca del Tocuyo de 1989, en el noroeste de Venezuela**

**Complex Source Characteristics of the 1989 Boca del Tocuyo Earthquakes in
Northwestern Venezuela**

by Gustavo Malavé¹ and Gerardo Suárez

Instituto de Geofísica, Universidad Nacional Autónoma de México, Mexico City, Mexico

¹Now at INTEVEP, S.A., Apartado Postal 76343, Caracas 1070A, Venezuela

Abstract The Boca del Tocuyo earthquake of April 30, 1989, has a special significance in assessing the seismic hazard of northern Venezuela. Although it was an event of moderate magnitude ($M_w=6.2$), the mainshock and its largest aftershock ($M_w=5.6$) produced considerable damage in low-rise structures mainly due to soil failure and induced intense liquefaction in most of the coastal towns near the epicentral area. Both earthquakes presented body-wave trains which are much longer than those expected for a single event of that magnitude. The reason for this anomalous duration was analyzed through the formal inversion of the P , SH , and SV waves recorded teleseismically. The results show that the Boca del Tocuyo main event and its largest aftershock were generated by multiple rupture processes composed of at least three and two subevents, respectively. Although the direction of rupture propagation could not be gleaned from the teleseismic body wave data, the epicentral relocation of the largest aftershock, the hypocentral distribution of about 60 aftershocks ($m_b < 4.5$), and the linearity of the coast, which is parallel to the

geologic structures in this area, suggest right-lateral, strike-slip faulting in a NW-SE direction. The Boca del Tocuyo earthquakes were apparently generated on a system of conjugate faults that are oblique to the east-west-trending, major fault systems in northern Venezuela.

Introduction

On April 30, 1989, Boca del Tocuyo and several neighboring coastal towns in northwestern Venezuela were severely damaged by a moderate-sized earthquake ($m_b=5.7$; $M_s=6.0$) (Fig. 1). This is the largest earthquake in central and western Venezuela since the magnitude 6.6 (M_w) Caracas event occurred on July 30, 1967. Four days later, on May 4, 1989, the largest aftershock ($m_b=5.4$; $M_s=5.2$) took place (Table 1). This aftershock caused concern among the inhabitants of this region and lightly damaged several low-rise dwellings.

The epicentral area of the Boca del Tocuyo seismic sequence lies close to the zone where the Oca-Ancón, Boconó, and Morón fault systems converge (Fig. 1). These fault systems have been proposed to represent the border between the Caribbean and South American plates in western Venezuela (e.g., Molnar and Sykes, 1969; Soulas, 1986). However, the present rates of motion of the Oca-Ancón fault system (2.5-4.0 mm/yr) (Soulas *et al.*, 1987) and of the Boconó fault system (0.3 cm/yr-1.4 cm/yr) (e.g., Schubert, 1982; Soulas, 1986) are lower than the predicted relative velocity between the Caribbean and South American plates (~2 cm/yr) proposed from kinematics plate motions (Jordan, 1975; Minster and Jordan, 1978; Stein *et al.*, 1988; Sykes *et al.*, 1982). Thus, the relative motion between the Caribbean and South American plates is apparently not absorbed on a single fault. This motion appears to be distributed over a wide zone of deformation along major right-lateral, strike-slip fault systems (e.g., Soulas, 1986) (Fig. 1).

Besides these major fault systems, several conjugate faults near the epicentral area of the Boca del Tocuyo earthquakes appear to be seismically capable (Soulas, 1986). These faults are oriented mainly in a NW-SE direction and they have been identified at sea, where they appear to cut the seafloor (Barbot *et al.*, 1979; Barbot *et al.*, 1980) (Fig. 1). As discussed later, this fault system apparently controls the orientation of the coastline in this area and presumably one of them ruptured during the Boca del Tocuyo seismic sequence.

The Boca del Tocuyo earthquake and its largest aftershock show several interesting aspects. The focal mechanisms reported by Dziewonski *et al.* (1990), the National Earthquake

Information Center (*NEIC*) (Sipkin, 1991), and *FUNVISIS* (Venezuelan Seismological Research Foundation) are all different (Fig. 2). The determination of a reliable fault plane solution for these events is important to correlate them with the active tectonics of the area.

The 1989 Boca del Tocuyo earthquakes are the only events reported in this region during both historical and instrumental seismological periods (Singer *et al.*, 1992). Furthermore, both earthquakes induced intense liquefaction in an area located ~25 km away from the epicenter. According to the relations proposed by Ambraseys (1988) (M_w vs. distance from the epicenter to the site liquefied), events of this magnitude are capable of causing the observed liquefaction. However, this phenomenon was particularly strong and widespread in Boca del Tocuyo.

In this study, the epicentral locations of the Boca del Tocuyo earthquake and its largest aftershock were evaluated. Furthermore, a detailed analysis of the long-period body waves using a formal least squares inversion algorithm (Nábelek, 1984) was carried out for both events in order to characterize their time history and the rupture process. The results suggest that the Boca del Tocuyo events originated from unusually complex and long rupture processes for earthquake of that magnitude.

Epicentral Location and Intensity Distribution

Epicentral Location of the Mainshock and of the Largest Aftershock

The epicentral locations of the main event and its largest aftershock were determined with the program *SE89* (Dewey, 1971), using the information collected from the Earthquake Data Report (*EDR*) of the *NEIC* (355 and 256 stations for the mainshock and aftershock respectively), and the 1968 seismological travel-time tables (Herrin *et al.*, 1968). In the calculation of those locations with the single-event method, arrival times showing large errors (residuals greater than 2 s) were eliminated in order to have a better quality control over the stations included in the database. After the last iteration, the number of stations in the database was reduced to 249 and 232 for the mainshock and aftershock, respectively.

There are some differences between these locations and those reported by the International Seismological Centre (*ISC*), *NEIC*, and *FUNVISIS* (Table 1). The epicentral locations of the mainshock reported by *ISC* and *NEIC* are on land, near the most severely damaged towns, whereas the locations reported by *FUNVISIS* and that determined in this study lie offshore, 15.5 km and 4.5 km away from the coast respectively (Fig. 2). On the other hand, the epicenters of the largest aftershock calculated by *ISC* and *NEIC* lie, on average, 5.5 km away from the coast and are very close to the mainshock epicentral location determined in this study (Fig. 2). *FUNVISIS* used in their hypocentral estimations only local seismological stations distributed to the south of the epicenter. In the determination of the epicentral locations in this study, besides the local stations used for *FUNVISIS*, many other regional and teleseismic stations were included to complete a good azimuthal coverage

Due to the variations obtained in the individual epicentral determination of both earthquakes, the largest aftershock was relocated with respect to the epicenter of the mainshock calculated in this study, using the Joint Hypocenter Determination (*JHD*) method (Dewey, 1971). The results show that the relocated epicenter of the largest aftershock lies two km to the NW of

the mainshock (Fig. 2). Unfortunately, no conclusive evidence may be drawn about the fault orientation based only on the location of the largest aftershock. However, the depth distribution of about 60 aftershocks ($m_b < 4.5$) located by *FUNVISIS* increases from NE to SW, suggesting a fault plane dipping towards the SW (Singer *et al.*, 1992) (Fig. 2). An attempt to relocate also a foreshock ($m_b = 4.9$) and two other smaller aftershocks ($m_b = 4.6$) was unsuccessful because they were not big enough to be detected by an adequate number of stations, resulting in epicenter locations with large 90% confidence ellipses.

Intensity Distribution

The intensity information collected by De Santis *et al.* (1991) shows a maximum value of VII Modified Mercalli Intensity (MMI) near the towns of Boca del Tocuyo, Tocuyo de la Costa, Chichiriviche, Boca del Mangle, and San Juan de los Cayos (Fig. 2). Most of the damage observed corresponds to fissures or to the collapse of walls in houses of defective masonry, and tilting of houses and water-tanks due to soil failure (De Santis *et al.*, 1991; Audemard and De Santis, 1991).

Both the main event and the largest aftershock induced liquefaction in the coastal area close to the epicenters. Isolated and aligned sand-boils, and vent-fractures were observed within a radius of about 25 km from the epicentral region.

The most spectacular liquefaction features occurred in the town of Boca del Tocuyo. There, the volume of water ejected inundated a zone of approximately 5000 m² with a water layer of 10 to 15 cm. The fact that the largest aftershock also induced liquefaction is demonstrated by the presence of overlapped sand-boils, where younger sand-boils cut older ones. No strong motion records are available in the near field and the accelerations estimated from empirical correlation and field observations are in the range of 0.25-0.30 g (De Santis *et al.*, 1991). Malaver (1990) estimated a maximum average acceleration of 0.38 g where liquefaction took place, and a value of 0.09 g outside this region.

Inversion of Body Waves

Data Preparation and Inversion Method

The source parameters of the Boca del Tocuyo earthquake and its largest aftershock were analyzed through the inversion of long-period P , SH , and SV waves recorded by the Global Digital Seismograph Network ($GDSN$). Only seismograms of stations within an epicentral distance range of 27° to 90° were included in the study. All seismograms were high-pass filtered with a cut-off period of 60 s in order to remove long-period noise. The crustal structure in the source region and below the recording stations was assumed to be a half-space with a compressional wave velocity of 6 km/s, a Poisson ratio of 0.25, and a density of 2.75 g/cm^3 . The anelastic attenuation along the propagation path was parameterized using a $t^* = 1 \text{ s}$ for P waves, and a $t^* = 4 \text{ s}$ for SH and SV waves.

The inversion procedure is discussed in detail by Nábelek (1984). Briefly, the method may be explained as follows. According to the size and complexity of the earthquake, the source time function is parameterized as a single point source or as an event composed of several point sources (subevents) separated in time and space. For each subevent, the model parameters include the fault plane solution (strike, dip, and rake), centroidal depth, seismic moment, source time function, and the relative location and time delay of each subevent with respect to the first one. The source time function is allowed to take an arbitrary shape. Theoretical seismograms are iteratively matched to the observed seismograms using a least squares criterion until a prescribed variance reduction is achieved. The seismic phases and stations used in the inversion procedure are shown on Tables 2 and 3.

Inversion Strategy

The observed waveforms strongly suggest that the Boca del Tocuyo mainshock and largest aftershock were complex events. The duration of the body wave trains was about 75 s. This

duration was, on average, twice as long as that expected for an earthquake of that magnitude. As a first step, the two events were analyzed assuming a single point source with a source time function duration of about four seconds. This source time function corresponds approximately to the duration of a single event of that magnitude. In both cases, the starting source mechanism for the inversion was the centroidal moment tensor solution (Dziewonski *et al.*, 1990) (Table 1: Fig. 2). Attempts to use the *NEIC* fault plane solution (Sipkin, 1991) as the initial source mechanism proved unsuccessful.

Assuming a single point source, only the initial part of the waveforms could be modeled (Table 4 and Fig. 3). Thus in order to synthesize the longer body-wave trains, we first investigated the possibility that the long duration was caused by local reverberation of body waves in the upper crust. Because the velocity structure of the Boca del Tocuyo region is not well known, a realistic velocity model of neighboring zones with similar conditions was used. Therefore, several inversions were attempted using the velocity model reported by Gajardo *et al.* (1986) for the east coast of Lake Maracaibo. To this velocity structure, low-velocity layers with high impedance contrasts were added in the upper crust.

The various source models including these low-velocity layers were tested as follows. First, a two-km-thick, low-velocity layer with a *P*-wave velocity ratio (V_1/V_2) of 2.9/6.0 km/s was added in the upper crust. Next, a second velocity model was prescribed where a low-velocity layer with a thickness of 3 km and with a *P*-wave velocity ratio (V_1/V_2) of 6.0/4.2 km/s was included in the upper crust, and a second low-velocity layer with a *P*-wave velocity ratio (V_2/V_3) of 4.2/8.2 km/s was placed above the Moho. All these attempts, however, were unsuccessful to reproduce the complexity and long duration of the observed waveforms.

There are several cases of moderate-sized earthquakes that have generated complex *P* waves, but very simple *SH* waveforms. Two recently studied examples are: the two aftershocks located north of Atka Island that occurred after the Andreanof Island earthquake of May 7, 1986 (Boyd and Nábelek, 1988), and the two events of January 10, 1979, that occurred in the Makran region (Byrne *et al.*, 1992). In both cases, because of the similarity of the *P* waveforms for each pair of events, and taking into account the simplicity of the *SH* waves, the authors concluded that

the complexities in the P waveforms were caused by near-source, crustal structure effects rather than by a complex source process. Boyd and Nábelek (1988), however, were unable to duplicate the waveforms adding low-velocity layers and a high-contrast layer above the Moho to the velocity structure. Byrne *et al.* (1992), on the other hand, were able to improve the fit of the waveforms adding a low-velocity zone to their prescribed velocity model.

It is worth stressing that contrary to the examples mentioned above, the Boca del Tocuyo earthquakes show an anomalously long duration and complexity not only in the P waveforms, but also on the SH and SV signals. Thus the possibility that the complexity of these waveforms is the result of a multiple rupture process was explored.

A Multiple Rupture Process

The source model of the Boca del Tocuyo events was obtained following a similar inversion strategy to that used by Suárez and Nábelek (1990) for the Caracas earthquake of July 30, 1967. First, it was assumed that the main event was caused by a single point source with a long source time function duration of 30 s. The inversion resulted in the average (centroidal) mechanisms indicated on Table 4. The resulting source time function shows that it is composed of three main subevents spaced in time (Fig. 4). A single point source with a long source time function prescribes the same focal mechanism for all subevents. Although the fit of the synthetic waveforms is not yet satisfactory, the resulting three subevents of the mainshock approximately match most of the observed seismograms for about 50 seconds (Fig. 4). A similar conclusion is reached in the case of the largest aftershock, where at least two subevents are needed to model the waveforms.

As a second step, each of the three subevents that resulted from the previous inversion using a single, long source time function was analyzed independently by freeing the parameters related only to a particular subevent. For example, in the case of the first subevent, the time series were inverted within a time frame that included only that particular subevent. After an adequate fit was obtained for this first subevent, the inversion was applied to the time frame corresponding

to the second subevent, and finally to the time window of the third one. Once this stepwise inversion of the waveforms was completed, all parameters were freed and the inversion was allowed to iterate freely to the best fitting solution using the complete waveforms (Figs. 5 and 6). The final results showing the parameters of the subevents of both earthquakes are summarized on Table 4 and Figure 7.

In the case of the mainshock, the second and third subevents triggered 12.4 s and 27.6 s after the origin time. The depths of the subevents decrease from 17.5 km for the first one to 10.8 km for the last. The total seismic moment release (tensor sum) of the mainshock is 2.4×10^{18} Nm, which corresponds to a moment magnitude $M_w=6.2$ (Hanks and Kanamori, 1979). The three subevents composing the mainshock indicate a strike-slip faulting mechanism (Fig. 5). Subevents 1 and 3 are the best resolved because they contribute most of the moment release on the seismograms (Table 4).

For the largest aftershock, the second subevent occurred 27 s after the first one. The depths of the subevents are 11 km and 12 km respectively and the total seismic moment (tensor sum) of the aftershock is 2.9×10^{17} Nm ($M_w=5.6$). The first subevent of the aftershock has a strike-slip-faulting mechanism similar to the mainshock. The second subevent, however, has a normal-faulting mechanism. The focal mechanism of the second subevent is not well resolved because the wavetrains arrive late and within the coda of the first burst of moment release. Nonetheless, in order to validate the result that the fault plane solution of the second subevent of the aftershock did not correspond to a strike-slip mechanism similar to that of the first subevent, several inversions were carried out fixing the initial parameters of the second subevent with a focal mechanism identical to the first subevent. The results of these inversions showed that the fit between the synthetics and observed seismograms was acceptable for *P*-waves, but not for the *SH*-waves. Furthermore, when the initial parameters of the second subevent were freed, the inversion continuously converged to a normal-faulting fault plane solution.

During the inversion, it was attempted to identify the direction of rupture propagation of the Boca del Tocuyo mainshock, based on a potential correlation with the preferential orientation of the aftershocks and with the strike indicated by the average focal mechanism. This was done by

testing whether a directivity pattern was observed in the body waves when the second and third subevents were displaced with respect to the first one. However, no preferred orientation of the rupture could be gleaned from the inversion by allowing the subevents to move relative to one another. The absence of a directivity pattern in the waveforms suggests that the three subevents of the mainshock nucleated very close to one another, probably as a result of episodic slip on the same fault or on neighboring faults.

Discussion

The analysis of the epicentral locations by the single, and calibration-event methods (Dewey, 1971) suggests that the Boca del Tocuyo earthquakes occurred offshore, very close to the coastal towns that were most damaged. The relocation of the largest aftershock with respect to the main event indicates that the aftershock was initiated approximately two km to the NW of the mainshock. Furthermore, the ~60 smaller aftershocks ($m_b < 4.5$) recorded by *FUNVISIS* using a local seismological network were also located at sea, with depths increasing from 0 to 24 km in a NE-SW direction.

The results of the inversion of the bodywaves show that the Boca del Tocuyo earthquakes originated as a result of a multiple rupture process. The complexity of the source caused an anomalously long duration of the body waves of both earthquakes. The duration of the *P* waves of a simple event of that magnitude is, on average, of about 35 s, whereas in the case of the Boca del Tocuyo mainshock it was of ~75 s. Although no local strong motion data are available, the teleseismic observations suggest that intense shaking took place near the epicentral region for over thirty seconds. That strong shaking was produced by the three subevents composing the mainshock, with the second and third subevents triggering about 12 and 28 s after the first one.

The strike-slip focal mechanisms obtained from the inversion of the Boca del Tocuyo mainshock and its largest aftershock are similar to those reported by Dziewonski et al. (1990). The analysis of which nodal plane of the mechanism corresponds to the ruptured fault is important from a tectonic point of view. As mentioned above, no historical or instrumental earthquakes had been reported in this area before the occurrence of the Boca del Tocuyo seismic sequence. Furthermore, recent studies of the active geological features in this region (Barbot et al., 1979; Barbot et al., 1980; Singer *et al.*, 1992) show evidence of a complex tectonic environment, related to the convergence of the major right-lateral, strike-slip fault systems (Boconó, Oca-Ancón, and Morón) and a set of smaller NW-SE oriented conjugate faults (Figs. 1 and 7).

A NW-SE oriented fault plane was selected as the nodal plane of the possible rupture process for the Boca del Tocuyo events based mainly on the depth distribution ($0 < h < 24$ km) of the ~60 smaller aftershocks ($m_b < 4.5$) located by *FUNVISIS* (Singer *et al.*, 1992) (Fig. 2). The depths of these aftershocks increase from NE to SW, suggesting a fault plane dipping to the SW. Furthermore, that fault plane coincides with the orientation of the NW-SE conjugate fault systems that apparently control the shape of the coastline in this region (Fig. 7). The focal mechanism of the Boca del Tocuyo earthquake could indicate right-lateral, strike-slip motion on a NW-SE oriented fault. Several right-lateral, strike-slip faults with a NW-SE orientation have been identified in northwestern Venezuela on both sides of the Peninsula of Paraguáná (Soulas *et al.*, 1987; Singer *et al.*, 1992) (Fig. 1). The correlation of this seismic sequence with a particular fault is difficult because the epicentral area is located at sea in a highly faulted zone.

The occurrence of moderate-sized earthquakes on those conjugate fault systems is important in understanding the tectonic regime in northern Venezuela. As mentioned before, there is an appreciable difference between the rate of motion of the Boconó and Oca-Ancón fault systems and the predicted relative velocity between the Caribbean and South American plates. That difference in motion between those plates is possibly being absorbed by slip on these conjugate fault systems, in a complex volumetric deformation.

Earthquakes with multiple rupture processes seem to be a relatively common occurrence in this complex tectonic environment of northern and western Venezuela. In addition to the earthquakes of Boca del Tocuyo, two more examples of multiple source events have been suggested: the great earthquake of March 26, 1812, and the Caracas earthquake of 1967. On the basis of damage reports, the earthquake of 1812 has been interpreted as consisting of at least two distinct events (Kelleher *et al.*, 1973). On the other hand, the Caracas earthquake of 1967 has been interpreted as the sum of at least three subevents (Rial, 1978; Suárez and Nábelek, 1990). These earthquakes reflect the presence of a complicated regional pattern associated with a wide deformation zone along the Caribbean-South America border.

The liquefaction induced by the Boca del Tocuyo earthquakes appears to be more intense and widespread than expected for earthquakes of that range of magnitudes. Liquefaction occurs in

soils when the pore-water pressure builds up under ground shaking and equals the confining pressure of the saturated and unconsolidated deposits. This produces a loss of the shear strength of the soil (e.g., Ambraseys and Sarma, 1969). This increase of pore pressure may be originated either by a rapid pulse of high stress or by a long train of comparatively weak pulses. In the latter case, liquefaction depends on the continuity and duration of the seismic excitation, both of which allow the pore-water pressure to build up gradually.

It could be speculated that the intensity and areal extent of the observed liquefaction induced by the Boca del Tocuyo events occurred mainly as a result of the local soil conditions, but enhanced by the long and sustained levels of intense shaking produced by the complex rupture process. Furthermore, the sequential initiation and stopping of the rupture process induced by this complex source, probably resulted in anomalously rich high-frequency waveforms. Unfortunately, no local recordings exist to confirm this.

In contrast, on July 12, 1988, a shallow event of magnitude $m_b=5.4$ occurred beneath Lake Maracaibo, in western Venezuela, near several places where soil conditions are very similar to those in Boca del Tocuyo. This event, however, did not produce liquefaction. The reason is perhaps that the 1988 Lake Maracaibo earthquake was a simple event (Malavé, 1992; Malavé and Suárez, 1993), whereas the Boca del Tocuyo earthquakes exhibited an anomalously long duration of the body-wave trains.

Summary and Conclusions

The Boca del Tocuyo earthquake of 1989 ($m_b=5.7$) is one of the largest instrumentally recorded events in western Venezuela. Both historical and instrumental records show a dearth of earthquakes in this coastal area before the seismic sequence of April and May, 1989. The inversion of the P , SH , and SV waves indicates that the source time functions of these two earthquakes are composed of three and two subevents, respectively, distributed over a time span of 30 s. The focal mechanisms of the three subevents of the mainshock show right-lateral, strike-slip faulting at an average depth of 14 km. The focal mechanism of the first subevent of the aftershock indicates strike-slip faulting similar to the fault plane solution of the mainshock. However, the focal mechanism of the second subevent shows tensional dip-slip faulting.

It was not possible to unequivocally identify the direction of rupture propagation using the inversion algorithm. However, the hypocenter distribution of about 60 small aftershocks ($m_b < 4.5$) located by local seismic stations shows a fault plane oriented in NW-SE direction with right-lateral, strike-slip displacement. This orientation coincides with the direction of a fault system which is conjugate to the east-west major fault systems that have been postulated as the current boundary between Caribbean and South American plates.

One may speculate that the intense liquefaction caused by these two earthquakes appears to be a consequence of the presence of water saturated, unconsolidated sediments, enhanced by the long and sustained duration of strong ground shaking induced by the multiple rupture process. Also, the resulting seismic waves near the epicentral area were probably rich in high-frequency content due to the complexity of the source time function.

References

- Ambraseys, N. and S. Sarma (1969). Liquefaction of soils induced by earthquakes. *Bull. Seism. Soc. Am.* 59 (2), 651-664.
- Ambraseys, N. (1988). Engineering Seismology. *Int. J. Earthquake Eng. Struct. Dyn.* 17, 1-105.
- Audemard, F. and F. De Santis (1991). Prospect-pit survey of liquefaction structures induced by recent moderate earthquakes. *Bull. Int. Assoc. Eng. Geol.* 44, 5-16.
- Barbot, J. P., J. Butenko, and J. I. Rodríguez (1979). Geologic and geotechnical analysis of Golfo Triste: its influence on offshore structures and drilling operations. *Congress COPPE/UFRJ*, Rio de Janeiro, 17 pp.
- Barbot, J. P., J. Butenko, E. Espinoza, J. Daza, and G. Malavé (1980). El cuaternario del Golfo de La Vela y su importancia geotécnica para la exploración y explotación petrolera. *Transactions 9th Caribbean Geological Conference*. Santo Domingo, 2, 541-553.
- Boyd, T. and J. Nábelek (1988). Rupture process of the Andean Islands earthquake of May 7, 1986. *Bull. Seism. Soc. Am.* 78 (5), 1653-1673.
- Byrne, D., L. Sykes, and D. Davis (1992). Great Thrust Earthquakes and Aseismic Slip Along the Plate Boundary of the Makran Subduction Zone. *J. Geophys. Res.* 97 (B1), 449-478.
- De Santis, F., C. Beltrán, F. Audemard, A. Fernández, A. Singer, A. Adrianza, L. Montes, M. Lugo, and C. Chacín (1991). Estudio de las manifestaciones de licuefacción de suelo ocurridas en Falcón Oriental durante los sismos de abril y mayo de 1989: aspectos geológicos y geotécnicos. *FUNFISIS*, Caracas, Venezuela.
- Dewey, J. W. (1971). Seismic studies with the method of Joint Hypocenter Determination, Ph.D. Thesis. Univ. of Calif., Berkeley. 164 pp.
- Dziewonski, A. M., G. Ekstrom, J. H. Woodhouse, and G. Zwart (1990). Centroid-moment tensor solutions for April-June 1989. *Phys. Earth Planet. Int.* 60, 243-253.
- Gajardo, E., J. L. Nicolle, B. Castejón, C. Márquez, and M. Urbáez (1986). Modelo de corteza de la Costa Oriental del Lago de Maracaibo. *III Congreso Venezolano de Geofísica*. Caracas, Venezuela, 102-111.

- Hanks, T. and H. Kanamori (1979). A moment magnitude scale, *J. Geophys. Res.* **84**, 2348-2350.
- Herrin, E., E. P. Arnold, B. A. Bolt, G. E. Clawson, E. R. Engdahl, H. W. Freedman, D. W. Gordon, A. L. Hales, J. L. Lohdell, O. Nuttli, C. Romney, J. Taggart, and W. Tucker (1968). 1968 seismological tables for *P* phases, *Bull. Seismol. Soc. Am.* **58**, 1196-1241.
- Jordan, T. H. (1975). The present-day motions of the Caribbean plate, *J. Geophys. Res.* **80**, 4433-4439.
- Kafka, A. and D. Weidner (1981). Earthquake focal mechanisms and tectonic processes along the southern boundary of the Caribbean plate, *J. Geophys. Res.* **86** (B4), 2877-2888.
- Kelleher, J., L. R. Sykes, and J. Oliver (1973). Possible criteria for predicting earthquake locations and their application to major plate boundaries of the Pacific and the Caribbean, *J. Geophys. Res.* **78**, 2547-2585.
- Malavé, G. (1992). Inversión de ondas de volumen de algunos sismos importantes del noroccidente de Venezuela: relación con la tectónica regional. *M.Sc.Thesis*, Universidad Nacional Autónoma de México, México D.F., México, 93 pp.
- Malavé, G. and G. Suárez (1993). Recent seismicity ($m_b \geq 5.4$) in western Venezuela: regional tectonic implications. *Second International Symposium on Andean Geodynamics*, Oxford, England, 111-114.
- Malaver, A. (1990). El sismo de Boca del Tocuyo del 30 de abril de 1989, *Memorias de las Segundas Jornadas de Ingeniería Sísmica*, Caracas, Venezuela.
- Minster, J. B. and T. H. Jordan (1978). Present-day plate motions, *J. Geophys. Res.* **83**, 5331-5334.
- Molnar, P. and L. Sykes (1969). Tectonics of the Caribbean and Middle America Regions from Focal Mechanisms and Seismicity, *Geol. Soc. Am. Bull.*, **80**, 1639-1684.
- Nábelek, J. L. (1984). Determination of earthquakes source parameters from inversion of body waves. Ph.D. Thesis. Massachusetts Institute of Technology, Cambridge. 361 pp.
- Rial, J. A. (1982). The Caracas, Venezuela, earthquake of July 1967; a multiple source event, *J. Geophys. Res.* **83**, 5405-5415.

- Schubert, C. (1982). Neotectonics of Boconó fault, western Venezuela. *Tectonophysics* **85**, 205-220.
- Singer, A., F. Audemard, C. Beltrán, J. A. Rodríguez, F. De Santis, A. Adrianza, C. Chacín, M. Lugo, J. Mendoza, and C. Ramos (1992). Actividad tectónica cuaternaria y características sismogénicas de los sistemas de fallas de Oca-Ancón (tramo oriental), de la península de Paraguaná y región de Coró y de la costa nororiental de Falcón, *FUNVISIS*, Caracas, Venezuela.
- Sipkin, S. and R. Needham (1991). Moment tensor solutions estimated using optimal filter theory: global seismicity, 1988-1989, *Phys. Earth Planet. Int.* **67**, 221-230.
- Soulas, J. P. (1986). Neotectónica y tectónica activa en Venezuela y regiones vecinas, *Memorias VI Congreso Geológico Venezolano X*, Caracas, Venezuela, 6639-6656.
- Soulas, J. P., C. Giraldo, D. Bonnot, and M. Lugo (1987). Actividad cuaternaria y características sismogénicas del sistema de fallas Oca-Ancón y de las fallas de Lagarto, Urumaco, Río Seco y Pedregal. Afinamiento de las características sismogénicas de las fallas de Mene Grande y Valera, *FUNVISIS*, Caracas, Venezuela.
- Stein, S., C. DeMets, R. G. Gordon, J. Brodholt, D. Argus, J. F. Engeln, P. Lungren, C. Stein, D. A. Wiens, and D. F. Woods (1988). A test of alternative Caribbean plate relative motion models, *J. Geophys. Res.* **93**, 3041-3050.
- Suárez, G. and J. Nábelek (1990). The 1967 Caracas Earthquake: Fault Geometry, Direction of Rupture Propagation and Seismotectonic Implications. *J. Geophys. Res.* **70**, 5065-5074.
- Sykes, L., W. R. McCann, and A. L. Kafka (1982). Motion of Caribbean plate during last 7 million years and implications for earlier Cenozoic movements, *J. Geophys. Res.* **87**, 10656-10676.

Table 1
Focal Parameters of the Boca del Tocufo Earthquake and its Largest Aftershock

Event	Source	Lat °N	Lon °W	Depth km	m_b	Strike deg	Dip deg	Slip deg	M_0 10^{18} Nm
Apr. 30, 1989	<i>ISC</i>	10.99	68.31	20.0	5.7	--	--	--	--
	<i>NEIC</i>	10.96	68.33	20.0	5.9	242	36	147	0.81
	<i>FUNVISIS</i>	11.10	68.18	11.1	5.7	75	45	-149	--
	<i>CMTS</i>	10.88	68.08	15.0	--	166	62	-168	0.98
	<i>This study</i>	11.01	68.25	14.0*	--	162*	82*	-177*	3.50*
May 4, 1989	<i>ISC</i>	11.07	68.26	10.0	5.4	--	--	--	--
	<i>NEIC</i>	11.04	68.27	16.0	5.4	--	--	--	--
	<i>FUNVISIS</i>	11.14	68.21	13.6	5.0	75	45	-149	--
	<i>CMTS</i>	10.96	68.42	15.0	--	145	51	-174	0.21
	<i>This study</i>	11.06	68.23	12.0*	--	130*	90*	-172*	0.24*
	<i>JHD89</i>	10.98	68.34	17.4	--	--	--	--	--

CMTS: Centroidal moment tensor solution (Dziewonski *et al.*, 1990).

- Best double-couple of the moment tensor sum of the subevents. Parameters of the subevents are resumed on Table 4.

Table 2
Seismic Stations Used in the Inversion of Boca del Tocuayo Mainshock

Station	Azimuth deg	Epicentral Distance °	Wave Type	Network
<i>KEV</i>	20.5	81.7	<i>P, SH</i>	<i>DIWSSN</i>
<i>KONO</i>	31.0	74.5	<i>P, SV, SH</i>	<i>ASRO</i>
<i>GRFO</i>	41.4	75.0	<i>P, SV, SH</i>	<i>SRO</i>
<i>TOL</i>	50.9	63.3	<i>P, SV, SH</i>	<i>DIWSSN</i>
<i>BCAO</i>	86.3	86.1	<i>P, SV, SH</i>	<i>SRO</i>
<i>ZOBO</i>	179.6	27.1	<i>P, SH</i>	<i>ASRO</i>
<i>ANMO</i>	310.8	42.1	<i>SV, SH</i>	<i>SRO</i>
<i>LON</i>	319.0	57.4	<i>P, SV, SH</i>	<i>DIWSSN</i>
<i>COL</i>	334.4	75.7	<i>P</i>	<i>DIWSSN</i>
<i>SCP</i>	345.8	30.9	<i>P, SV, SH</i>	<i>DIWSSN</i>
<i>GAC</i>	351.3	35.2	<i>P, SV, SH</i>	<i>SRO</i>

Table 3
Seismic Stations Used in the Inversion of Boca del Tocuyo Aftershock

Station	Azimuth deg	Epicentral Distance °	Wave Type	Network
<i>KONO</i>	31.0	74.4	<i>SH</i>	<i>ASRO</i>
<i>GRFO</i>	41.4	74.9	<i>SH</i>	<i>SRO</i>
<i>ANTO</i>	49.1	91.3	<i>SH</i>	<i>SRO</i>
<i>BCAO</i>	86.3	86.0	<i>SH</i>	<i>SRO</i>
<i>ZOBO</i>	179.7	27.1	<i>P</i>	<i>ASRO</i>
<i>ANAO</i>	310.7	42.1	<i>P, SH</i>	<i>SRO</i>
<i>LON</i>	319.0	57.4	<i>SH</i>	<i>DIWSSN</i>
<i>SCP</i>	345.7	30.8	<i>P</i>	<i>DIWSSN</i>
<i>GAC</i>	351.3	35.2	<i>P, SH</i>	<i>SRO</i>

Complex Source Characteristics of the 1989 Boca del Tocuyo Earthquakes

Table 4

Source Parameters of the Boca del Tocuyo Earthquakes Determined by the Inversion of Long-Period Body Waves

Seismograms

Event	Subevent	Strike deg	Dip deg	Slip deg	Depth km	M_0 10^{18} Nm	Delay sec	Duration sec
Apr. 30, 1989	SSTF ¹	162±2	78±1	-178±1	17.0±0.4	1.32±0.06	-	4.00±0.04
	1	162±2	77±1	-179±2	17.5±0.4	1.20±0.06	-	4.00±0.05
	2	159±8	41±4	-161±12	12.5±2.0	0.25±0.04	12.4±0.5	4.00±0.16
	3	164±2	83±1	-174±1	10.8±0.7	0.98±0.06	27.6±0.2	4.00±0.06
	Average ²	162±1	82±1	-177±1	14.3±0.3	3.5	-	30
May 4, 1989	SSTF ¹	133±2	83±1	-172±1	10.2±0.7	0.17±0.01	-	4.00±0.04
	1	137±1	76±1	-172±1	11.0±0.5	0.15±0.01	-	4.00±0.03
	2	178±2	56±1	-72±2	12.4±0.6	0.14±0.01	26.9±0.2	4.00±0.04
	Average ²	130±2	90±2	-172±1	12.0±1.4	0.24	-	30

¹SSTF: Best double-couple using a short source time function.

²Average: Best double-couple of the moment tensor sum of the subevents.

Figure Captions

Figure 1. Major active fault systems in northern Venezuela (after Singer *et al.*, 1992; Soulas, 1986; Soulas *et al.*, 1987). The solid triangle shows the epicentral location of the Boca del Tocuyo seismic sequence, where a maximum intensity of VII (MMI) was assigned by De Santis *et al.* (1991). The opposing arrows indicate the relative motion of the faults. Bathymetry is in meters.

Figure 2. Epicentral locations determined by the *ISC* (triangle), *NEIC* (square), *FUNVISIS* (diamond), Dziewonski *et al.* (1990) (cross; mainshock is offshore), and this study (circle) for the Boca del Tocuyo main event (solid symbols) and its largest aftershock (open symbols). The uncertainties in the epicentral locations determined in this study are shown as 90% confidence ellipses. The hatched circle indicates the relocation of the largest aftershock using the *JHD* method of Dewey (1971). The location of the smaller aftershocks ($m_b < 4.5$) are shown for depths ranging from 0 to 9 km (open circles) and from 10 to 24 km (solid circles). The black quadrants in the focal mechanisms indicate compressional arrivals projected in a lower hemisphere projection. The open and solid circles in the mechanisms correspond to the position of the *T* and *P* axes on the focal sphere, respectively. The dashed lines are active fault traces (Singer *et al.*, 1992). Solid lines at sea are bathymetric curves in meters.

Figure 3. Results of the simultaneous inversion of the long-period (top) P , (middle) SH , and (bottom) SV waves of the Boca del Tocuyo mainshock using a single point source with a source time function duration of 4 s. The theoretical seismograms (dashed lines) match well only the first part of the observed waveforms (solid lines) at all the stations. The focal mechanisms are shown in a lower hemisphere projection. The hatched areas in the *P* waves fault plane solution represent compressional first motion. Amplitudes of the waveforms are normalized to an instrumental magnification of 1500 and a geometrical spreading corresponding to an epicentral distance of 40° .

Figure 4. Comparison between long-period theoretical seismograms (dashed lines) and observed (top) P , (middle) SH , and (bottom) SV waves for the Boca del Tocuyo mainshock, using a point source with a single, long source time function (same focal mechanism for all resulted subevents) with a duration of 30 s. The fit is better than for the shorter source time function (Fig. 3) and shows that at least three point sources are present in the rupture process. Other symbols and amplitude normalization are the same as on Figure 3.

Figure 5. Results of the simultaneous inversion of the long-period body waves of the Boca del Tocuyo mainshock using three point sources (subevents): a) P waves; b) SH waves; and c) SV waves. The focal mechanism of the first subevent is shown together with the theoretical seismograms (dashed lines) and observed waveforms (solid lines). The fault plane solutions of the second (left) and third (right) subevents are shown at the bottom. The symbols and amplitude normalization are the same as on Figure 3.

Figure 6. Results of the simultaneous inversion of the long-period body waves P and SH for the Boca del Tocuyo aftershock using two point sources (subevents). The focal mechanism of the first subevent is shown together with the theoretical seismograms (dashed lines) and observed waveforms (solid lines). The fault plane solution of the second subevent is shown to the right of the first one. Other symbols and amplitude normalization are the same as for Figure 3.

Figure 7. Summary of focal mechanisms obtained from the long-period body waves inversion of the Boca del Tocuyo main event ($M1$, $M2$, and $M3$ are the mechanisms of the three subevents) and for the largest aftershock ($A1$ and $A2$). The solid quadrants in the fault plane solutions indicate compressional arrivals. The open and solid circles in mechanisms correspond to the position of the T and P axes, respectively, on the focal sphere. The dashed lines are possible active faults in this region (after Singer *et al.*, 1992).

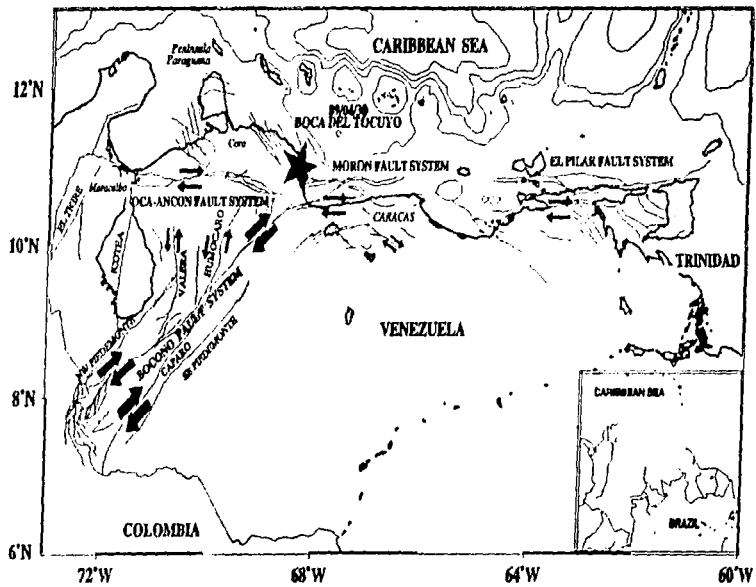


Figure 1

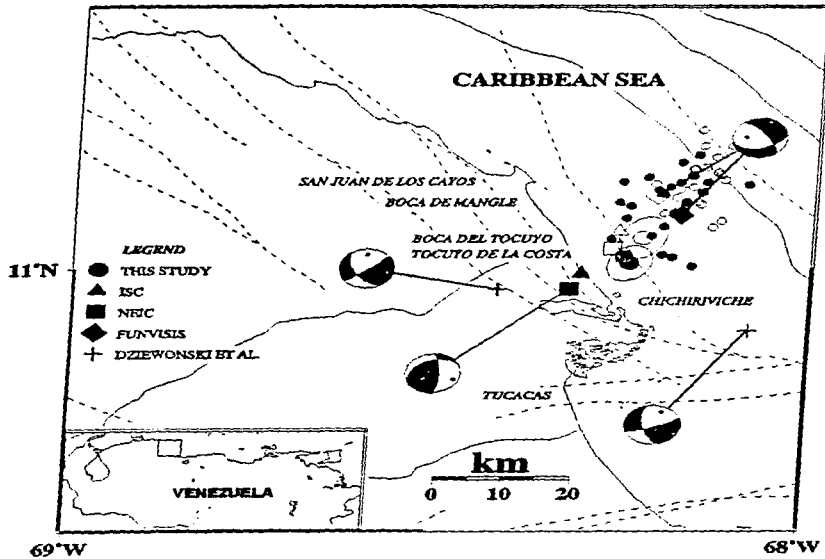


Figure 2

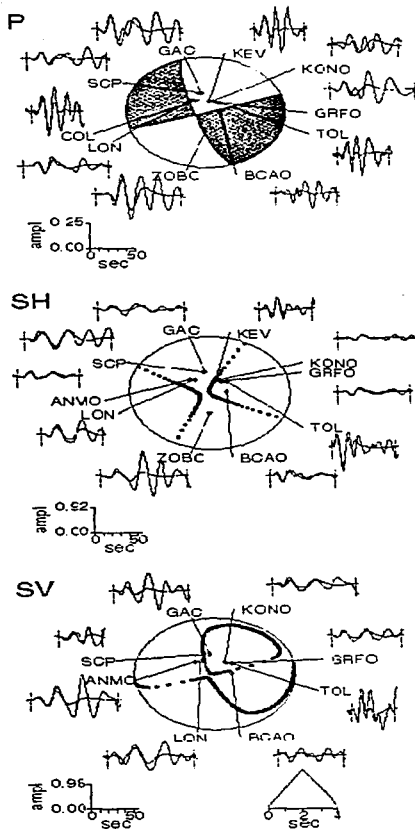


Figure 3

Complex Source Characteristics of the 1989 Boca del Tocuyo Earthquakes

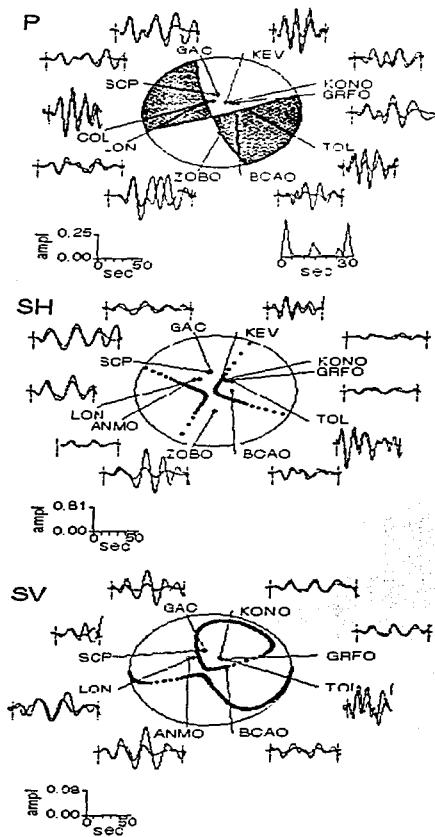


Figure 4

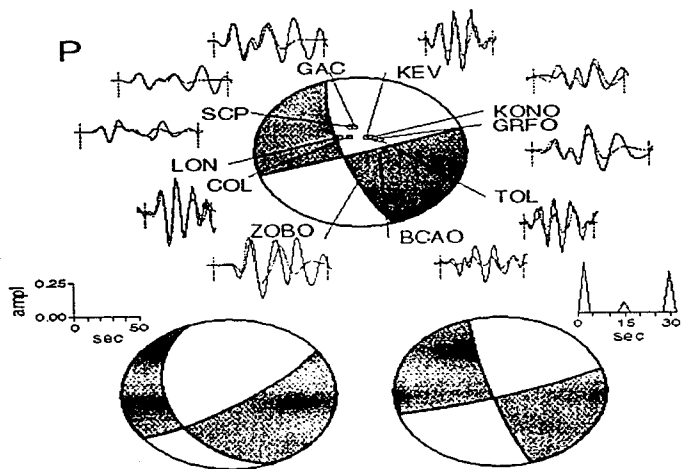


Figure 5a

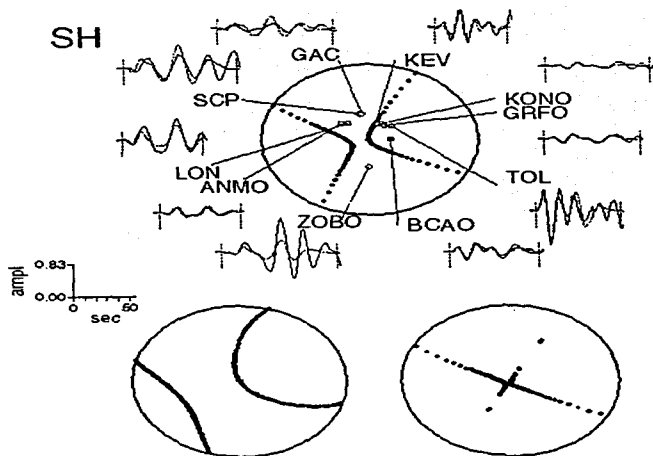


Figure 5b

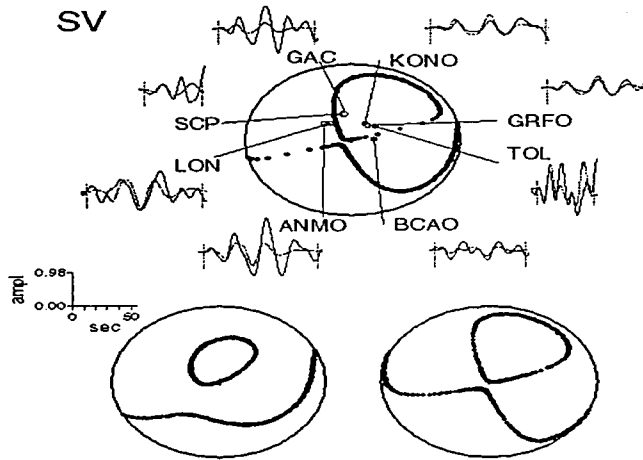


Figure 5c

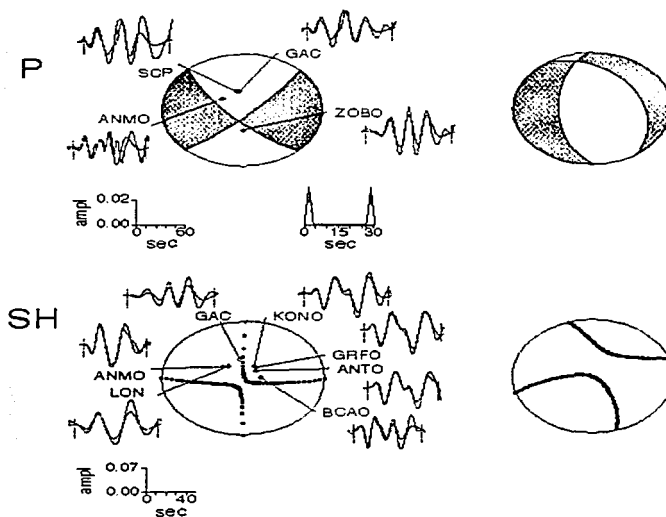


Figure 6

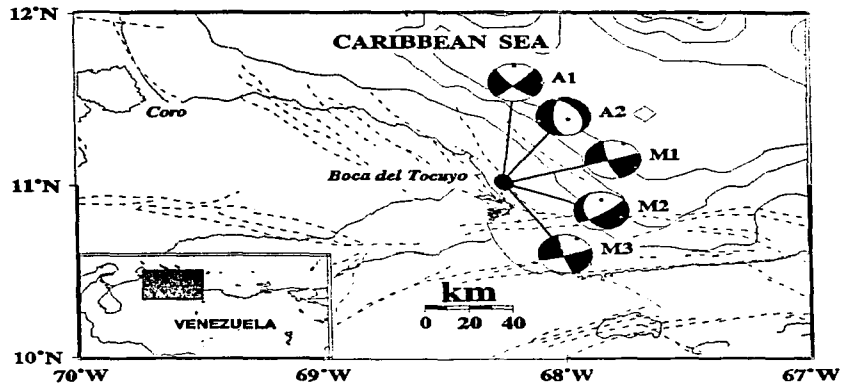


Figure 7

**IV. Deformación cortical y sismicidad superficial reciente al oeste de Venezuela:
implicaciones tectónicas regionales**

**Crustal deformation and recent shallow seismicity
in western Venezuela: regional tectonic implications**

Gustavo Malavé¹ and Gerardo Suárez

Instituto de Geofísica, Universidad Nacional Autónoma de México, D.F., México

¹ also at INTEVEP, S.A. Apartado Postal 76343, Caracas 1070A, Venezuela

Abstract. The source parameters of shallow, moderate-sized earthquakes that have occurred in western Venezuela from 1964 to 1994 were evaluated to understand the complex tectonic environment in this region and its relationship to the interaction between the Caribbean and South American plates. The results indicate that most of the earthquakes nucleated on secondary fault systems, instead of on the major fault systems of Boconó and Oca-Ancón. The average direction of the *P*-axes clearly divides the region of western Venezuela into two zones: north and south of latitude 10°N. In the northern area, the *P*-axes rotate from a NW-SE to NNE-SSW direction; whereas in the southern zone, the *P*-axes are approximately oriented E-W. The determination of the compressional strain rate in the overall region over 30-years period of time is $5.9 \times 10^{-10} \text{ yr.}^{-1}$ and is oriented almost N-S. According to the seismic activity on the secondary faults, the border between the Caribbean and South American plates may be distributed over a wide zone of deformation instead of a major

single fault. The correlation between the left-lateral, strike-slip faults trending roughly NNE-SSW, the focal mechanisms and the Quaternary geological data suggest that the kinematics of the faulting pattern behave as a bookshelf faulting mechanism.

Introduction

The location and the nature of the border between the Caribbean and South American plates in western Venezuela has been a source of controversy for several years and is crucial in understanding the tectonics of the Caribbean region (Figure 1). The motion on the southeastern Caribbean plate boundary is presumably accommodated mainly by the major right-lateral, strike-slip faults of El Pilar and Morón. Towards the west, however, the continuation of the plate boundary is unclear. The Boconó fault system, also characterized by right-lateral strike-slip faulting, has been postulated to be the current boundary between these two plates in western Venezuela [e.g., Dewey, 1972; Schubert, 1982; Soulas, 1986]. Other workers, however, have also proposed the Southern Caribbean Deformed Belt as the limit between plates and consider the Boconó fault system as evidence of intraplate deformation [e.g., Kellogg and Bonini, 1982; 1985] (Figure 1).

Large earthquakes have occurred in this region during the last four centuries that are apparently related to the Boconó fault system [Centeno-Grau, 1940] (Figure 2). The rate of motion between the Caribbean and South American plates is relatively low (~ 2 cm/yr), and this probably implies long recurrence periods for large earthquakes. Moreover, the occurrence of moderate-size events ($5.4 \leq m_b \leq 6.2$) is sparse, rendering more difficult the interpretation of the tectonic regime and seismic hazard in this zone.

Several previous studies have been carried out to understand the tectonic deformation in western Venezuela. Some of these studies were based on the evaluation of the seismicity recorded either locally by temporary networks or by using teleseismic information, neotectonic field evidence, and focal mechanisms determined from first motion data and from Rayleigh-wave inversion. For example, Dewey [1972] relocated all the teleseismically recorded seismicity that occurred in western Venezuela from 1930 to 1970 and evaluated 540 days of data obtained with local seismographs near the Boconó fault. Moreover, he determined the fault plane solutions of five shallow events, based on the polarities of first arrivals (Table 1) and concluded that the Boconó fault zone is seismically active. Kafka and Weidner [1981] analyzed the same five focal

mechanisms studied by *Dewey* [1972], using a moment-tensor inversion of the Rayleigh waves. Their resulting focal mechanisms suggest right-lateral, strike-slip faulting parallel to the Boconó fault. Table 1 and Figure 3 show compiled fault-plane solutions from *Dewey* [1972], *Kafka and Weidner* [1981], *Pérez and Aggarwal* [1980], *Pennington* [1981], *Dziewonski et al.* [1985; 1987a, 1987b, 1987c; 1987d; 1988a, 1988b; 1988c; 1989; 1990, 1992], and *Sipkin and Needham* [1991].

Besides the right-lateral, strike-slip Boconó and Oca-Ancón fault systems, there are others faults in western Venezuela that may be capable of generating earthquakes of moderate size [*Soulas*, 1986] (Figure 2). Some of them are oriented NE-SW, parallel to the Boconó fault (e.g., Caparo, NW Piedemonte, SE Piedemonte); other faults, however, show a NNE-SSW orientation and splinter off the Boconó fault (e.g., Valera, Carache, Humocaró, Icotea). Moreover, other conjugate faults that are oriented mainly in a NW-SE direction have been identified either on land and at sea in northern Venezuela [*Barbot et al.*, 1979; 1980] and several moderate-magnitude events have occurred in this region recently, but only a few of them have been studied in detail.

The hypocenters were evaluated by using a single-event location method [*Dewey*, 1971]. The focal parameters were obtained from the inversion of body waves recorded at teleseismic distances [*Nábelek*, 1984]. In most cases, long-period body waves were used in the inversion scheme. However, some events were analyzed through the waveform inversion of short-period *P*-waves because, due to their small magnitude, the signal-to-noise ratio on the long-period seismograms was too low. The motivation for recomputing the previously-determined focal mechanisms was to use a more reliable and powerful methodology than those utilized by previous workers.

Consequently, we combined the Quaternary geological data (e.g., active faults, rate of motion) with the source parameters of the recent shallow seismicity, in an effort to understand the complex tectonic deformation occurring in this zone of interaction between two major plates and its relationship with the different sets of fault systems mentioned above. In total, the focal parameters of fourteen earthquakes of magnitude $m_b \geq 5.4$ that occurred in western Venezuela since 1964 were analyzed, and then correlated with the mapped active faults. On the basis of that correlation, a kinematic model was proposed to explain the mechanism controlling the tectonic environment in western Venezuela.

Tectonics and Seismicity of Western Venezuela

Tectonic Setting

Several alternative models have been proposed to explain the motion of the Caribbean relative to its neighboring plates [Jordan, 1975; Minster and Jordan, 1978; Stein et al., 1988; Sykes et al., 1982]. In general, these different models conclude that the Caribbean plate has a low absolute velocity in a hot-spot reference frame, and that it is moving in a south-southwest direction with respect to the Cocos plate, and predominantly eastward with respect to both the North and South American plates [e.g., Dewey and Suárez, 1991]. However, the models differ in the relative plate velocities and in the direction of plate motion.

The southeastern Caribbean plate boundary is generally considered to be a right-lateral, strike-slip fault system. However, the relative motion between the Caribbean and South American plates does not seem to be concentrated along a single fault system as a transform fault. Apparently, the motion is distributed over a wide zone of deformation along the Boconó, Morón, and El Pilar fault systems [e.g., Soulas, 1986] (Figure 2).

Major Active Faults in Western Venezuela

The major active faults in central and western Venezuela are the Morón, Boconó, and Oca-Ancón right-lateral, strike-slip fault systems (Figure 2). These faults have been well studied by marine high-resolution seismic profiles and by neotectonic field works onshore.

The Morón fault zone presumably defines the plate boundary between the Caribbean and South American plates in north central Venezuela (Figure 2). It is a system of en-echelon, right-lateral strike-slip faults oriented east-west [Schubert and Krause, 1984; Soulas, 1986]. It has been suggested that during the earthquake of 26 March 1812, in addition to slip on the Boconó fault, a segment of the Morón fault zone may have been involved in the rupture [Dewey and Suárez, 1991]. Also, the Caracas earthquake of 30 July 1967 probably occurred on one of these east-west, strike-

slip faults [Molnar and Sykes, 1969]. Rial [1978] originally proposed a north-south fault orientation for the source of the Caracas earthquake on the basis of modeling *P* and *S* waveforms. Suárez and Nábelek [1990], however, showed that an east-west fault matches the *P* and *S* waveforms better and agrees with the observed intensity data and the location of aftershocks.

The Oca-Ancón fault system shows right-lateral, strike-slip movement from the Paleocene to Pliocene times [e.g., Vásquez and Dickey, 1972; Soulas *et al.*, 1987]. Geologic data suggest that the Pliocene average rate of motion of the Oca-Ancón fault system was higher than 6.4 mm/yr. [Soulas *et al.*, 1987]. However, the present rate of motion on the Oca-Ancón fault system is in the range of 2.5 to 4.0 mm/yr. [Soulas *et al.*, 1987]. This rate of motion is about one order of magnitude lower than the predicted relative velocity between the Caribbean and South American plates. Also, no large earthquakes have been associated with this fault during this century.

The Boconó fault system supposedly accommodates an important fraction of the displacement between the undeformed interiors of the Caribbean and South American plates [Schubert, 1982]. Slip rates of the Boconó fault, measured from the offset of Pleistocene moraines, range from 0.3 cm/yr. to 1.4 cm/yr. [e.g., Schubert, 1982; Soulas, 1986]. Aggarwal *et al.* [1983] postulated that the Venezuelan Andes represent the border between the Caribbean and South American plates, and that they are the result of the oblique collision between these two lithospheric plates. Aggarwal *et al.* [1983] also suggested that the present movement observed in the Boconó fault system began probably only since the Pliocene or Pleistocene. They suggested that before that, the border between the Caribbean and South American plates was a convergent margin where the Caribbean lithosphere was being subducted below the South American plate. The last great earthquake ($M_s=7.8$) on the Boconó fault zone occurred on 26 March 1812 [Centeno-Grau, 1940; Grases, 1980]. According to Soulas [1985], the lower velocity observed on the southwest segment of the Boconó fault takes place because the Caparo fault to the south, absorbs a fraction of the right-lateral, strike-slip motion.

Data and Methodology

Hypocentral Relocation

The hypocenters of the events studied here were recalculated utilizing the single-event method (*SE89*) of Dewey [1971], and both the *ISC* (International Seismological Centre) and the *NEIC* (National Earthquake Information Center) earthquake databases. This was done in an effort to reduce the errors in the hypocentral locations determined by *ISC* and *NEIC*. For this purpose, readings showing high residuals were filtered out in order to have a better quality control over the stations listed in the catalogs. In general, the epicentral locations determined here are similar to those reported by *ISC* and *NEIC* (Table 1). For most events, these latter epicenters are in most events within the 90% confidence ellipses estimated by *SE89*. The focal depths obtained from the single-event method were used as a priori information in the inversion scheme.

Body-Wave Inversion

The focal mechanism, depth, and seismic-moment of the earthquakes studied here were analyzed through the inversion of body waves recorded teleseismically by the World-Wide Standardized Seismograph Network (*WWSSN*) and/or by the Global Digital Seismograph Network (*GDSN*). In most cases, long-period body waves were used in the inversion scheme. However, due to a low signal-to-noise ratio in long-period seismograms of several smaller events, the short-period *P*-waves were inverted. Only seismograms of stations within an epicentral distance range of 27 to 90 were included in the inversion. Within this distance range, the Green's functions for a source embedded in a layered earth are simple to calculate and can be accurately estimated [e.g., *Nábelek*, 1984].

The long-period seismograms were high-pass filtered with a cut-off period of 60 s in order to remove long-period noise. The analog records were hand-digitized with a sampling rate of 0.5 s. The short-period seismograms were high-pass filtered with a cut-off period of 2.5 s. In general, the

crustal structure in the source region and below the recording stations was assumed to be a half-space with a compressional wave velocity of 6 km/s, a Poisson ratio of 0.25, and a density of 2.75 g/cm³. The anelastic attenuation along the propagation path was parameterized for the long-period body waves using a $t^* = 1$ s for P waves, and a $t^* = 4$ s for SH and SV waves. In the case of short-period P -waves, the inversions were performed to fit only the shape of the waveforms. A single point source with a variable source-time function duration was used in the inversion scheme.

Although this procedure is discussed in detail by *Nábelek* [1984], the method may be explained briefly as follows. According to the size of the earthquake, the source time function is parameterized as a single point source or as an event composed of several point sources (subevents) separated in time and space. For each subevent, the model parameters include the focal mechanism (strike, dip, and rake), centroidal depth, seismic moment, source time function, and the relative location and time delay of each subevent with respect to the first one. Each source time function is allowed to take an arbitrary shape. Theoretical seismograms are iteratively matched to the observed seismograms using a least squares criterion until a prescribed variance reduction is achieved.

Focal Mechanisms and their Correlation with Active Faults

The focal mechanisms obtained in this study and by previous workers in western Venezuela are summarized in Table 1 and Figures 3 and 4. In order to understand the relationship between the seismicity and the main tectonic features, these fault-plane solutions were correlated to the mapped active faults of the region. This correlation between the Quaternary geological features and the focal mechanisms will be the basis to determine the average, regional orientation of the stress field and suggest a kinematic tectonic model of this region. The main characteristics and the results of the formal inversion achieved in this study are shown in Table 2 and Appendix.

Boconó Fault System

During the last 30 years, only the 19 July 1965 earthquake (event 1) appears to take place on the Boconó fault system, indicating a right-lateral, strike-slip focal mechanism. Due to the magnitude of this event (*ISC*: $m_b=5.4$; *NEIC*: $m_b=5.3$), the signal-to-noise ratio on the long-period seismograms is relatively low. Nevertheless, several *P*, *SH*, and *SV* waves were used to perform the inversion and constrain the focal depth and the fault-plane solution (see Appendix). The focal mechanism resulting from the inversion agrees in general with those solutions determined by *Dewey* [1972] and by *Kafka and Weidner* [1981] (Figure 3). The resulting focal depth is 14 km. The mechanism suggests a trend of approximately N38E in agreement with the Boconó fault.

Oca-Ancón Fault System

Along its whole length of ~500 km, from western Colombia to Golfo Triste in Venezuela, there is little seismic activity directly correlated to the Oca-Ancón fault system. To the west of longitude 69°W, no clear seismic evidence is shown and to the east of that longitude, only the earthquake that occurred on 19 May 1970 (event 6) may be an indication of seismic activity on the Oca-Ancón fault system (Figures 3 and 4).

The epicenter of the earthquake of 20 October 1969 ($m_b=5.7$) (event 4) is located about 30 km south of the Oca-Ancón fault system and approximately 25 km west of El Tigre fault (Figure 3). Dewey [1970] suggested that this event may have occurred on the Oca fault. Later, Pennington [1981] obtained a mainly tensional focal mechanism for this earthquake and interpreted it as the result of a complicated local stress pattern near the southern Caribbean margin. The results obtained here for the event of 20 October 1969 (Figure 4) show a strike-slip fault plane solution that may be correlated either to the right-lateral, strike-slip motion of the Oca-Ancón fault system [e.g., Vásquez and Dickey, 1972; Soulas *et al.*, 1987] or to the left-lateral, strike-slip movement of the El Tigre fault [Rod, 1956].

Another earthquake occurred near the Oca-Ancón fault system on 18 July 1986 ($m_b=5.8$) (event 18) (Figure 4). The inversion of the *P*, *SH*, and *SV* waves show a shallow (7 km) reverse-faulting focal mechanism, with nodal planes trending approximately in a NE-SW direction (see Appendix). The fault plane solution obtained in this study agrees with the mechanism determined by Dziewonski *et al.* [1987d]. Due to its focal mechanism, it is not clear whether this event originated on the Oca-Ancón fault system. Nevertheless, the trend of the *P*-axis on the source mechanism (328°) presents an orientation similar to the compressive field currently acting over the Oca-Ancón fault system.

The event of 19 May 1970 (event 6) may be correlated to the Oca-Ancón fault system (Figure 3). Unfortunately, due to its low magnitude ($m_b=5.1$), a formal teleseismic, body-wave inversion to determine its focal mechanism was not possible in this study. Furthermore, an attempt to obtain a fault plane solution from first-motion polarities was unsuccessful. Dewey [1972], from first-motion data, determined for this event a right-lateral, strike-slip focal mechanism that could correspond to the relative movement described for that fault. Kafka and Weidner [1981], however, obtained a mechanism different to that estimated by Dewey [1972] (event 6). There are no arguments to define at this point which mechanism is correct, since there are other conjugate faults striking roughly NW-SE in the region that may agree with either mechanism.

Caparo Fault

The Caparo fault is one of the most seismically active features in the region during the last three decades. According to *Soulas* [1985], this fault plays an important role in absorbing a large fraction of the Caribbean-South American relative movement. The earthquake of 5 May 1979 (*JSC*: $m_b=5.4$; *NEIC*: $m_b=5.6$) (event 12) was generated apparently on this fault. Because of the low magnitude of the event and the time period when it occurred, only the *P*, *SH*, and *SV* waves recorded in three digital teleseismic stations were available. The inversion scheme was then performed solely to fit the shape of the waveforms (see Appendix). The right-lateral, strike-slip focal mechanism resulting from the inversion agrees with the relative motion of the Caparo fault described by *Soulas* [1985].

There are two other earthquakes that probably nucleated on the southwestern extremity of the Caparo fault: the 27 January 1970 and the 4 July 1982 earthquakes (events 5 and 16) (Figure 4). The focal mechanisms of both earthquakes, determined using short-period *P*-waves, also show right-lateral, strike-slip-faulting (see Appendix). *Pérez and Aggarwal* [1980] reported a composite fault-plane solution that corresponds to a northeast-trending reverse fault. However, the focal mechanisms obtained in this study for the earthquakes of 27 January 1970, 5 May 1979, and 4 July 1982 indicate right-lateral, strike-slip motion on the Caparo fault trending between 29° and 46°, and with depths ranging from 11 km to 17 km.

SE Piedemonte Fault

The earthquakes of 5 March 1975 and 11 December 1977 (events 7 and 9) are apparently related to the SE Piedemonte fault. *Pennington* [1981] proposed that the northern Andes is part of a separate crustal block that is being compressed and underthrust from the east by the South American plate. Nevertheless, both focal mechanisms (see Appendix) show reverse faulting instead of the expected low-angle faulting that would reflect the underthrusting indicated by *Pennington* [1981]. Also, their nodal planes trend approximately in a N-S direction instead of the NE-SW

mapped-fault direction, and dip ~ 45 to the west (Figure 4). The fault-plane solution determined by Pérez and Aggarwal [1980] for the earthquake of 5 March 1975 shows pure reverse-faulting trending $N43^\circ E$.

NNE-SSW Secondary Fault System

Humocaro fault. One of the more recent earthquakes of magnitude $m_b \geq 5.4$ in western Venezuela occurred on 17 August 1991 (event 22). Both, this earthquake and that of 5 April 1975 (event 8) ($m_b = 5.5$), appear to have nucleated on the Humocaro fault, a NNE-SSW left-lateral, strike-slip fault (Figure 4). The recent seismic activity of this fault is appreciable. Besides these two moderate-sized events analyzed here, another earthquake ($m_b = 5.2$) (event 17) occurred on 14 June 1984, whose focal mechanism was determined by *Dziewonski et al.* [1985].

The results from the inversion of the 5 April 1975 and the 17 August 1991 earthquakes (events 8 and 22) show fault-plane solutions that correspond to left-lateral, strike-slip faulting. The difference in the orientation of the fault planes between the event of 5 April 1975 (NNE-SSW) and the earthquakes of 14 June 1984 (event 17) [*Dziewonski et al.*, 1985] and 17 August 1991 (NNW-SSE) apparently reflects changes of direction in the Humocaro-fault trace (Figures 3 and 4). The event of 5 April 1975 probably nucleated on the northern segment of the fault, whereas the two other earthquakes were generated on the southern part of the fault. The reason of this change in the trend of the Humocaro fault is discussed below.

Icotea fault. On 12 July 1988 ($m_b = 5.4$) (event 19), a predominantly tensional event occurred beneath Lake Maracaibo (see Appendix and Figure 4). The structural pattern in this area is relatively well known from the oil exploration efforts undertaken in the past 40 years. Unfortunately, the epicenter of this earthquake lies on a broad fault system, making it difficult to correlate it with a specific fault. However, the regional trend in Lake Maracaibo shows several en-echelon, left-lateral strike-slip faults oriented in a N-S direction and pull-apart basins developing

between the faults. Presumably, this event beneath Lake Maracaibo was associated with one of these pull-apart basins.

Faulting in the Southwestern Terminus of the Boconó-Caparo Fault System

The southwestern region of the study area is the most active from a seismic point of view. Besides the two events described above that were possibly originated on the southwestern extremity of the Caparo fault (the 27 January 1970 and the 4 July 1982 events), several earthquakes have nucleated in this region, including the recent 31 May 1994 event of magnitude 6.1 (m_b). In this area, the Boconó fault system sharply changes direction and turns to the south, modifying its style of deformation to almost purely reverse faulting with an important component of left-lateral, horizontal displacement [Soulas, 1985] (Figures 2 and 3). The complexity of this zone of deformation is demonstrated by the higher rate of seismicity relative to the northeastern area and the diversity of focal mechanisms obtained from the inversion.

The event of 31 May 1994 (event 24) is one of the larger earthquakes in Venezuela in the last thirty years. The focal mechanism of the mainshock obtained from the inversion of P and SH waves show reverse faulting trending roughly in a N-S direction (Figure 4). This earthquake induced an aftershock of magnitude 5.6 (m_b) a few hours later. The fault-plane solution of this aftershock (event 25) determined by *Dziewonski et al.* [quick solution] shows a mechanism similar to that of the mainshock (Figure 3). On the other hand, earthquakes with fault-plane solutions corresponding to reverse faulting combined with left-lateral, strike-slip motion also occur in this zone. That is the case of the earthquake of 18 October 1981 ($m_b=5.4$) (event 15) (see Figure 4 and Appendix).

On 22 July 1993 ($m_b=6.1$), an earthquake occurred about 60 km south of the Colombian-Venezuelan border (event 23) (Figure 4 and Appendix). The inversion of the body waves shows a tensional focal mechanism with nodal planes striking approximately in a N-S direction, and at a depth of 18 km. The seismograms indicate the presence of a small pre-event about three seconds before the mainshock, which is reflected by the source-time function obtained from the inversion. The epicenter of this earthquake is located clearly outside (~80 km to the east) of the compression

zone related to the southwestern terminus of the Boconó fault system. It was not possible to correlate this earthquake with a specific tectonic feature in the region because no faults have been mapped in this area. However, several tensional faults trending NE-SW that have been identified in the Barinas-Apure basin (southeastern Venezuelan Andes) could extend to the region where this earthquake occurred. The origin of these faults could be associated with bending in the upper crust due to the overriding of the Venezuelan Andes over the plains.

Offshore NW-SE Trending Faults

There was an important seismic sequence in northwestern Venezuela during April-May 1989 (events 20 and 21). The mainshock ($m_b=5.9$) and its largest aftershock ($m_b=5.4$) occurred on 30 April 1989 and 4 May 1989, respectively. Both earthquakes had the peculiarity of being multiple rupture processes that originated long, body-wave trains. These earthquakes were generated apparently on a fault system trending in the NW-SE direction, with a right-lateral, strike-slip mechanism [Malavé and Suárez, 1996].

Stress Field and Caribbean-South America Plate Interaction in Western Venezuela

The orientation of the stress field in a region where lithospheric plates are interacting is a crucial observation in understanding the tectonic processes induced by the relative movement of the plates. The complex tectonic environment in northwestern South America has motivated that the direction of the compressive stress field in this area has been a matter of discussion for more than twenty years. Several authors concluded that the direction of the compressive stress field is oriented east-west due to the underthrusting of the Nazca plate beneath the South American plate [e.g., Dewey, 1972; Pennington, 1981; Kafka and Weidner, 1981, Soulas, 1985]. Other workers, however, reported a principal compressive direction oriented in the northwest-southeast direction induced by the underthrusting of the Caribbean plate beneath the South American plate in northern Colombia and northwestern Venezuela [e.g., Kellogg and Bonini, 1982; 1985]. Both directions of the stress field suggested by previous studies agree, in general, with that expected to induce the dextral relative movement between the Caribbean and South American plates.

The focal mechanisms obtained in this study clearly suggest two different direction of the compressive stress field in western Venezuela. The earthquakes located in southwestern Venezuela consistently indicate a compressive stress field oriented east-west. However, focal mechanisms of earthquakes in northwestern Venezuela (approximately north of latitude 10°N) show a general rotation of *P*-axes from the NW-SE to NNE-SSW direction (Figure 5).

These two well defined sets of directions of the compressive stress field acting over western Venezuela motivated a comparison between the rate of strain in both northern and southern areas considered individually with that in the whole region. The correlation between the focal mechanisms and the active mapped faults shows that seismic energy release is not occurring on a single, major fault boundary such as the Boconó or the Oca-Ancón system. Instead, seismicity nucleates on faults with different orientations distributed over a large seismogenic volume. In this case, it is more convenient to follow Kostrov [1974] and use the seismic moment tensor (M_{ij}) to calculate the strain resulting from the volumetric deformation of the region. Kostrov [1974] showed

that the mean rate of irrotational strain ϵ_{ij} in a volume V over a time period τ produced by the slip on n different faults is

$$\epsilon_{ij} = \frac{1}{2 \mu V \tau} \sum_{n=1}^N M_{ij}$$

In this analysis, the region was studied first as one block and then divided into two sections: north and south of 10°N . The areal dimensions of the deformed volume are shown on Figure 6. A thickness of 15 km was assumed in according to the average of the depths of the earthquakes analyzed in this study. A time period of 30 years (1964-1994) was considered in the estimations.

Firstly, all events studied here were included in the analysis. The results suggest a principal value of compressive strain rate of $5.9 \times 10^{-10} \text{ yr}^{-1}$ oriented almost N-S (about 1° west of north). Afterwards, we excluded the event of 22 July 1993 in the calculations because it appears to be generated in a different tectonic environment than the other events. The result is a compressive strain rate of $5.6 \times 10^{-10} \text{ yr}^{-1}$ oriented approximately N-S (4° east of north). The principal values of compressive strain rate when the area was divided into the north and south zones are $1.6 \times 10^{-9} \text{ yr}^{-1}$ oriented about $\text{N}5^{\circ}\text{E}$ and $1.7 \times 10^{-9} \text{ yr}^{-1}$ oriented $\sim 99^{\circ}$ east of north, respectively.

The results obtained from this study show that when the region is divided into north and south areas, the principal values of compressive strain rate in each zone, as was expected, have a similar orientations than those obtained from the average of the P -axes mentioned above. In the northern part, the almost N-S maximum compressive strain is probably due to the underthrusting of the Caribbean plate beneath northwestern South America [e.g., Kellogg and Bonini, 1982; Ladd *et al.* 1984, Freymueller *et al.*, 1993]; whereas the approximately E-W maximum compressive strain in the southern part of the study area is presumably produced by the Nazca-South American plates convergence [e.g., Pennington, 1981]. However, when the overall deformed volume is considered, the direction of the compressive strain rate is almost N-S, indicating that the compression in this direction is predominating in the region rather than the E-W compression.

In the effort to estimate a relative velocity between the Caribbean plate (north of Oca-Ancón fault system) and South American plate (south of Boconó fault system) based on the seismic

moment tensors, the earthquakes studied here were assumed that occurred along Boconó fault system instead of others faults. According to *Jackson and McKenzie* [1988], the relative velocity between two plates (v_{12}), when the length (l) of the deformation zone is much greater than its width, can be calculated by

$$v_{12} = \frac{1}{\mu \tau l h} \sum_{n=1}^N M_{12}$$

where τ is the time period and h is the depth of the fault. The calculation shows a relative velocity of 2.12×10^{-3} cm/yr. for the last 30 years, which is three orders of magnitude lower that the relative velocity measured on the Boconó fault system. This difference may be the result, as suggested by *Dewey and Suárez* [1991], of that Boconó fault system ruptures infrequently in very large earthquakes but that is quiescent at both high and low-magnitude.

Tectonic in Western Venezuela: A Bookshelf Faulting Case

As mentioned above, the predicted relative movement between the Caribbean and South American plates is on the order of 2 cm/yr. However, the rates of motion measured on the Boconó, El Pilar, and Oca-Ancón fault systems during the last 1.8 m.y. are not greater than 1.3 cm/yr. [Pérez and Aggarwal, 1981; Schubert, 1982; Soulas, 1986; 1987]. That means that a fraction of the relative motion between those plates is being either accumulated in seismic energy or absorbed by internal volumetric deformation associated with secondary fault systems, or by a combination of both. This zone of deformation has been defined from the east to the central part of Venezuela of ~100 km wide, along the El Pilar and Morón fault systems [Soulas, 1985]. Towards the west, however, this zone of deformation becomes wider and includes part of the Venezuelan Andes and the Maracaibo basin.

The interior of this latter area of deformation is highly faulted and contains several sets of conjugate faults trending in different directions: E-W, NE-SW, NNE-SSW, and NW-SE. The fact that most of the recent earthquakes in western Venezuela are occurring on these faults within the deformation zone may indicate that part of the relative motion between the Caribbean and South American plates is being accommodated by internal volumetric deformation related to the secondary faults. The manner of how these secondary faults are acting with respect to the major fault systems will be explained as follows.

The left-lateral, strike-slip faults in western Venezuela trending roughly NNE-SSW (El Tigre, Icotea, Valera, Humocaró, Carache) appear to define elongated blocks. These blocks are apparently limited by the Oca-Ancón fault system to the north and the Boconó fault system to the south (Figure 7a). The current left-lateral slip in several of these NNE-SSW faults has been demonstrated by geological field works, by seismic reflection profiles, and by neotectonic studies and trenching [e.g., Soulas, 1985]. Moreover, some focal mechanisms determined in this study indicate that kind of displacement.

The Humocaró fault is an excellent example of the current sinistral motion on these faults. Three earthquakes that probably originated on that fault (5 April 1975, 14 June 1984, and 17

August 1991) reflect that motion. As discussed before, the orientation of the fault plane of the event of 5 April 1975 indicates a change in direction towards the east in the northernmost segment of the Humocaro fault relative to its southern trace. On the other hand, the earthquake of 20 October 1969 (event 4), whose epicenter is located near the El Tigre fault, may have been nucleated on that fault indicating recent left-lateral motion.

Kinematically, the geological and seismological evidence suggest that the deformation observed in northwestern Venezuela may be explained as bookshelf faulting. This type of bookshelf mechanism occurs where faults oriented at high angles have left-lateral slip antithetic to the right-lateral shear couple, rotating individual blocks clockwise [e.g., Mandl, 1987; Kleinrock and Hey, 1989]. The name bookshelf derives from the similarity of shearing a row of books on a shelf by moving their tops from left to right and observing the left-lateral shear on the planes separating the books (Figure 7b).

In western Venezuela, however, the right-lateral shear couple, in this case the Boconó and Oca-Ancón fault systems are not parallel. Furthermore, we have to take into account that those shear faults are not moving at the same rate; there is approximately a 3:1 ratio of relative velocity between them. On Figure 8, an schematic representation of the bookshelf model in western Venezuela is shown. When applying the shear stress, either individually on each shear fault or on both, the NNE-SSW faults separating the blocks experience left-lateral slip and the blocks rotate independently clockwise.

This type of deformation is supported by the observation of James [1985] that the sinistral displacements of the NNE-SSW faults transform in their northern and southern extremities into NE-SW to E-W trending thrusts as they approach the Oca-Ancón and Boconó fault systems, (Figure 8). James [1985] explained this variation as a result of the northeastward movement of the Maracaibo block towards the Caribbean, along the Boconó fault. He also cited the Valera fault as an example of this sinistral transformation into thrusting as the Boconó system fault approaches. That transformation into a thrusting fault will depend on the component of normal stress acting on the Boconó and Oca-Ancón faults. The presence of horizontal *P*-axes oblique to either Boconó and

Oca-Ancón faults, demonstrated in this study, ensure the existence of a significant component of normal stress on these faults.

The bookshelf mechanism has also been observed on individual faults in western Venezuela, but in a smaller scale. *Mandl* [1987] used the Icotea fault as an example to explain tectonic deformation by rotating parallel fault using a bookshelf mechanism. He described a set of rotated parallel faults, with predominant dip-slip, associated with shearing along two subparallel branches of the Icotea fault. More recently, *Lugo* [1992] presented a detailed analysis of the tectonic evolution of the Icotea fault in the Maracaibo basin. He concluded that the Icotea fault, from middle Late Eocene through Late Miocene, acted as left-lateral, strike-slip fault. Using a "domino" style analogy, he interpreted 15° of clockwise rotation for the northern Icotea fault-bounded blocks. Furthermore, there is evidence that the Maracaibo Basin has rotated ~45° since the Middle Cretaceous [*Perarnau et al.*, 1988]. *Lugo* [1992] also proposed that since the Pleistocene, the northern segment of the Icotea fault has behaved as a west-vergent compressional fault associated with a regional E-W compressive regime.

It is possible that during the Late Eocene-Pliocene times the NNE-SSW faults could have experimented larger slip than during the present due to the higher average velocity of the Oca-Ancón fault during that period. Nevertheless, both Boconó and Oca-Ancón fault systems continue moving at the present time, suggesting that the bookshelf mechanism is still occurring today. It could be speculated that the recent compressional regime identified by *Lugo* [1992] in the northern segment of Icotea fault could be possibly related to the transformation of sinistral to thrust faulting reported by *James* [1985].

In summary, the resulting deformation from the interaction between the Caribbean and South American plates in western Venezuela is being absorbed through a wide zone of deformation instead of a single major fault. This deformation zone may be defined from the northernmost part of Colombia and Venezuela to the Venezuelan Andean region. This argument seems to resolve the old problem of why the Caribbean-South American pole is unconstrained (large 95% confidence ellipse) by using data along the Boconó fault system [*Jordan*, 1975], which motivated others workers to suggest another pole that could adjust much better.

Summary and Conclusions

The source parameters of shallow ($h < 30$ km), moderate-sized ($5.4 \leq m_b \leq 6.1$) earthquakes occurred in western Venezuela during the last three decades were analyzed to understand the complex tectonic environment in this region and its relationship to the interaction between the Caribbean and South American plates. The focal parameters were evaluated through the moment-tensor inversion, using long and short period teleseismic P , SH , and SV waves. The results show that most of the earthquakes are apparently associated with secondary fault systems and only the 19 July 1965 event nucleated on the Boconó fault system, considered by several authors as the main plate boundary in the region.

The average direction of the P -axes obtained from the focal mechanisms clearly divides the region of western Venezuela into two zones: north and south of latitude 10°N . In the northern area, the direction of the P -axes, in general, rotate from a NW-SE to NNE-SSW direction; whereas in the southern zone, the P -axes are approximately oriented E-W. The determination of the compressional strain rate in the overall region over 30-years period of time is $5.9 \times 10^{-10} \text{ yr}^{-1}$ and is oriented almost N-S. This result is probably due to the underthrusting of the Caribbean plate beneath western South America.

According to the seismic activity occurring on the secondary faults, the border between the Caribbean and South American plates is distributed over a wide zone of deformation instead of a major single fault. This may be one of the reasons for the large uncertainties in the determination of the instantaneous Caribbean-South American pole.

The left-lateral, strike-slip faults trending roughly NNE-SSW in western Venezuela define elongated small blocks limited by the Oca-Ancón fault system to the north and the Boconó fault system to the south. The focal mechanisms and the Quaternary geological data suggest that the kinematics of the faulting pattern behave as a bookshelf faulting mechanism.

Acknowledgments. The authors thank C. Mendoza for valuable review and comments of the manuscript. M. Zirbes (*USGS*) made available copies of the *GDSN* digital seismograms. M. Benites and J. Taggart helped us to make copies of the *WWSSN* analog seismograms. This paper was partially written while one of the authors (GM), as a graduate student of the Universidad Nacional Autónoma de México, was visiting the U. S. Geological Survey in Golden, CO. The use of facilities is greatly appreciated. He (GM) received financial aid in the form of an INTEVEP, S.A. Fellowship.

References

- Aggarwal, Y. J. P. Soulas, and D. García. Contemporary Tectonics of the Venezuelan Andes and Northern Colombia. *X Caribbean Geological Conference*, Cartagena, Colombia (abstract), 1983.
- Aki, K. and P. Richards, *Quantitative Seismology*, W. H. Freeman, San Francisco. 557 pp., 1980.
- Barbot, J. P., J. Butenko, and J. I. Rodríguez, Geologic and geotechnical analysis of Golfo Triste: its influence on offshore structures and drilling operations. *Congress COPPE/UFRJ*, Rio de Janeiro. 1979.
- Barbot, J. P., J. Butenko, E. Espinoza, J. Daza, and G. Malavé, El cuaternario del Golfo de La Vela y su importancia geotécnica para la exploración y explotación petrolera, *Transactions 9th Caribbean Geological Conference*, Santo Domingo, 2, 541-553, 1980.
- Centeno-Grau, M., *Estudios Sismológicos: Caracas, Litografía del Comercio*, 555 p., 1940.
- Chen, W. and P. Molnar, Focal depths of intracontinental and intraplate earthquakes and their implications for the thermal and mechanical properties of the lithosphere, *J. Geophys. Res.*, 88, B5, 4183-4214, 1983.
- De Toni, B. and J. Kellogg, Seismic evidence for blind thrusting of the northwestern flank of the Venezuelan Andes, *Tectonics*, 12, 1393-1409, 1993.
- Dewey, J., Seismicity studies with the method of joint hypocenter determination. Ph.D. thesis, University of California, Berkeley. 1971.
- Dewey, J., Seismicity and tectonics of western Venezuela. *Bull. Seismol. Soc. Am.*, 62, 1711-1751, 1972.
- Dewey, J., and G. Suárez, Seismotectonics of Middle America. in Slemmons, D. B., E. R. Engdahl, M. D. Zoback, and D. D. Blackwell, eds., *Neotectonics of North America: Boulder, Colorado. Geological Society of America, Decade Map Volume 1*, 1991.
- Dziewonski, A. M., G. Ekström, J. E. Franzen, and J. H. Woodhouse. Global seismicity of 1977: Centroid-moment tensor solutions for 471 earthquakes, *Phys. Earth Planet. Int.*, 45, 11-36, 1987.

- Dziewonski, A. M., G. Ekström, J. E. Franzen, and J. H. Woodhouse. Global seismicity of 1978: Centroid-moment tensor solutions for 512 earthquakes, *Phys. Earth Planet. Int.*, 46, 316-342, 1987.
- Dziewonski, A. M., G. Ekström, J. E. Franzen, and J. H. Woodhouse. Global seismicity of 1979: Centroid-moment tensor solutions for 524 earthquakes, *Phys. Earth Planet. Int.*, 48, 18-46, 1987.
- Dziewonski, A. M., G. Ekström, J. E. Franzen, and J. H. Woodhouse. Global seismicity of 1980: Centroid-moment tensor solutions for 515 earthquakes, *Phys. Earth Planet. Int.*, 50, 127-154, 1988.
- Dziewonski, A. M., G. Ekström, J. E. Franzen, and J. H. Woodhouse. Global seismicity of 1981: Centroid-moment tensor solutions for 542 earthquakes, *Phys. Earth Planet. Int.*, 50, 155-182, 1988.
- Dziewonski, A. M., G. Ekström, and M. P. Salganik. Centroid-moment tensor solutions for July-September 1991, *Phys. Earth Planet. Int.*, 72, 1-11, 1992.
- Dziewonski, A. M., G. Ekström, J. H. Woodhouse, and G. Zwart. Centroid-moment tensor solutions for July-September 1986, *Phys. Earth Planet. Int.*, 46, 305-315, 1987.
- Dziewonski, A. M., G. Ekström, J. H. Woodhouse, and G. Zwart. Centroid-moment tensor solutions for July-September 1988, *Phys. Earth Planet. Int.*, 56, 165-180, 1989.
- Dziewonski, A. M., G. Ekström, J. H. Woodhouse, and G. Zwart. Global seismicity of 1982 and 1983: additional centroid-moment tensor solutions for 553 earthquakes, *Phys. Earth Planet. Int.*, 53, 17-45, 1988.
- Dziewonski, A. M., G. Ekström, J. H. Woodhouse, and G. Zwart. Centroid-moment tensor solutions for April-June 1989, *Phys. Earth Planet. Int.*, 60, 243-253, 1990.
- Dziewonski, A. M., J. E. Franzen, and J. H. Woodhouse. Centroid-moment tensor solutions for April-June 1984, *Phys. Earth Planet. Int.*, 37, 87-96, 1985.
- Frey Mueller, J. T., J. N. Kellogg, and V. Vega. Plate motions in the North Andean region, *J. Geophys. Res.*, 98, 21853-21893, 1993.

- Grases, J., Investigación sobre los sismos destructores que han afectado el centro y occidente de Venezuela, 3 vol., INTEVEP, S.A., Caracas, Venezuela, 1980.
- Hanks, T. and H. Kanamori, A moment magnitude scale, *J. Geophys. Res.*, 84 (B5), 2348-2350, 1979.
- Jackson, J. and D. McKenzie, The relationship between plate motions and seismic moment tensors, and the rates of active deformation in the Mediterranean and Middle East, *Geophys. J.*, 93, 45-73, 1988.
- James, K., Marco tectónico, estilos estructurales y habitat de hidrocarburos cretácicos, Venezuela, *VI Venezuelan Geological Congress Mem.*, 2452-2469, 1985.
- Jordan, T. H., The present-day motions of the Caribbean plate, *J. Geophys. Res.*, '80, 4433-4439, 1975.
- Kafka A. and D. Weidner, Earthquake focal mechanisms and tectonics processes along the southern boundary of the Caribbean plate, *J. Geophys. Res.*, 86, 2877-2888, 1981.
- Kellogg, J. N. and W. E. Bonini, Subduction of the Caribbean plate and basement uplifts in the overriding South American plate, *Tectonics*, 1 (3), 251-276, 1982.
- Kellogg, J. N. and W. E. Bonini, Reply: *Tectonics*, 4 (7), 785-790, 1985.
- Kleinrock, M. and R. Hey, Migrating transform zone and lithospheric transfer at the Galapagos 95.5°W propagator, *J. Geophys. Res.*, 94, 13859-13878, 1989.
- Kostrov, V. V., Seismic moment and energy of earthquakes, and seismic flow of rock, *Izv. Acad. Sci. USSR Phys. Solid Earth*, 1, 23-44, 1974.
- Ladd, J. W., M. Truchan, M. Talwani, P. L. Stoffa, P. Buhl, R. Houtz, A. Manfrett, and G. Westbrook, Seismic reflection profiles across the southern margin of the Caribbean, in Bonini, W. E. *et al.*, eds., The Caribbean-South America plate boundary and regional tectonics, *Geol. Soc. Am. Mem.*, 162, 239-261, 1984.
- Lugo, J., Historia tectónica a lo largo de los sistemas de fallas de Icotea y Pueblo Viejo, Cuenca de Maracaibo, *VI Venezuelan Geophysical Congress Mem.*, 118-124, 1992.
- Malavé, G. and G. Suárez, Complex source characteristics of the 1989 Boca del Tocuyo earthquakes in northwestern Venezuela, submitted to *Bull. Seism. Soc. Am.*, 1996.

- Malavé, G. and G. Suárez. Intermediate-depth earthquakes in northern Colombia and western Venezuela and its relationship to Caribbean plate subduction, *Tectonics*, 14 (3), 617-628, 1995.
- Mandl, G., Tectonic deformation by rotating parallel faults: the bookshelf mechanism, *Tectonophysics*, 141, 277-316, 1987.
- Minster, J. and T. Jordan, Present-day plate motions, *J. Geophys. Res.*, 83, 5331-5354, 1978.
- Molnar, P. and L. R. Sykes, Tectonics of the Caribbean and Middle America regions from focal mechanisms and seismicity, *Geol. Soc. Am. Bull.*, 80, 1639-1684, 1969.
- Nábelek, J., Determination of earthquake source parameters from inversion of body waves. Ph.D. thesis, Massachusetts Institute of Technology, Cambridge, 361 p.
- Pennington, W., Subduction of the Eastern Panama Basin and Seismotectonics of Northwestern South America, *J. Geophys. Res.*, 86, 10753-10770, 1981.
- Perarnau, A., J. Castillo, and W. Gose, Paleomagnetismo de unidades del Cretácico en Los Andes y la Serranía de Perijá: Implicaciones tectónicas, *IV Venezuelan Geophysical Congress Mem.*, 399-405, 1988.
- Pérez, O. and Y. Aggarwal, Estudios de microsismicidad en el sistema Uribante-Caparo, Estado Táchira, *FUNVISIS*, Caracas, Venezuela, 1980.
- Pérez, O. and Y. Aggarwal, Present-day tectonics of the southeastern Caribbean and northeastern Venezuela, *J. Geophys. Res.*, 86, 10791-10804, 1981.
- Rial, J. A., The Caracas, Venezuela, earthquake of July 1967; a multiple source event. *J. Geophys. Res.*, 83, 5405-5415, 1978.
- Rod, E., Strike-slip faults of northern Venezuela, *Am. Assoc. Pet. Geol. Bull.*, 40, 457-476, 1956.
- Schubert, C., Neotectonics of Boconó fault, western Venezuela, *Tectonophysics*, 85, 205-220, 1982.
- Schubert, C. and F. Krause, Morón fault zone, north-central Venezuelan borderland: identification, definition, and neotectonic character, *Mar. Geophys. Res.*, 6, 257-273, 1984.
- Singer, A., F. Audemard, C. Beltrán, J. A. Rodríguez, F. De Santis, A. Adrianza, C. Chacín, M. Lugo, J. Mendoza, and C. Ramos, Actividad tectónica cuaternaria y características sismogénicas de los sistemas de fallas de Oca-Ancón (tramo oriental), de la península de

- Paraguaná y región de Coro y de la costa nororiental de Falcón. *FUNVISIS*. Caracas. Venezuela, 1992.
- Sipkin, S. and R. Needham. Moment-tensor solutions estimated using optimal filter theory: global seismicity, 1988-1989, *Phys. Earth Planet. Int.*, 67, 221-230, 1991.
- Soulas, J. P., C. Rojas, A. Singer, C. Beltrán and M. Lugo. Actividad cuaternaria y características sismogénicas de las fallas de Boconó, Valera, Tuñame, Piñango, Piedemonte, Burro Negro-Mene Grande y otras, *FUNVISIS*, Caracas. Venezuela, 1985.
- Soulas, J. P., Neotectónica y tectónica activa en Venezuela y regiones vecinas. *Memorias VI Congreso Geológico Venezolano*, Caracas, X, 6639-6656, 1986.
- Soulas, J. P., C. Giraldo, D. Bonnot, and M. Lugo. Actividad cuaternaria y características sismogénicas del sistema de fallas Oca-Ancón y de las fallas de Lagarto, Urumaco, Río Seco y Pedregal, *FUNVISIS*, Caracas, Venezuela, 1987.
- Stein, S., Ch. DeMets, R. G. Gordon, J. Brodholt, D. Argus, J. F. Engeln, P. Lundgren, C. Stein, D. A. Wiens, and D. F. Woods, A test of Alternative Caribbean plate Relative Motions Models. *J. Geophys. Res.*, 93, 3041-3050, 1988.
- Suárez, G. and J. Nábelek, The 1967 Caracas Earthquake: Fault Geometry, Direction of Rupture Propagation and Seismotectonic Implications. *J. Geophys. Res.*, 70 (20), 5065-5074, 1990.
- Sykes, L., W. R. McCann, and A. L. Kafka, Motion of Caribbean plate during last 7 million years and implications for earlier Cenozoic movements. *J. Geophys. Res.*, 87, 10656-10676, 1982.
- Vásquez, E. and P. Dickey, Major faulting in north-western Venezuela and its relation to global tectonics. *VI Caribbean Geological Conference Mem.*, 191-202, 1972.

Table 1. Compilation of Results Obtained by Previous Workers and in This Study.

Event	Date	Lat °N	Long °W	Depth km	m_b	Strike deg	Dip deg	Slip deg	P-axis Tr°/Pl°	F-axis Tr°/Pl°	M_0	Source
1	Jul. 19, 1965	9.20	70.38	20	5.3	145	80	0	100/7	10.7	--	A
		9.25	70.44	4	5.3	240	60	-160	97/34	192.8	0.78	B
		9.25	70.38	14±1	--	38±1	82±1	172±1	264.0	354/11	1.10	H
2	Dic. 21, 1967	7.04	72.02	29	5.4	58	83	166	105/5	13/15	--	A
		7.04	72.06	55	5.4	240	60	-160	97/34	192.8	1.19	B
3	May 13, 1968	9.00	71.06	29	4.8	228	60	118	298/11	186.63	--	A
		9.06	71.08	1	4.9	240	60	-150	95/41	188.3	0.21	B
4	Oct. 20, 1969	10.90	72.40	36	--	154	67	-131	18/50	272/12	--	C
		11.00	72.38	8±1	--	15±1	73±1	-22±1	334/27	65.3	6.30	H
5	Jan. 27, 1970	7.54	71.95	49	5.7	0	66	90	90/21	270.69	--	A
		7.49	72.09	55	5.6	240	60	-150	95/41	188.3	1.09	B
*		7.51	72.08	12±1	--	36±1	61±1	171±1	357/26	1.49	--	H
6	May 19, 1970	10.89	68.93	--	5.1	88	58	-143	302/47	32/1	--	A
		10.99	68.92	6	5.1	285	52	-20	238/14	137/39	1.17	B
7	Mar. 5, 1975	9.04	69.95	--	5.5	43	45	90	133/0	0/90	--	B
		9.06	69.90	14±1	--	184±3	47±1	93±1	272/2	140/87	2.90	H
8	Apr. 5, 1975	10.10	69.60	--	--	204	80	10	158/0	68/14	--	C
		10.01	69.67	10±1	--	21±1	75±1	-2±1	337/9	245/12	9.5	H
9	Dic. 11, 1977	9.52	69.56	18	5.6	170	38	83	85/7	296/82	1.87	E
		9.52	69.54	8±1	--	173±2	42±1	75±2	94/4	342/79	10.06	H
10	Jan. 21, 1978	6.38	72.38	15	5.1	94	35	-12	73/42	312/30	1.59	E
11	Aug. 8, 1978	6.96	72.14	51	5.1	161	35	90	71/10	251/80	0.66	E
12	May 5, 1979	8.36	70.99	22	5.6	119	53	4	79/23	336/28	1.52	E
**		8.38	70.94	16±1	--	29±1	89±1	161±1	76/16	341/19	4.06	H
13	May 2, 1980	7.21	72.17	15	5.1	226	28	147	95/26	227/54	1.29	E
14	Nov. 26, 1980	8.05	72.44	40	5.0	57	64	170	282/12	17/25	0.86	E
15	Oct. 18, 1981	8.12	72.53	26	5.4	251	43	173	109/27	220/35	9.16	E
		8.13	72.47	28±1	--	349±1	77±1	28±1	118/10	214/29	8.2	H
16	Jul. 4, 1982	7.66	72.19	96	5.5	52	69	169	278/7	11/22	1.21	E
		7.65	72.11	11±1	--	46±2	78±1	166±1	93/1	2/18	1.68	H
17	Jun. 14, 1984	10.01	69.74	18	5.2	340	65	-11	300/25	205.10	1.02	E
18	Jul. 18, 1986	10.72	69.51	15	5.8	64	41	106	323/5	78/78	1.78	E
		10.76	69.41	7±1	--	49±1	41±1	78±1	328/5	207/81	1.40	H
19	Jul. 12, 1988	9.85	71.37	15	5.4	59	16	-47	91/55	294/33	0.78	E
		9.83	71.34	13±1	--	83±4	52±2	-43±3	59/56	322.5	0.30	H
20	Apr. 30, 1989	11.00	68.32	15	5.9	166	62	-168	25/28	121/12	9.83	E
		10.96	68.33	20	--	242	36	147	113/20	332.53	8.10	F
-		11.01	68.25	14±1	--	162±1	78±1	-178±1	26/10	117.7	35.10	G
21	May 4, 1989	11.07	68.28	15	5.5	145	51	-174	1/30	105/23	2.13	E
		11.06	68.23	12±1	--	133±2	83±1	-172±2	358/11	267/1	2.40	G
22	Aug. 17, 1991	10.02	69.91	15	5.5	344	86	-3	299/5	209/1	2.58	E
		--	--	15±1	--	75±2	69±2	-169±2	293/22	26.7	1.20	H
23	Jul. 22, 1993	6.50	71.22	24	6.1	21	39	-92	124/84	292.6	13.20	E

Seismicity in western Venezuela

		6.47	71.21	20	--	352	46	-115	184/72	279/2	15.00	F
		--	--	18±1	--	331±5	43±2	-131±2	162/62	269/9	15.30	H
24	May. 31, 1994	7.40	72.10	17	6.1	130	33	50	68/17	301/63	12.10	E
--		7.35	72.11	17	6.1	144	41	99	48/4	174/83	9.70	F
		--	--	11±1	--	3±5	53±2	75±4	104/7	223/76	10.40	H
25	May. 31, 1994	7.30	72.10	--	5.6	232	27	153	96/29	229/51	1.07	E

Source: (A) Dewey [1972]; (B) Kafka and Weidner [1981]; (C) Pennington [1981]; (D) Pérez and Aggarwal (1980); (E) Harvard centroid-moment tensor solution; (F) USGS moment-tensor solution; (G) Malavé and Suárez [1996]; (H) This study.

Convention of focal mechanisms follows Aki and Richards [1980].

* Short-period *P* waves inversion (only waveform).

** Long-period waveform inversion only.

+ Multiple source event.

Tr: Trend; Pl: Plunge; M_0 Seismic-moment ($\times 10^{17}$ Nm).

Table 2: Types of waves used and source time function for the moment tensor inversion of the earthquakes analyzed in this study

Event	Date	Instrument	Waves Inverted	STFD (s) ^a
1	Jul. 19, 1965	Long-period	<i>P, SV, SH</i>	4
4	Oct. 20, 1969	Long-period	<i>P, SV, SH</i>	4
5	Jan. 27, 1970	Short-period	<i>P</i>	1
7	Mar. 5, 1975	Long-period	<i>P, SV, SH</i>	3
8	Apr. 5, 1975	Long-period	<i>P, SV, SH</i>	6
9	Dic. 11, 1977	Long-period	<i>P, SV, SH</i>	4
12	May. 5, 1979	Long-period	<i>P, SV, SH</i>	4
15	Oct. 18, 1981	Long-period	<i>P, SV, SH</i>	4
16	Jul. 4, 1982	Short-period	<i>P</i>	1
18	Jul. 18, 1986	Long-Period	<i>P, SV, SH</i>	2
19	Jul. 12, 1988	Long-period	<i>P, SV, SH</i>	4
22	Aug. 17, 1991	Long-period	<i>P, SV, SH</i>	4
23	Jul. 22, 1993	Long-period	<i>P, SH</i>	4
24	May 31, 1994	Long-period	<i>P, SH</i>	3

^aSTFD: Source time function duration

Figure Captions

Figure 1. Seismicity ($m_b \geq 5.0$) related to the interaction of the Caribbean plate and its neighboring plates (Atlantic, Cocos, Nazca, North America, and South America). The arrows indicate the direction of relative plate motion. The seismicity is shown as open circles; the darker areas thus reflect a high concentration of earthquakes.

Figure 2. Major active fault systems in northern Venezuela [after *Singer et al.*, 1992; *Soulas*, 1986; *Soulas et al.*, 1987]. The rectangular areas indicate the places where most of the major historical earthquakes (before 1900) occurred. The numbers near these regions are the years when these large earthquakes occurred. The arrows indicate the relative motion of the faults. Bathymetry is in meters.

Figure 3. Compilation of focal mechanisms of earthquakes that occurred in western Venezuela reported in previous studies. The fault plane solutions are shown in a lower-hemisphere projection. The numbers nearby the mechanisms are the same as those on Table 1. The letters are the identification of the information source: (A) *Dewey* [1972]; (B) *Kafka and Weidner* [1981]; (C) *Pennington* [1981]; (D) *Pérez and Aggarwal* [1980]; (E) *Dziewonski et al.* [1985; 1987a, 1987b, 1987c; 1987d; 1988a, 1988b; 1988c; 1989; 1990, 1992]; (F) *Sipkin and Needham* [1991]. The faults are from *Soulas* [1986] and *Singer et al.* [1992]. The arrows denote the direction of relative motion of the faults. The black quadrants in the focal mechanisms indicate compressional arrivals. The small open and solid circles in the mechanisms correspond to the position of the T and P axes on the focal sphere, respectively. Bathymetry is in meters.

Figure 4. Focal mechanisms determined in this study for earthquakes $m_b \geq 5.4$ that occurred in western Venezuela since 1964. The fault plane solutions are shown in a lower-hemisphere projection. The faults are from *Soulas* [1986] and *Singer et al.* [1992]. The arrows indicates the direction of relative motion of the faults. The black areas in focal mechanisms indicate compressional arrivals. The small open and solid circles in the mechanisms correspond with the position of the T and P axes on the focal sphere respectively. The numbers near the

mechanisms are the same on Table 2. The solid triangles are the epicenters of the earthquakes of magnitude $5.0 \leq m_b \leq 5.3$ reported by the *NEIC* in western Venezuela since 1964. Bathymetry is in meters.

Figure 5. Lower hemisphere projection of the *P* and *T*-axes of the focal mechanisms determined in this study. The axes are plotted in two groups: Northwestern Venezuela (left) and Southwestern Venezuela (right). In the former region, the *P*-axes rotate from the NW-SE to NNE-SSW direction, whereas in the latter area the *P*-axes are oriented in a E-W direction.

Figure 6. Areal dimensions considered to estimate the maximum compressive strain rate in western Venezuela, following *Kostrov* [1974]. The thick solid line shows the overall zone. The dashed line at latitude 10°N divides the region in north and south sections. In the north section is where the focal mechanisms show *P*-axes trending approximately in the NW-SE direction; whereas in the south section the *P*-axes are oriented roughly in the E-W direction.

Figure 7. An example of how the bookshelf mechanism works. a) Original position of the row of books on a shelf; b) The row of books shears by displacing the boundaries, in this case in a right-lateral motion. Notice the left-lateral shear on the planes separating the books; c) The books rotate as the right-lateral shear couple continues displacing.

Figure 8. Bookshelf-faulting mechanism in western Venezuela: a) Regional-faulting pattern from *Soulas* [1986] and *Singer et al.* [1992]; b) Diagram of the bookshelf-faulting mechanism in western Venezuela. The Boconó and Oca-Ancón fault systems act as a right-lateral shear couple. The dashed lines show the original position of the N-S trending faults, whereas the solid lines are the current fault traces. The arrows indicate the relative movement of the faults.

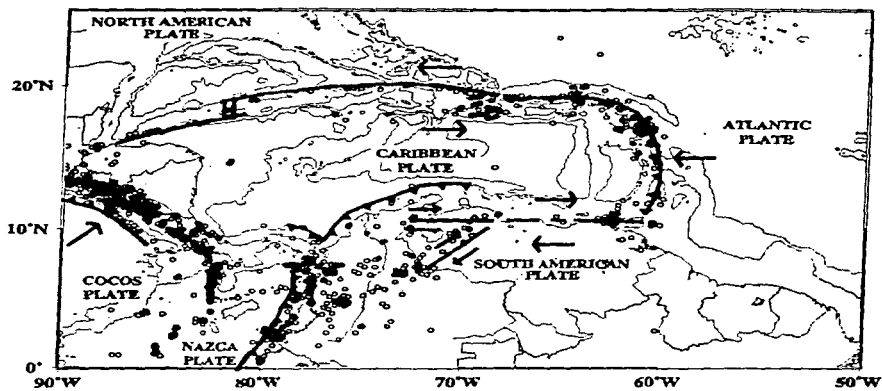
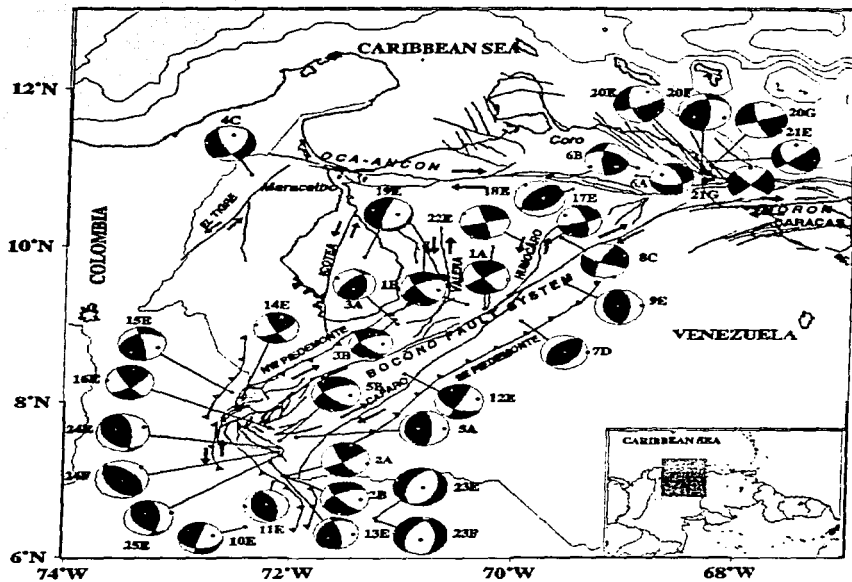


Figure 1



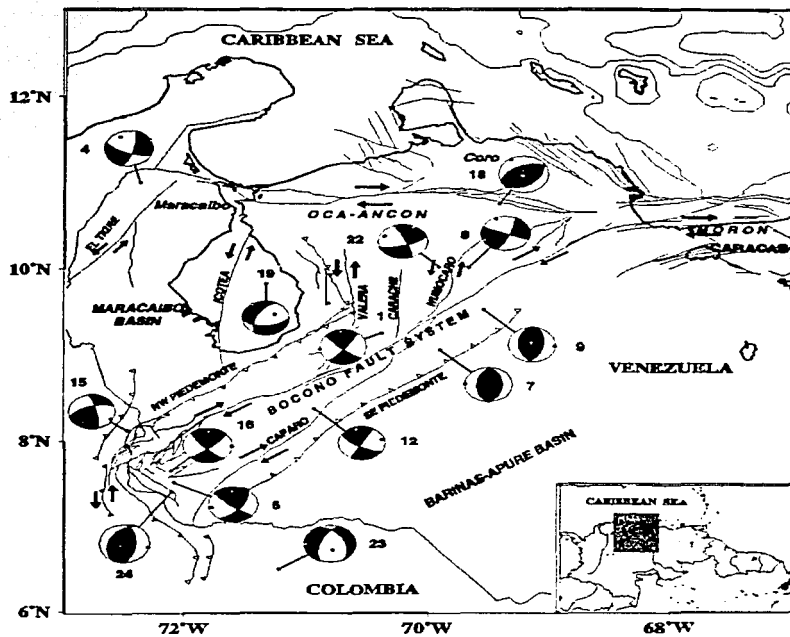
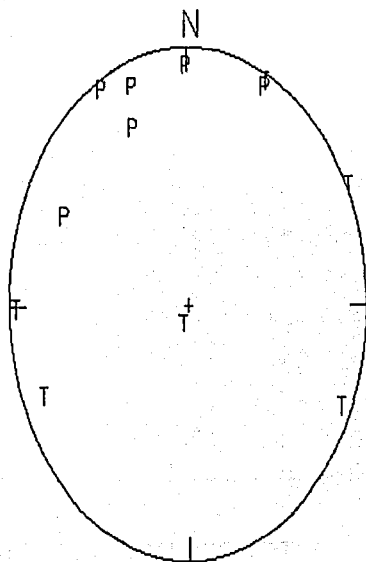


Figure 4

NORTHWESTERN
VENEZUELA



SOUTHWESTERN
VENEZUELA

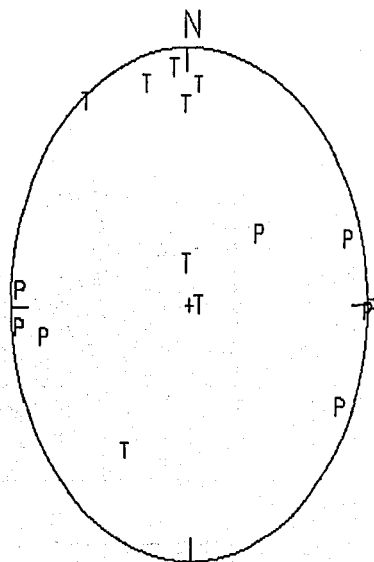


Figure 5

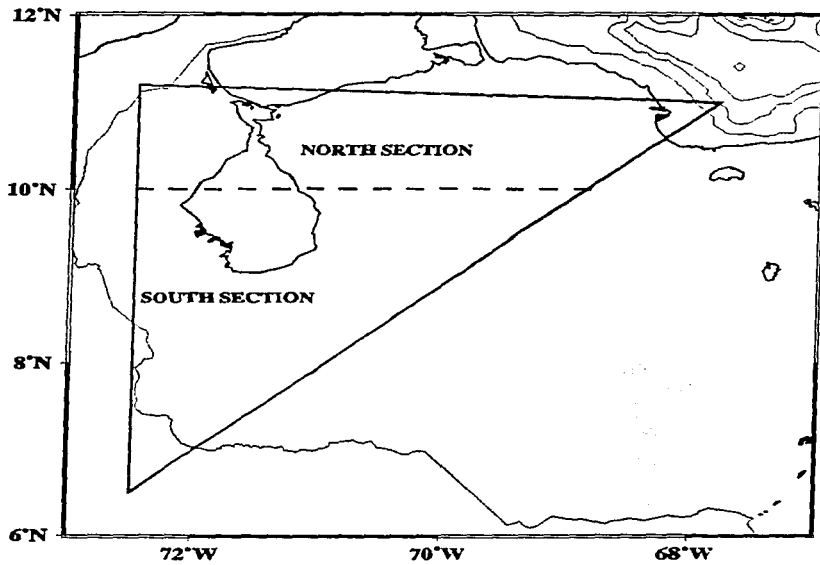
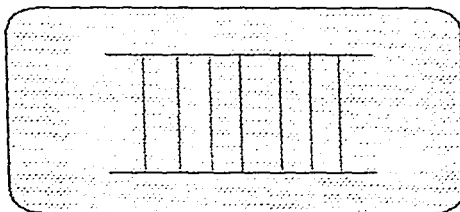


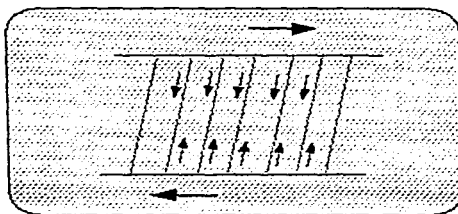
Figure 6

BOOKSHELF MECHANISM

A



B



C

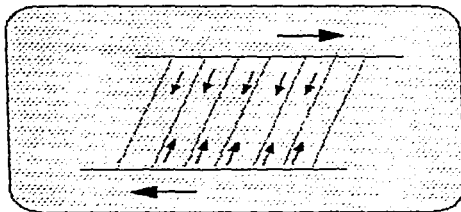


Figure 7

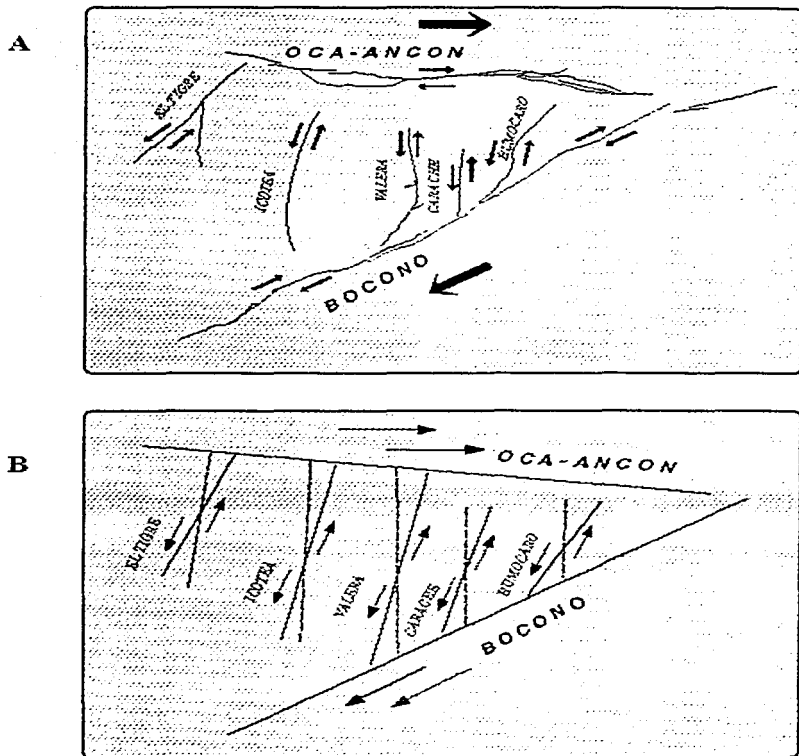
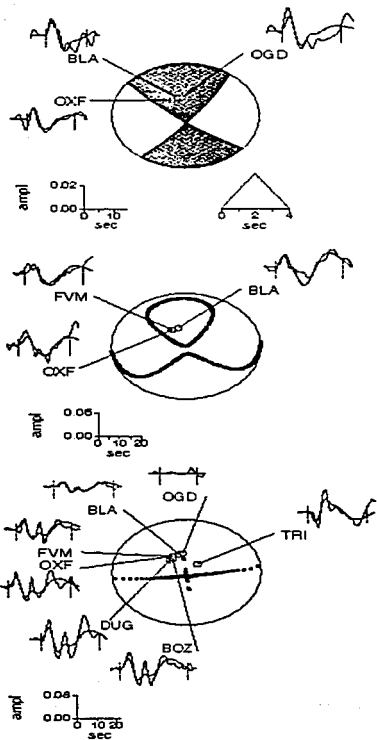


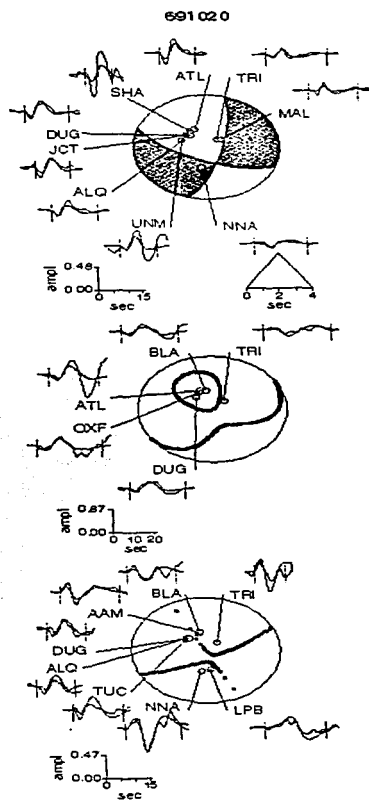
Figure 8

APPENDIX

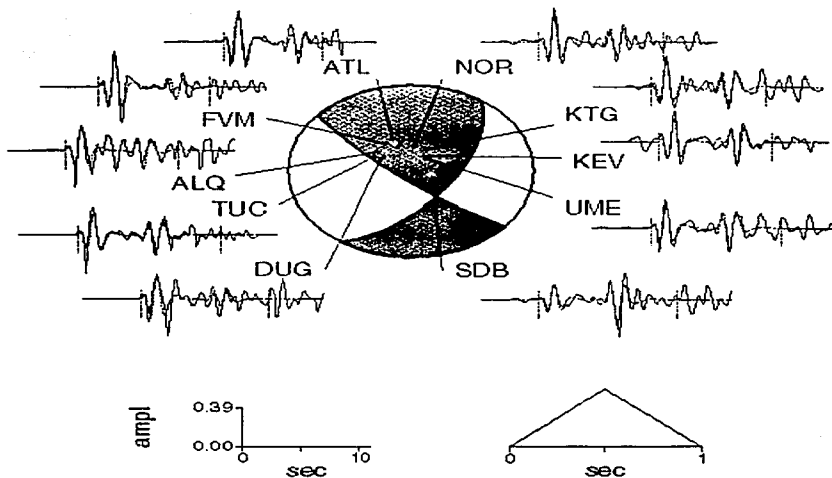
Results of the inversion of the waveforms determined in this study. The focal mechanisms are shown in a lower hemisphere projection. The theoretical seismograms are indicated by dashed lines, whereas the observed waveforms are shown as solid lines. The dark quadrants in the P -waves focal mechanisms represent compressional arrivals. Amplitudes of the waveforms are normalized to an instrumental magnification of 1500 and a geometrical spreading corresponding to an epicentral distance of 40° . A single point source was used in all inversions.

650719

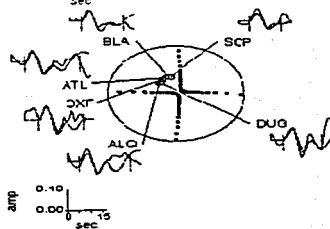
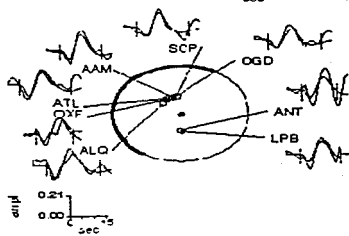
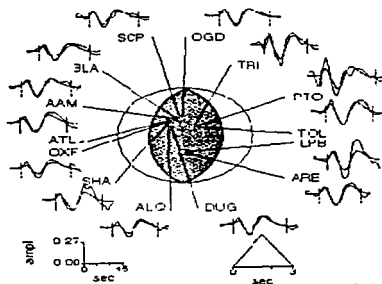




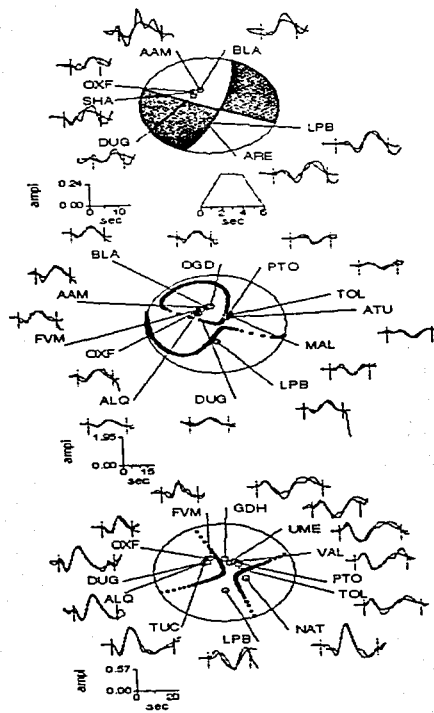
700127



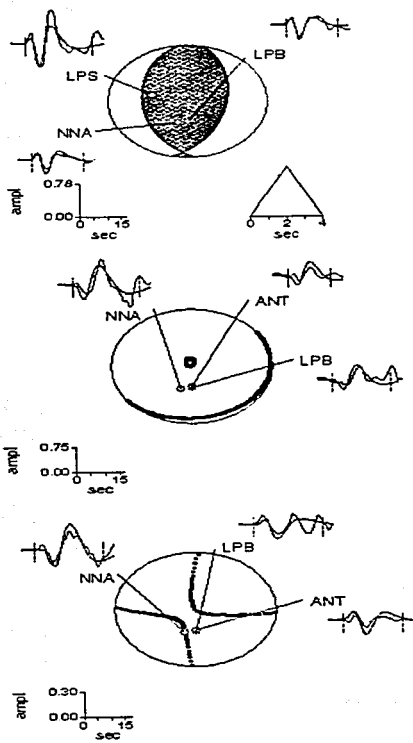
750305



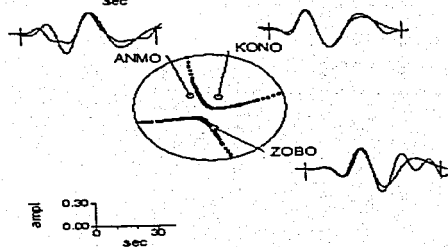
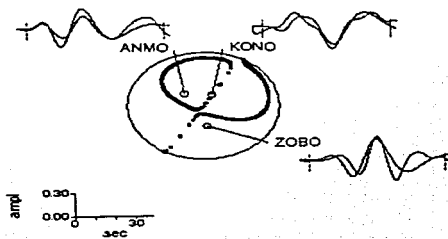
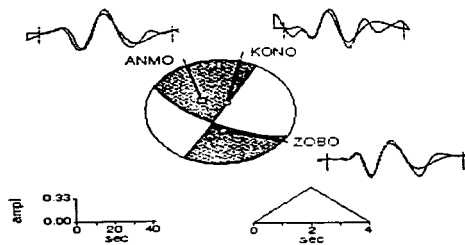
750405



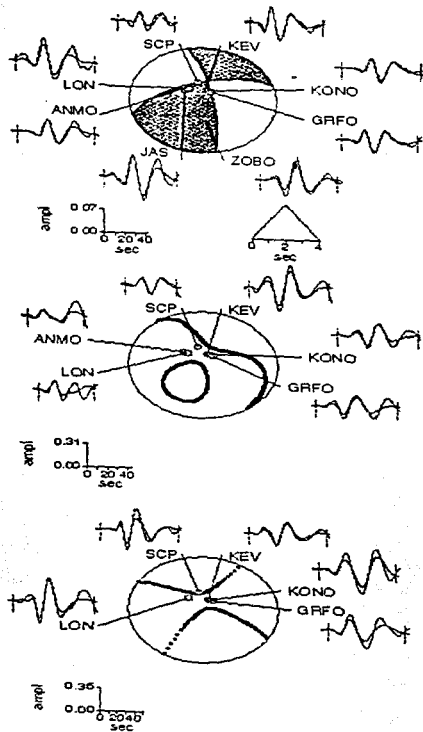
771211



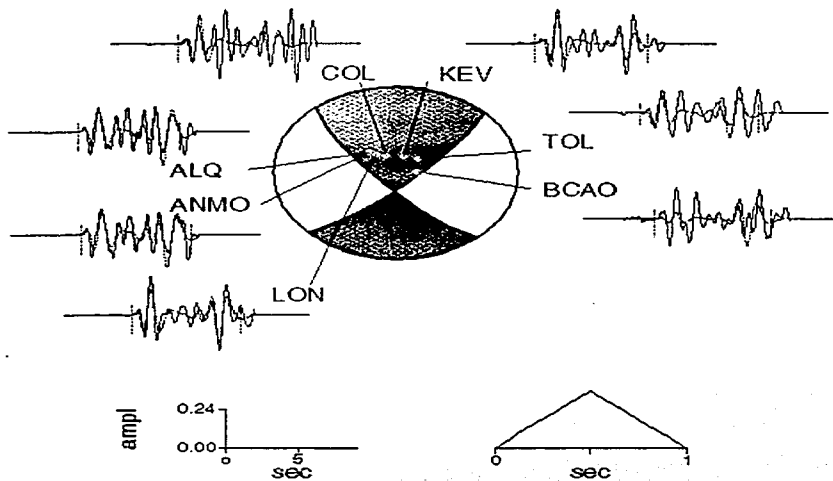
790505



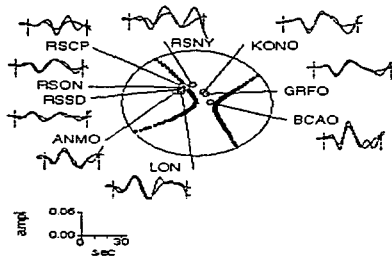
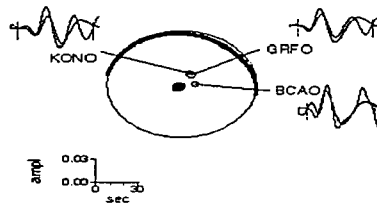
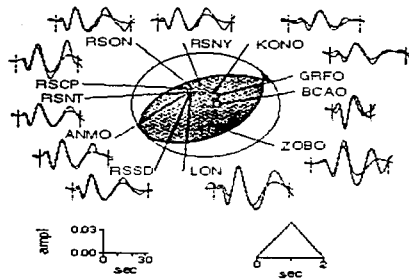
811018



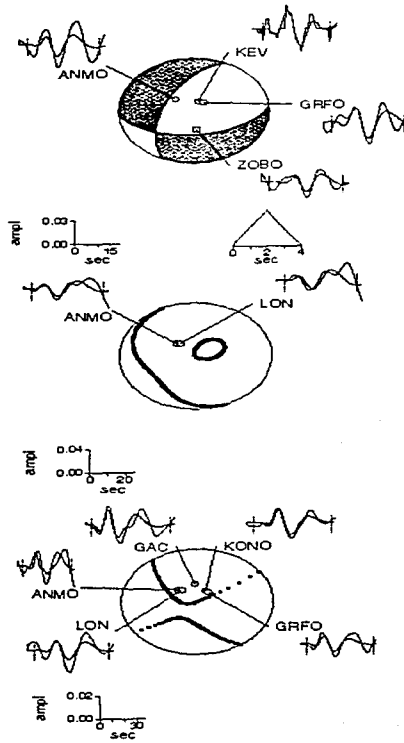
820704



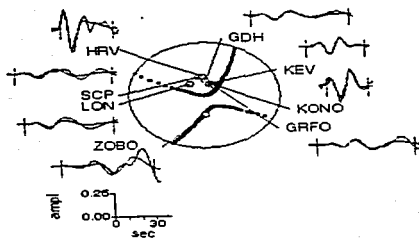
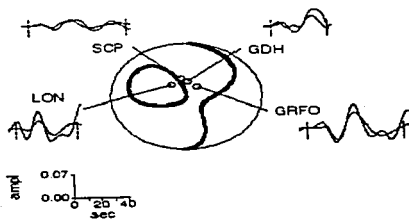
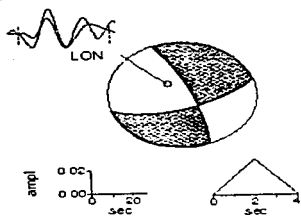
850718



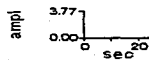
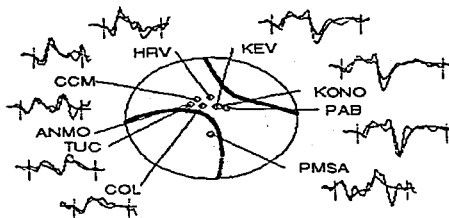
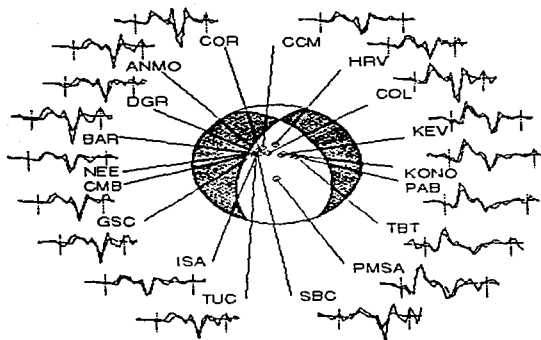
880712



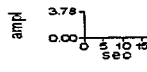
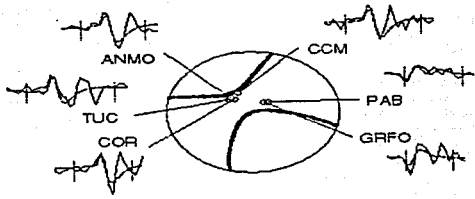
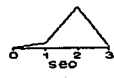
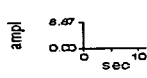
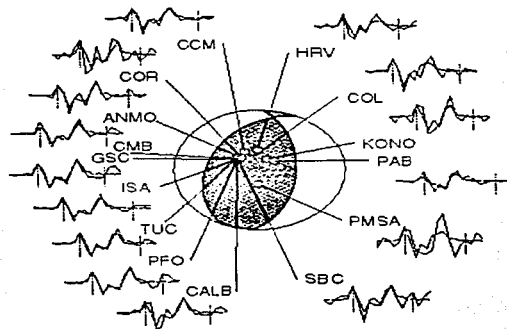
910817



930722



940531



V. Determinación de mecanismos focales mediante sismogramas regionales de período largo. Factibilidad de aplicación de esta técnica al oeste de Venezuela

**Determination of focal mechanisms using long period regional seismograms.
Feasibility to apply this technique in western Venezuela**

By Gustavo Malavé^{1,2}, Carlos Mendoza³, and Gerardo Suárez¹

¹Instituto de Geofísica, Universidad Nacional Autónoma de México, México, D.F.04510

²INTEVEP, S.A., Apartado Postal 76343, Caracas 1070A, Venezuela

³U. S. Geological Survey, *NEIC*, Denver Federal Center MS 967, Denver, CO.

Abstract Forward modeling and moment-tensor inversion processes were analyzed in this study to obtain focal mechanisms using long-period seismograms recorded at regional distances. The motivation of this study was to determine the fault plane solutions of moderate earthquakes ($m_b \leq 5.3$) occurred in western Venezuela. However, due to only two broadband stations were deployed at regional distances from western Venezuela during the development of this study, seven moderate earthquakes that occurred in western United States during 1993 and 1994 were evaluated, instead. Only for an earthquake nucleated on July 22, 1993, near the Colombia-Venezuela border, we were able to access a recorded seismogram at station *SJG*, located at ~1400 km from the epicenter. In general, the results obtained from the moment-tensor inversions, using regional seismograms recorded from earthquakes originated in western United States, satisfied the initial expectative prescribed at the beginning of this study. In most

of the cases studied, the focal mechanisms obtained from the inversion using the Central United States and the Basin and Range models, agreed with the fault plane solutions determined by previous workers. In conclusion, considering the initial condition of developing a tool for working as an automatic routine, the results are acceptable. Nevertheless, the results obtained from the forward modeling and the moment-tensor inversion methodologies clearly show the importance of knowing realistic crustal structures to reach better results.

Introduction

The complex tectonic in western Venezuela is directly related to the interaction of the Caribbean, Nazca, and South American plates (Fig. 1). The analysis of the seismicity in this region shows that most of the events of moderate magnitude ($m_b \geq 5.4$) are occurring on secondary fault systems located in a wide deformation zone between the major fault systems of Boconó and Oca-Ancón (e.g., Dewey, 1972; Kafka and Weidner, 1982; Malavé and Suárez, 1997). The epicenters determined by the National Earthquake Information Center (*NEIC*) for the low-magnitude seismicity ($5.0 \leq m_b \leq 5.3$) also show a similar behavior (Fig. 2). Only three of ~30 events appear to have nucleated on the Boconó fault system. Furthermore, some smaller events originated apparently on faults where no moderate or large events ($m_b \geq 5.4$) have occurred during the last three decades (Icotea, Valera, NW Piedemonte faults). Attempts to determine well constrained, first-motion focal mechanisms of these smaller events were unsuccessful. Focal mechanisms for the moderate size earthquakes provide important information about the regional and local tectonics. Then, the feasibility of using regional recordings for determining earthquake faulting parameters of those smaller events was considered in this study.

Several methodologies for estimating earthquake focal parameters using seismograms at teleseismic distances (30° - 90°) have been developed (e.g., Langston and Helmberger, 1975; Kanamori and Stewart, 1976; Dziewonski *et al.*, 1981; Sipkin, 1982; Nábelek, 1984), also at a very close distances ($\Delta < 1^\circ$) when strong-motion data are available (e.g., Hartzell and Heaton, 1983; Wald *et al.*, 1991). Nevertheless, a few attentions have been paid to evaluate earthquake source parameters using seismograms at regional distances (1° - 12°), due to the complex propagation effects in the earth crust.

The availability of regional waveforms has contributed the development of numerous methodologies for analyzing the regional signals for earthquake source parameters. Some of the recent developments include inversions of broadband P_{nl} signals (e.g., Wallace and Helmberger, 1982; Dreger and Helmberger, 1993; Lay *et al.*, 1994a, 1994b), simultaneous broadband body and surface waveform inversions (e.g., Zhao and Helmberger, 1994), spectral inversions of short-

period surface waves (e.g., Patton and Zandt, 1991; Romanowicz *et al.*, 1993; Thio and Kanamori, 1995), near-field waveform inversion (Kanamori *et al.*, 1990; Uhrhammer, 1992), empirical Green's function deconvolutions (e.g., Kanamori *et al.*, 1992b; Ammon *et al.*, 1993), and complete time domain, waveform inversion of long-period signals (e.g., Ritsema and Lay, 1993; Giardini *et al.*, 1993).

In this case, we concentrate efforts to evaluate two of the methodologies mentioned above. First of all, we analyzed a forward modeling, using the Saikia and Burdick (1991) code for generating accuracy regional seismograms. This program is a modified version of the Wang and Herrmann (1980) method and Herrmann and Wang (1985) regional seismogram's code. Several tests were achieved using the September 21, 1993, Klamath Falls earthquake and an event that occurred near the Colombian-Venezuelan border on July 22, 1993. Second, we made a regional seismogram, moment-tensor inversion for earthquakes occurred in western United States, thinking on an automatic routine that may be used in regional seismological networks. The focal mechanisms determined in this study were compared with those obtained by previous workers (e.g., Dziewonski *et al.*, 1994a; 1994b; 1994c; 1994d; 1995; Sipkin and Needham, 1994; Nábelek and Xia, 1995; Braunmiller *et al.*, 1995; Ritsema and Lay, 1995; Sipkin and Zirbes, 1996).

Finally, the feasibility of applying this inversion scheme for earthquakes occurred in western Venezuela was evaluated, considering the new stations that had been deployed recently in the Caribbean, Central and South American regions.

Regional Seismograms Forward Modeling

Methodology

An evaluation of P_{nl} seismograms forward modeling was considered as a first step in this study. P_{nl} waveforms can be synthesized at regional distances by a variety of techniques. The two most practical are generalized rays and wavenumber integration. The generalized ray approach is the most efficient for a layer over a half-space model and has been used in most previous P_{nl} studies. It becomes difficult to obtain exact results in a multilayered model because the ray sum becomes intractably large. Alternate approaches to computing synthetic seismograms are the frequency-wave number ($f-k$) scheme (Wang and Herrmann, 1980; Bouchon, 1981) and the reflectivity approach (Kennett, 1980; Mallick and Frazer, 1987).

In this case, the Saikia and Burdick (1991) code was used to generate the theoretical seismograms. This code is a vectorized computer program based on the formulation presented by Wang and Herrmann (1980). The synthetic signals are generated through a two-step procedure: first, the program *filon* calculates the theoretical seismograms in the frequency domain and then the program *wvint* produces the time series. The input parameters for *filon* are: source depth, epicentral distance, sample rate, number of points, crustal structure (thickness, V_P , V_S , density), attenuation values for P and S waves, and a phase velocity filter. The input parameters for *wvint* are the output of *filon*, and some aspects regarding to whether the seismograms will be in displacement, velocity or acceleration, the source type (impulse, trapezoid or parabolic), and duration.

The output of the Saikia and Burdick (1991) code generates the following ten Green's functions: vertical and radial components for a 45° dip-slip mechanism (strike: 0° ; dip: 45° ; rake: 90°); vertical, radial, and transverse components for a vertical dip-slip faulting (strike: 0° ; dip: 90° ; rake: 90°); vertical, radial, and transverse components for a vertical strike-slip mechanism (strike: 0° ; dip: 90° ; rake: 0°); and vertical and radial components for an explosion. These Green's functions are then combined to calculate three-component seismograms for a specific fault plane

solution and seismic moment. The three-component signals were configured to be plotted using both the *Buplot* libraries developed by R. Buland at the U.S. Geological Survey, Golden, Colorado, and the *SAC* (Lawrence Livermore National Laboratory: Seismic Analysis Code) program.

Due to the existence of only two stations located at regional distances from western Venezuela (*BOCO*, Colombia; *SJG*, Puerto Rico), we decided to look for another event that occurred in a different place that had been recorded for several stations at regional ranges. The September 21, 1993, Klamath Falls earthquake was the one selected to evaluate this methodology. Nevertheless, we generated synthetic seismograms for an event that occurred on July 22, 1993, near the Colombia-Venezuela border (Fig. 2).

The September 21, 1993, Klamath Falls Earthquake

The September 21, 1993, (03:28:55.4), Klamath Falls earthquake is an event of magnitude $m_b=5.8$ (*NEIC*) that occurred at 25 km northwest of Klamath Falls, in the southern part of the state of Oregon (Fig. 3). This was one of several events that occurred in that state during 1993 and the first of two stronger shocks that originated on September 21. The focal mechanisms determined by Dziewonski *et al.* (1994b), Sipkin and Needham (1994), and Braunmiller *et al.* (1995) show a tensional faulting striking approximately in the NW-SE direction (Fig.3). These fault plane solutions agree with the tectonics of the region, which is dominated by normal-faults trending in the north to northwest direction.

Crustal Models for Western United States Events

Several crustal structures were evaluated to estimate a preferred model. First, we used the simplified crustal model composed of a simple one layer over a half-space (Table 1), introduced by Helmberger and Engen (1980). This simplified crustal structure has been used in several studies to model P_{nl} globally. The general success of this simple model is due to the fact that at

long period the earth behaves like a layer over a half-space at these ranges. The detailed nature of the crust is not significant (Saikia and Burdick, 1991).

Second, we used a variation of the preferred crustal model selected by Saikia and Burdick (1991). The variation consisted in the substitution of their first 9 layers of 0.67 km thick each one, for only one layer of 6 km thick. The parameters of this crustal model are shown in Table 2. The near surface Q_β structure was taken from Lin (1989) and is appropriate for Basin and Range of the western United States. A relationship of $Q_\alpha=2Q_\beta$ was used for Q_α .

Third, we selected independent crustal structures for the path from the hypocenter to every station considered in the modeling, trying to generate the theoretical seismograms with realistic models (Zucca *et al.*, 1986; Mooney and Weaver, 1987; Pakiser, 1989). In this case, we also varied the values of Q_α and Q_β proposed by Lin (1989), Al-Khatib and Mitchell (1991), and a variation of the last one with a lower value of Q_β for the half-space (Tables 3-8).

Forward modeling

The stations included in the forward modeling were: *WDC* (azimuth=193°; Δ =198 km), *COR* (azimuth=338°; Δ =273 km), *CMB* (azimuth=163°; Δ =495 km), *SJO* (azimuth=175°; Δ =618 km), *ISA* (azimuth=156°; Δ =798 km), *DUG* (azimuth=104°; Δ =805 km), and *PAS* (azimuth=157°; Δ =967 km) (Fig. 3).

The data recorded at the stations mentioned above was retrieved from *IRIS* (Incorporated Research Institutions for Seismology) database at a sample rate of 20 samples/s. The instrument response was removed from the data and filtered with a four-pole Butterworth band-pass filter with corner frequencies of 0.01 and 8 Hz and cutoff frequencies of 0.005 and 10 Hz.

The synthetic seismograms calculated from the Saikia and Burdick (1991) were obtained in displacement, with a source depth of 11 km, and using a triangle, source time function of 2 s. To attenuate the presence on the theoretical signals of wave trains arriving after the *P*-waves, a phase velocity filter was included in the input parameters. The high cutoff and corner velocities of the phase velocity filter were fixed to 10000 and 30 km/s respectively in all cases considered in the forward modeling. However, the low corner and cutoff velocities varied according to the crustal

structures. For the low corner and cutoff velocities, we used the maximum value of V_S and the 91% of that figure respectively (Tables 3-8). The focal mechanism and the seismic moment determined by Dziewonski *et al.* (1994b) were utilized to generate the three-component seismograms for each station (Table 9).

The theoretical and observed signals were filtered using a third-order Butterworth low-pass frequency of 0.2 Hz. The time window of interest in this P_{nl} study varied from 60 to 150 s after the first arrival, according to the epicentral distance.

At station *WDC*, the results show a good visual correlation between the predicted and the observed seismograms for all the crustal structures considered in the modeling (Fig. 4). However, there are some differences related to the maximum amplitude of the signals. The smaller difference was obtained with the Zucca *et al.* (1986) crustal model (Fig. 4C) and the larger one with the modified Saikia and Burdick (1991) model (Fig. 4B).

At station *COR*, the theoretical seismograms also matched very well the recorded data (Fig. 5). In this case, with the modified Saikia and Burdick (1991) crustal model, the maximum amplitude of the synthetics and data were almost identical, whereas the larger difference was reached with the realistic model obtained from Mooney and Weaver (1989), but including a lower value of Q_β in the half-space. Also at station *CMB*, the minor difference in amplitude was observed when the modified Saikia and Burdick (1991) crustal model was used (Fig. 6). Here, on the contrary that we were expecting, the larger differences between the predicted and the observed data were reached with the three different more reliable models.

In general, the theoretical signals fit very well the recorded data in most of the models considered for station *SAO*; however, the modified Saikia and Burdick (1991) model reproduced better the waveforms and showed the second smaller difference in the amplitude (Fig. 7). At station *ISA*, undoubtedly the better visual correlation and the smaller differences in amplitude were achieved with the realistic crustal model taken from Mooney and Weaver (1989), combined with the Q_β values obtained from Al-Khatib and Mitchell (1991) (Fig. 8).

All the theoretical seismograms matched well the recorded signals at station *DUG*, except for that generated with the simplified crustal model (Fig. 9). The maximum amplitudes of the

predicted seismograms determined in this study coincided with the maximum amplitude of the recorded data.

The waveforms of the predicted seismograms calculated using the realistic crustal structure proposed by Mooney and Weaver (1989), combined with the values of Q_β determined by Al-Khatib and Mitchell (1991), fit very well the recorded data at station *PAS* (Fig. 10). Nevertheless, they presented the larger differences in amplitude.

On the basis of the results shown on Figures 4-10 and the knowledge that the Earth has a strong, though laterally varying, free surface gradient, we attempted to select a preferred model from those shown in Tables 1-8. The comparison revealed that the best visual correlation between the synthetic and the observed signals corresponds with the reliable crustal structures selected from the references. Nevertheless, for the case that we are interested on, that is the determination of a reliable fault plane solution, all the models utilized in the forward modeling permitted a very good visual correlation between the predicted and the recorded data, taking in account the parameters mentioned at the beginning of this section.

The July 22, 1993, Colombia-Venezuela Border Earthquake

The July 22, 1993, Colombia-Venezuela earthquake is an event of magnitude $m_b=6.1$ (*NEIC*) that occurred at about 60 km from the border of Colombia and Venezuela (Fig. 2). This has been one of the larger earthquakes that has occurred in this region during the last three decades. The focal mechanisms determined by Dziewonski *et al.* (1994b), by Sipkin and Needham (1994), and by Malavé and Suárez (1997) show a tensional faulting striking approximately in the N-S direction.

Only the station *SJG* (azimuth=23°; $\Delta=1396$ km) was included in the forward modeling. Unfortunately the another station available at regional distance from western Venezuela (*BOCO*, Colombia) was not in operation during the occurrence of this event. The data recorded at the station *SJG* was retrieved from *IRIS* database at a sample rate of 20 samples/s. The instrument

response was removed from the data and filtered with a four-pole Butterworth band-pass filter with corner frequencies of 0.01 and 8 Hz and cutoff frequencies of 0.005 and 10 Hz.

The synthetic seismograms calculated from the Saikia and Burdick (1991) were obtained in displacement, using the modified version of the preferred crustal structure suggested by them (Table 2). The source parameters obtained by Malavé and Suárez (1997) were utilized in this study as the input parameters to generate the seismograms: a source located at 18 km depth, a trapezoidal, source time function of 5 s, and a focal mechanism defined by a strike of 331° , a dip of 43° , and a rake of -131° . To attenuate the presence on the theoretical signals of wave trains arriving after the *P*-waves, a phase velocity filter was included in the input parameters. The high cutoff and corner velocities of the phase velocity filter were 10000 and 30 km/s respectively; whereas the low corner and cutoff velocities, were the maximum value of V_S (4.5 km/s) and the 91% of that figure (4.1 km/s), respectively.

The theoretical and observed data were filtered using a four-pole Butterworth band-pass filter with a low corner frequency of 0.01 Hz and a high corner frequency of 0.1 Hz. The time window of interest in this *P_{nl}* study was 150 s after the first arrival.

At station *SJG*, the results show a good visual correlation between the calculated and the observed seismograms (Fig. 11). However, there is a considerable difference between the maximum amplitudes measured on the theoretical (2.01×10^{-4}) and on the observed (3.41×10^{-4}) seismograms. It could be a consequence of being very close to the limit on distance of using the *P_{nl}* waves (12.6°).

Moment Tensor Inversion Using Regional Seismograms

In this section, we outline a technique to analyze the regional waveforms through out the moment tensor inversion and its application to several earthquakes occurred in western United States during 1993-94. The earthquakes included in this study are: the March 25, 1993, Scotts Mills event; the September 21, 1993, and the December 4, 1993, Klamath Falls earthquakes; the February 3, 1994, Wyoming event; the September 12, 1994, California-Nevada earthquakes (mainshock and aftershock); and the September 13, 1994, Colorado event (Fig. 12). The source parameters for each one of these events determined by different seismological agencies, institutions, or individual workers, are described in Table 9: the origin time, the epicenter location, the magnitude, the focal depth, the fault plane solution, and the seismic moment.

Methodology

Our aim in this work was to compile different existent tools to generate focal mechanisms as an *automatic routine*, using regional seismograms. In that sense, for each event, the following procedure was followed. The observed waveforms were retrieved from the *USNSN* (United States National Seismographic Network), using the program *ttimes*, based on the *tau-spline* method of Buland and Chapman (1983) to determine the stations included at regional ranges ($\Delta \leq 12^\circ$) from the epicenter. The data was transformed from the *Retrieve* format to *SAC* format, since most of the other codes in the procedure use that format. In some cases, the data was retrieved from the *IRIS* database in the *SEED* format and then converted to *SAC* format. The instrument response was removed from the broadband data and filtered with a four-pole Butterworth band-pass filter with corner frequencies of 0.01 and 8 Hz and cutoff frequencies of 0.005 and 10 Hz.

The synthetic seismograms were generated using a code (*mijkennett*) written by Randall (1994). The input parameters for *mijkennett* are: the source depth, the epicentral distance, the station azimuth, the sample rate, the number of points in the time series, the crustal model (thickness, V_P , V_S , density), the attenuation values for *P* and *S* waves, and the phase velocity

filter. In the automatic procedure, the number of points in the seismograms was estimated in according to the epicentral ranges. For distances between 0 and 499 km, the time series were defined for 256 points; whereas for ranges greater than 500 km, the number of points was 512. Those numbers of points are large enough to avoid the truncation of the signals, assuming a maximum frequency of 0.5 Hz, that implies a sample rate of one sample per second. For each event analyzed in this study, we used a crustal structure suggested by Ammon (1994, personal communication) for the Central United States (*CUS*) (Table 10) and the Basin and Range (*BASIN*) crustal model proposed by Patton and Taylor (1984) (Table 11). In both cases, the phase velocity filter was designed to permit the entire seismograms.

The output of the *mijkennett* program is the file *mspec*, which contains the spectral Green's functions that are transformed to time-domain Green's functions by the program *tsynth*. In *tsynth*, it must be specified whether the output will be in displacement or velocity, and the type of source you want to use: an impulse or a step function. The program *tsynth* generates eighteen (18) Green's functions for each station, which correspond with the radial, transverse, and vertical components of the six elements of the seismic moment tensor. The Green's functions are combined to obtain three-component seismograms for the three basic focal mechanisms: vertical strike-slip (0,90,0), vertical dip-slip (0,90,90), and 45° dip-slip (0,45,90).

The observed and theoretical seismograms were band-pass filtered and windowed using macros running on the *SAC* code, and then, they were prepared for the inversion. The low-pass cutoff frequency was chosen on the basis of the initial magnitude estimated. A single band-pass filter was applied to the entire waveform. Thus, high-amplitude fundamental mode surface wave seismograms dominate the inversion.

The beginning of the time-window inversion is fixed on the synthetic seismograms, using a program (*marktime*) that calculates the theoretical first arrival-time, based on the same crustal structure used in the program *mijkennett* to generate the synthetic seismograms. The beginning of the time-window inversion is fixed on the observed data using the readings of the first arrivals determined by the *NEIC*.

The moment-tensor inversion scheme was achieved through a program written by Ammon (1994, personal communication) called *mintv*. The observed and synthetic seismograms must have the same amount of points in order to have the inversion routine to work. The predicted and observed signals were not realigned during the inversion. Thus, *the results are strongly dependent on the crustal models and on how well the theoretical travel-times match the NEIC first-arrival readings*. No source depths were estimated in this study, since it has been observed a variance reduction of less than 10% in the inversion results for earthquakes occurred in the upper crust (Ritsema and Lay, 1995).

In order to have the whole process working as an automatic routine, several shell programs and *SAC* macros were developed to follow the procedure described previously.

The March 25, 1993, Scotts Mills Earthquake

The Scotts Mills earthquake of March 25, 1993 ($m_b=5.5$; *NEIC*), was the first of several unusually strong earthquakes felt in Oregon during 1993 (Nábelek and Xia, 1995). It occurred in the foothills of the Cascade mountains, at ~35 km east of Salem, Oregon. The fault plane solutions of this event determined by Dziewonski *et al.* (1994a) and by Nábelek and Xia (1995) show a compressional faulting, combined with a component of lateral movement, striking in the northeast direction; whereas the focal mechanism calculated by Ritsema and Lay (1995) indicates an almost strike slip lateral motion, trending in the northeast direction (Fig. 13).

The regional stations and components used in the moment tensor inversion of this earthquake are indicated in Table 12. The records of those stations were retrieved from *IRIS* database at 20 samples per second, and then converted to *SAC* format. The synthetic seismograms were determined assuming a source depth of 15 km. The theoretical and observed waveforms were filtered using a four-pole Butterworth band-pass filter with a low corner frequency of 0.010 Hz and a high corner frequency of 0.033 Hz. The time window of interest in this study varied from 5 s before to 400 s after the first arrival, according to the epicentral ranges (Table 12).

The results obtained from the moment tensor inversion using regional seismograms are shown on Figures 14 and 15. The predicted seismograms at the transverse component of all stations fit very well the observed data. However, at the radial and vertical components, the correlation is not as good as at the transverse. The focal mechanisms obtained from the inversion procedure using both the *CUS* and the *BASIN* models are similar (Table 9; Fig. 13). They indicate a compressional faulting, as determined by Dziewonski *et al.* (1994a) and by Nábelek and Xia (1995), but with nodal planes striking in the almost north-south direction.

The September 21, 1993, Klamath Falls Earthquake

As mentioned before, several earthquakes ruptured in the State of Oregon during 1993. On September 21, 1993, two stronger shocks of magnitude $m_b=5.8$ and 5.5 (*NEIC*) occurred at 25 km northwest of Klamath Falls, in the southern part of the state. The origin times of these earthquakes are 03:28:55.4 and 05:45:34.0 (Figs. 16 and 17). The focal mechanisms for the first of these events obtained by Dziewonski *et al.* (1994b), Sipkin and Needham (1994), Braunmiller *et al.* (1995), and Ritsema and Lay (1995) show a tensional faulting striking approximately in the *NW-SE* direction (Fig.16). The fault plane solutions of the second earthquake estimated by Dziewonski *et al.* (1994b), Braunmiller *et al.* (1995), and Ritsema and Lay (1995) indicate a tensional faulting similar than one of the previous event, but with nodal planes trending in the north-south direction. All these fault plane solutions agree with the tectonics of the region, which is dominated by normal-faults trending in the north to northwest direction. In this study, we analyzed only the first of those events, whose results are presented later.

The regional stations and components used in the moment tensor inversion of this earthquake are shown in Table 13. The records of those stations were retrieved from *USNSN* database in the *Retrieve* format at 20 samples per second, and then converted to *SAC* format. The synthetic seismograms were calculated assuming a source depth of 11 km, determined by the *NEIC* using broadband displacement seismograms. The predicted and observed waveforms were filtered using a four-pole Butterworth band-pass filter with a low corner frequency of 0.010 Hz

and a high corner frequency of 0.033 Hz. The time window of interest in this study varied from 5 s before to 250 s after the first arrival, according to the epicentral ranges (Table 13).

The results obtained from the moment-tensor inversion using the *CUS* and *BASIN* crustal structures are very similar (Figs. 18 and 19). The fit between the predicted and the observed waveforms is good in almost all the station/components. The focal mechanisms calculated in this study exhibit normal faulting trending in the *N-S* direction (Fig. 16; Table 9); whereas the nodal planes of the previous workers in average strike in the *NW-SE* direction. However, the solutions determined in this study have nodal planes as those estimated by previous workers for the second shock

The December 4, 1993, Klamath Falls Earthquake

On December 4, 1993 (22:15:19.5), another moderate earthquake of magnitude $m_b=5.2$ (*NEIC*) occurred in the area of Klamath Falls, State of Oregon. The focal mechanisms determined by Dziewonski *et al.* (1994c) and Braunmiller *et al.* (1995) are similar than those obtained by them for the events ruptured on September 21, 1993 (03:28:55.4) (Fig. 20). Those mechanisms indicate normal faulting striking in the *NW-SE* direction.

The regional stations and components used in the moment tensor inversion of this earthquake are exhibited in Table 14. The seismograms of those stations were retrieved from *IRIS* and the *USNSN* databases at a sample rate of 20 samples per second. The theoretical seismograms were calculated assuming the source depth of 8 km estimated by the *NEIC*. The theoretical and the recorded data were filtered using a four-pole Butterworth band-pass filter with a low corner frequency of 0.010 Hz and a high corner frequency of 0.033 Hz. The time window of interest in this study varied from 5 s before to 300 s after the first arrival, according to the epicentral ranges (Table 14).

The fit between the synthetic and the observed seismograms is good in most of the cases, except in the vertical component of station *DUG* and in the transverse components of stations *CMB* and *ISA* (Figs. 21 and 22). The focal mechanisms obtained from the inversion procedure in

this study are similar to those determined by Dziewonski *et al.* (1994c) and Braunmiller *et al.* (1995) (Fig. 20; Table 9). All of them show tensional faulting with nodal planes trending in the *NW-SE* direction.

The February 3, 1994, Wyoming Earthquake

On February 3, 1994 (09:05:04.2), an earthquake of magnitude $m_b=5.4$ (*NEIC*) nucleated close to the Idaho-Wyoming border (Fig. 23). This event was felt in the epicentral area, where some damage (VII) was reported. The focal mechanisms calculated for this earthquake by Dziewonski *et al.* (1994d), Oregon State University, Ritsema and Lay (1995), and Sipkin and Zirbes (1996), indicate tensional faulting (Fig. 23). The nodal planes of the fault plane solutions of the first three authors strike approximately in the north-south direction, whereas the planes of the Sipkin and Zirbes' solution trend in the northeast-southwest direction.

The regional stations and components used in the moment tensor inversion of this earthquake are shown in Table 15. The records of those stations were retrieved from *IRIS* database at 20 samples per second. The synthetic seismograms were assuming a source depth of 8 km, estimated from broadband displacement seismograms by the *NEIC*. The synthetic and observed data were filtered using a four-pole Butterworth band-pass filter with a low corner frequency of 0.010 Hz and a high corner frequency of 0.033 Hz. The time window of interest in this study varied from 5 s before to 250 s after the first arrival, according to the epicentral ranges (Table 15).

The results obtained from the moment-tensor inversion in this study using both the *CUS* and the *BASIN* crustal models did not fit well the recorded seismograms (Figs. 24 and 25). Only in the transverse component of station *ALQ*, and the vertical and radial components of station *NEW*, the predicted seismograms matched well the first arrivals, but not the entire seismograms. The focal mechanisms calculated in this study differ from the mechanisms determined by previous workers (Fig. 23; Table 9). In spite of all the solutions estimated for this event indicate

normal faulting, the orientation of the nodal planes obtained here differ by almost 90° from those determined by previous workers.

The September 12, 1994, California-Nevada Earthquakes (Mainshock and Aftershock)

On September 12, 1994 (12:23:42.2), an earthquake of magnitude $m_b=5.1$ ($M_L=6.3$; *NEIC*) occurred close to the California-Nevada border, at about 30 km east-southeast of South Lake Tahoe, California (Fig. 26). The same day, at about 11.5 hours later (23:57:08.4), an aftershock of magnitude $m_b=4.6$ ($M_L=5.3$, *NEIC*) occurred (Fig. 27). This aftershock was felt in the epicentral area and as far away as San Francisco, California. The focal mechanisms obtained for the mainshock by Dziewonski *et al.* (1995), the Earthquake Research Institute, and Sipkin and Zirbes (1996) show a predominant strike-slip faulting, combined with a small component of normal fault, with one of the nodal planes oriented in the northwest-southeast direction. No fault plane solution was obtained for the aftershock before this study.

The regional stations and components used in the moment-tensor inversion of the mainshock and aftershock are shown in Tables 16 and 17. The records of those stations were retrieved from the *USNSN* database at a sample rate of 20 samples per second. The synthetic seismograms were calculated assuming a source depth of 10 km, estimated from broadband displacement seismograms. The predicted and the recorded data were filtered using a four-pole Butterworth band-pass filter with a low corner frequency of 0.010 Hz and a high corner frequency of 0.05 Hz for the mainshock and a low corner frequency of 0.010 Hz and a high corner frequency of 0.033 Hz for the aftershock. The time window of interest in this study varied from 5 s before to 400 s after the first arrival, according to the epicentral ranges (Tables 16 and 17).

The comparison between the synthetic and the observed data for the mainshock are shown on Figures 28 and 29. In general, the fit between the theoretical and recorded waveforms is not as good as in other events. The focal mechanisms obtained in this study using both crustal structures agree with those estimated by previous workers (Fig. 26, Table 9). They correspond with a mainly strike-slip fault, combined with a small component of tensional movement.

The match between the predicted and the recorded seismograms, even though is better than that for the mainshock, is not as good as expecting (Figs. 30 and 31). The focal mechanisms obtained from the inversion procedure are exhibit in Fig. 27 and in Table 9. In this case, we did not have any fault plane solution to compare, since no fault plane solution was determined by another worker before this study. Anyway, the focal mechanisms calculated using both the *CUS* and the *BASIN* models show normal faulting trending in the northwest-southeast direction.

The September 13, 1994. Colorado Earthquake

On September 13, 1994, a moderate earthquake of magnitude $m_b=4.5$ ($M_L=4.6$; *NEIC*) occurred in western Colorado, at about 30 km south-southwest of Montrose, Colorado (Fig. 32). This earthquake was felt strongly in the epicentral area and as far north as Grand Junction, Colorado. No focal mechanism of this event was reported previously due to its low magnitude, which did not permitted to be recorded at teleseismic distances with a good signal-to-noise ratio.

The regional stations and components used in the moment tensor inversion of this earthquake are shown in Table 18. The records of those stations were retrieved from *USNSN* database in the *Retrieve* format at a sample rate of 20 samples per second, and then converted to *SAC* format. The theoretical seismograms were assuming a source depth of 10 km. The synthetic and observed data were filtered using a four-pole Butterworth band-pass filter with a low corner frequency of 0.01 Hz and a high corner frequency of 0.1 Hz. In this case, it was necessary to filter in a higher range of frequencies due to the absence of energy at longer periods. The time window in the seismograms considered in this study varied from 5 s before to 175 s after the first arrival, according to the epicentral distances (Table 18).

The comparison between the predicted and the observed data are shown on Figure 33 for the *CUS* model and on Figure 34 for the *BASIN* model. In both cases, the fit between the theoretical and the recorded seismograms is satisfactory only in the components of station *GOL*. The fault plane solutions obtained for this event are included on Table 9 and Figure 30. This was the only case of all events studied here that the focal mechanisms differ from the *CUS* to the

BASIN models. The first one corresponds with an almost vertical dip-slip faulting, whereas the mechanism obtain with the *BASIN* model indicates a predominant strike-slip fault plane.

Attempts to Analyze Earthquakes in Western Venezuela

One of the critical aspects in applying the techniques described above in western Venezuela is the amount of stations available at regional distances. As a first step, we decided to analyze the earthquakes with magnitude $m_b \geq 5.4$ for which an inversion of teleseismic body-waves was achieved by *Malavé and Suárez* (1997).

For earthquakes that occurred before 1978, only the seismograms recorded at stations from the *WWSSN* (World-Wide Standard Seismograph Network) were available. At regional distances, we considered the stations: *BOG* (Colombia), *CAR* (Venezuela), *QUI* (Ecuador), *UPA* (Panama), *SJG* (Puerto Rico), and *TRN* (Trinidad). None of the earthquakes that occurred from 1964 to 1978 could be analyzed due to the low signal-to-noise ratio on the seismograms.

For earthquakes that occurred after 1978, seismograms at stations from the *GDSN* (Global Digital Seismograph Network) were collected. Unfortunately, only a few stations were available at regional distances during this time period. The station *BOCO* (Colombia) was operating as a *SRO* (Seismic Research Observatory) station since March 13, 1978, until November 11, 1987. On June 6, 1994, *BOCO* was transformed in a *GSN* (Global Seismograph Network) station. Other *GSN* seismological stations at regional distances from western Venezuela are: *SJG*, deployed in San Juan, Puerto Rico, on May 26, 1993; *SDV*, which has been operating in Santo Domingo, Venezuela, since August 19, 1994; *JTS*; deployed in Costa Rica on April 23, 1995; *PTG.A*, which has been operating in Brazil since November 15, 1995. The station (*CAR*) is planned to be installed in Caracas, Venezuela, on July, 1997.

With the stations mentioned above in operation, we will be able to test the routines considered in this study (forward modeling and moment tensor inversion) for earthquakes that will occur in western Venezuela in the near future.

Discussion and Conclusions

Forward modeling and moment tensor inversion processes were analyzed to obtain focal mechanisms using long-period seismograms recorded at regional distances. The motivation of this study was to determine fault plane solutions of moderate-sized earthquakes ($m_b \leq 5.3$) that occurred in western Venezuela, that help us to understand the complex tectonic environment in this region. However, only two broadband stations were deployed in western Venezuela during the development of this study. Instead, several moderate-sized earthquakes that occurred in western United States during 1993 and 1994 were taken into account to evaluate the methodologies. Only for an earthquake nucleated on July 22, 1993, near the Colombia-Venezuela border, we were able to access a recorded seismogram at station *SJG*, located at ~1400 km from the epicenter.

For the *P_{nl}* forward modeling analysis, we used the September 21, 1993, Klamath Falls earthquake and the July 22, 1993, Colombia-Venezuela border. For the first one, we generated synthetic waveforms using different crustal structures that varied from a simple layer over a halfspace to more reliable crustal models obtained by previous workers for every station included in this study. The waveforms obtained for all the crustal models, in general, matched very well the recorded seismograms. However, they differ in the maximum amplitude of the signals, reflecting attenuation problems related to the crustal structures.

The results obtained from the moment tensor inversions, using regional seismograms recorded from earthquakes originated in western United States, satisfied the initial expectation established at the beginning of this study. In most of the cases studied, the focal mechanisms calculated from the inversion using the *CUS* and the *BASIN* models are consistent with the fault plane solutions determined by previous workers. In conclusion, considering the initial condition of developing a tool for working as an automatic routine, the results are acceptable of using with the models mentioned above.

Several aspects influenced in our results. The first one and the most important is related to the crustal structure. Undoubtedly, we need to consider more reliable crustal models to reduce the

path effects and to minimize the uncertainties in the estimation of the theoretical first arrival-time. This value is used on the synthetics to fix the beginning of the time-window inversion. Another point is related to the station azimuthal coverage. Adequate sampling of the Love and Rayleigh wave radiation must be available for stable inversions (Fukushima *et al.*, 1989), but this is ensured by the regional distribution of stations. In most of the events analyzed in this study, we were not able to compile information with a good azimuthal coverage.

The phase mismatches, arising from unmodeled propagation effects, were not corrected by realigning the waveforms. No source depth tests were made in this study, but the source depths considered in all the cases can be considered as reliable values, since most of them were computed using broadband displacement seismograms. Moreover, long-period surface waves are relatively insensitive to source depth variations.

The advantage of this moment-tensor inversion method over the forward modeling using body waves is that it is easier to be made into an automatic process suitable for real-time purposes. Another advantage is the determination of reliable estimates of seismic moments on a routine basis for moderate-sized events.

In a near future, we will be able to determine the earthquake source parameters in western Venezuela, based on regional data. We are concerned about the possibility to do this work as a near-real time, automatic routine in this region due to the unavailability of data in a short time after the occurrence of an earthquake. However, the fact of having access to those tools that permit us to obtain focal mechanisms using regional seismograms, could be a great contribution to the knowledge and understanding of the regional tectonics in western Venezuela. Furthermore, it would be useful for several post-earthquake hazard response activities. We accept that we need to do several tests to have this tool ready working in this area, but the experience gained on this study permit us to augur good results when we will have the stations ready.

Acknowledgments. This work was performed while one of the authors (*GM*) was visiting the U. S. Geological Survey in Golden, Colorado. The use of facilities is greatly appreciated. We thank C. Saikia, G. Randall, and C. Ammon for giving us a copy of their codes. H. Benz made us easy the contact with G. Randall and C. Ammon.

References

- Al-Khatib, H. H. and B. J. Mitchell (1991). Upper mantle anelasticity and tectonic evolution of the western United States from surface wave attenuation, *J. Geophys. Res.* **96**, 18129-18146.
- Ammon, C. J., A. A. Velasco, and T. Lay (1993). Rapid determination of rupture directivity: Application to the 1992 Landers ($M_S=7.4$) and Cape Mendocino ($M_S=7.2$) California earthquakes, *Geophys. Res. Lett.* **20**, 97-100.
- Bouchon, M. (1981). A simple method to calculate Green's functions for elastic layered media, *Bull. Seismol. Soc. Am.* **71**, 959-971.
- Braunmiller, J., J. Nábelek, B. Leitner, and T. Qamar (1995). The 1993 Klamath Falls, Oregon, earthquake sequence: Source mechanisms from regional data, *Geophys. Res. Lett.* **22**, 105-108.
- Buland, R. and C. Chapman (1983). The computation of seismic travel times, *Bull. Seismol. Soc. Am.* **73**, 1271-1302.
- Dewey, J. (1972). Seismicity and tectonics of western Venezuela, *Bull. Seismol. Soc. Am.* **62**, 1711-1751.
- Dreger, D. S. and D. V. Helmberger (1993). Determination of source parameters at regional distances with three-component sparse network data, *J. Geophys. Res.* **98**, 8107-8125.
- Dziewonski, A. M., A. T. Chou, and J. H. Woodhouse (1981). Determination of earthquakes source parameters from waveform data for studies of global and regional seismicity, *J. Geophys. Res.* **86**, 2825-2852.
- Dziewonski, A. M. G. Ekström, and M. P. Salganik (1994a). Centroid-moment tensor solutions for January-March 1993, *Phys. Earth Planet. Int.* **82**, 9-17.
- Dziewonski, A. M. G. Ekström, and M. P. Salganik (1994b). Centroid-moment tensor solutions for July-September 1993, *Phys. Earth Planet. Int.* **82**, 165-174.
- Dziewonski, A. M. G. Ekström, and M. P. Salganik (1994c). Centroid-moment tensor solutions for October-December 1993, *Phys. Earth Planet. Int.* **85**, 215-225.

- Dziewonski, A. M. G. Ekström, and M. P. Salganik (1994d). Centroid-moment tensor solutions for January-March 1994, *Phys. Earth Planet. Int.* **86**, 253-261.
- Dziewonski, A. M. G. Ekström, and M. P. Salganik (1995). Centroid-moment tensor solutions for July-September 1994, *Phys. Earth Planet. Int.* **90**, 1-11.
- Fukushima, T., D. Suetsugu, I. Nakanishi, and I. Yamada (1989). Moment tensor inversion for near earthquakes using long-period digital seismograms, *J. Phys. Earth*, **37**, 1-29.
- Giardini, D., E. Boschi, and B. Palombo (1993). Moment tensor inversion from Mednet data. (2) Regional earthquakes of the Mediterranean, *Geophys. Res. Lett.* **20**, 273-276.
- Hartzell, S. H. and T. H. Heaton (1983). Inversion of strong ground motions and teleseismic waveform data for the fault rupture history of the 1979 Imperial Valley, California earthquake, *Bull. Seismol. Soc. Am.* **73**, 1553-1583.
- Helmberger, D. V. and G. R. Engen (1980). Modeling the long period body waves from shallow earthquakes at regional ranges, *Bull. Seismol. Soc. Am.* **70**, 1699-1714.
- Herrmann, R. B. and C. Y. Wang (1985). A comparison of synthetic seismograms, *Bull. Seismol. Soc. Am.* **75**, 41-56.
- Kafka A. and D. Weidner (1981). Earthquake focal mechanisms and tectonics processes along the southern boundary of the Caribbean plate, *J. Geophys. Res.* **86**, 2877-2888, 1981.
- Kanamori, H. and G. S. Stewart (1976). Mode of the strain release along the Gibbs Fracture Zone, Mid-Atlantic ridge, *Phys. Earth Planet Inter.* **11**, 312-332.
- Kanamori, H., J. Mori, and T. H. Heaton (1990). The 3 December 1988, Pasadena earthquake ($M_L=4.9$) recorded with the very broadband system in Pasadena, *Bull. Seismol. Soc. Am.* **80**, 483-487.
- Kanamori, H., H. K. Thio, D. Dreger, and E. Hauksson (1992). Initial investigation of the Landers, California, earthquake of 28 June 1992 using TERRAScope, *Geophys. Res. Lett.* **19**, 2267-2270.
- Kennett, B. L. N. (1980). Seismic wave propagation in stratified media, Cambridge University Press, New York, 342 pp., 1980.

- Langston, C. A. and D. V. Helmberger (1975). A procedure for modeling shallow dislocation sources, *Geophys. J. R. Astron. Soc.* **42**, 117-130.
- Lay, T., J. Ritsema, C. J. Ammon, and T. Wallace (1994). Rapid source mechanism analysis of the April 29, 1993 Cataract Creek (MW=5.3), Northern Arizona earthquake. *Bull. Seismol. Soc. Am.* **84**, 451-457.
- Lay, T., C. J. Ammon, A. A. Velasco, J. Ritsema, T. C. Wallace, and H. J. Patton (1994). Near-real-time seismology: Rapid analysis of earthquake faulting. *GSA Today* **4**, 129, 132-134.
- Lin, W. J. (1989). Rayleigh wave attenuation in basin and range province. M.S. thesis, 54 pp., Saint Louis University, St. Louis, Mo.
- Malavé, G. and G. Suárez (1997). Recent shallow seismicity in western Venezuela: regional tectonic implications, submitted to *J. Geophys. Res.*
- Mallick, S. and L. N. Frazer (1987). Practical aspects of reflectivity modeling. *Geophysics* **52**, 1355-1364.
- Mooney, W. and C. Weaver (1989). Regional crustal structure and tectonics of the Pacific Coastal States; California, Oregon, and Washington. *Geol. Soc. Am.*, memoir **172**, 129-161.
- Nábelek, J. (1984). Determination of earthquake source parameters from inversion of body waves, Ph.D. thesis, Massachusetts Institute of Technology, Cambridge, 361 p.
- Nábelek, J. and G. Xia (1995). Moment-tensor analysis using regional data: Application to the 25 March, 1993, Scotts Mills, Oregon earthquake. *Geophys. Res. Lett.* **22**, 13-16.
- Pakiser, L. C. (1989). Geophysics of the Intermontane system. *Geol. Soc. Am.*, memoir **172**, 235-247.
- Patton, H. J. and S. R. Taylor (1984). Q structure on the Basin and Range from surface waves. *J. Geophys. Res.* **89**, 6929-6940.
- Patton, H. J. and G. Zandt (1991). Seismic moment tensors of western United States earthquakes and implications for the tectonic stress field. *J. Geophys. Res.* **96**, 18245-18259.
- Randall, G. (1994). Efficient calculation of complete differential seismograms for laterally homogeneous earth models. *Geophys. J. Int.* **118**, 245-254.

- Ritsema, J. and T. Lay (1993). Rapid source mechanism determination of large ($M_H \geq 5$) earthquakes in the western United States. *Geophys. Res. Lett.* **20**, 1611-1614.
- Ritsema, J. and T. Lay (1995). Long-period regional wave moment tensor inversion for earthquakes in the western United States. *J. Geophys. Res.* **100**, 9853-9864.
- Romanowicz, B., D. Dreger, M. Pasyanos, and R. Uhrhammer (1993). Monitoring of strain release in central and northern California using broadband data. *Geophys. Res. Lett.* **20**, 1643-1646.
- Saikia, C. K. and L. J. Burdick (1991). Fine structure of *P*nt waves from explosions. *J. Geophys. Res.* **96**, 14383-14401.
- Sipkin, S. A. (1982). Estimation of earthquake source parameters by the inversion of waveform data: synthetic seismograms, *Phys. Earth Planet. Int.* **30**, 242-259.
- Sipkin, S. A. and R. E. Needham (1994). Moment-tensor solutions estimated using optimal filter theory: global seismicity, 1993, *Phys. Earth Planet. Int.* **86**, 245-252.
- Sipkin, S. A. and M. D. Zirbes (1996). Moment-tensor solutions estimated using optimal filter theory: global seismicity, 1994, *Phys. Earth Planet. Int.* **93**, 139-146.
- Thio, H. K. and H. Kanamori (1995). Moment tensor inversion for local earthquakes using surface waves recorded at TERRAScope, *Bull. Seismol. Soc. Am.* **85**, 1021-1038.
- Uhrhammer, R. (1992). Broadband near-field moment tensor inversion, *EOS Trans. AGU.*, **73**.
- Wald, D. J., D. V. Helmberger, and T. H. Heaton (1991). Rupture model of the 1989 Loma Prieta earthquake from the inversion of strong-motion and broadband teleseismic data. *Bull. Seismol. Soc. Am.* **81**, 1540-1572.
- Wallace, T. C. and D. V. Helmberger (1982). Determining source parameters of moderate-size earthquakes from regional waveforms. *Phys. Earth Planet. Inter.* **30**, 185-196.
- Wang, C. Y. and R. B. Herrmann (1980). A numerical study of P, SV, and SH wave generation in a plane layered medium, *Bull. Seismol. Soc. Am.* **70**, 1015-1036.
- Zhao, L. S. and D. V. Helmberger (1994). Source estimation from broadband regional seismograms. *Bull. Seismol. Soc. Am.* **84**, 91-104.

Zucca, J. J., G. S. Fuis, B. Milkereit, W. Mooney, and R. D. Catchings (1986). Crustal structure of northeastern California, *J. Geophys. Res.* **91**, 7359-7382, 1986.

Table 1
Simplified crustal model used in the forward modeling

Layer	Thickness km	V_P km/s	V_S km/s	Density g/cm ³	Q_α	Q_β
1	30	5.81	3.40	2.8	600	300
2	Half-space	8.00	4.70	3.1	5000	2500

Table 2
A variation of the crustal model used by Saikia and Burdick (1991).

Layer	Thickness km	V_P km/s	V_S km/s	Density g/cm ³	Q_α	Q_β
1	6	5.80	3.28	2.4	120	60
2	26	6.20	3.50	2.7	1200	600
3	Half-space	8.20	4.50	3.4	5000	2500

Table 3
Crustal model (Zucca *et al.*, 1986) used to generate the synthetic P_{nl} signals at station *WDC*.
The values of Q_β are from (1) Lin (1989); (2) Al-Khatib and Mitchell (1991);
and (3) the same values of (2), except for a low Q_β in the half-space.

Layer	Thickness km	V_P km/s	V_S km/s	Density (1) g/cm ³	Q_β (1)	Density (2,3) g/cm ³	Q_β (2)	Q_β (3)
1	3	5.50	3.18	2.40	40	2.65	28	28
2	11	6.40	3.70	2.70	150	2.79	29	29
3	26	7.00	4.05	2.85	600	2.86	80	80
4	Half-space	8.00	4.62	3.40	2500	3.40	2500	315

Table 4

Crustal model (Mooney and Weaver, 1989) used to generate the synthetic P_{nl} signals at station *COR*. The values of Q_{β} are from (1) Lin (1989); (2) Al-Khatib and Mitchell (1991); and (3) the same values of (2), except for a low Q_{β} in the half-space.

Layer	Thickness km	V_p km/s	V_s km/s	Density (1) g/cm ³	Q_{β} (1)	Density (2,3) g/cm ³	Q_{β} (2)	Q_{β} (3)
1	3	4.50	2.60	2.20	60	2.48	28	28
2	26	6.20	3.58	2.70	500	2.75	35	35
3	13	7.00	4.05	2.85	600	2.86	100	100
4	Half-space	7.70	4.45	3.10	2500	3.10	2500	315

Table 5

Crustal model (Mooney and Weaver, 1989) used to generate the synthetic P_{nl} signals at station *SAO*. The values of Q_{β} are from (1) Lin (1989); (2) Al-Khatib and Mitchell (1991); and (3) the same values of (2), except for a low Q_{β} in the half-space.

Layer	Thickness km	V_p km/s	V_s km/s	Density (1) g/cm ³	Q_{β} (1)	Density (2,3) g/cm ³	Q_{β} (2)	Q_{β} (3)
1	6	4.50	2.60	2.30	60	2.48	28	28
2	2	5.50	3.18	2.40	500	2.65	28	28
3	6	6.10	3.53	2.60	600	2.74	29	29
4	6	6.80	3.93	2.70	600	2.82	29	29
5	6	7.30	4.22	2.85	600	2.95	40	40
6	Half-space	8.00	4.62	3.30	2500	3.30	2500	80

Table 6

Crustal model (Mooney and Weaver, 1989) used to generate the synthetic P_{nl} signals at stations *CMB*, *ISA*, and *PAS*. The values of Q_{β} are from Lin (1989).

Layer	Thickness km	V_p km/s	V_s km/s	Density g/cm ³	Q_{β}
1	6	4.50	2.60	2.30	60
2	2	5.50	3.18	2.40	500
3	6	6.10	3.53	2.60	600
4	6	6.80	3.93	2.70	600
5	6	7.30	4.22	2.85	600
6	Half-space	8.00	4.62	3.30	2500

Table 7

Crustal model (Mooney and Weaver, 1989) used to generate the synthetic P_{nl} signals at stations *CMB*, *ISA*, and *PAS*. The values of Q_{β} are from (2) Al-Khatib and Mitchell (1991) and (3) the same values of (2), (3) except for a low Q_{β} in the half-space.

Layer	Thickness km	V_p km/s	V_s km/s	Density (2,3) g/cm ³	Q_{β} (2)	Q_{β} (3)
1	6	5.20	3.01	2.60	28	28
2	19	6.20	3.58	2.75	29	29
3	23	6.90	3.99	2.85	200	200
4	Half-space	7.90	4.57	3.20	2500	315

Table 8

Crustal model (Pakiser, 1989) used to generate the synthetic P_{nl} signals at station *DUG*.

The values of Q_β are from (1) Lin (1989); (2) Al-Khatib and Mitchell (1991);

and (3) the same values of (2), except for a low Q_β in the half-space.

Layer	Thickness km	V_p km/s	V_s km/s	Density (1) g/cm ³	Q_β (1)	Density (2,3) g/cm ³	Q_β (2)	Q_β (3)
1	19	6.00	3.47	2.40	150	2.71	55	55
2	12	6.70	3.87	2.70	500	2.83	135	135
3	Half-space	8.00	4.62	3.30	2500	3.30	2500	470

Determination of focal mechanisms using regional data

 Table 9
 Focal parameters obtained by previous workers for the events analyzed in this study.

Event	Origin Time	Lat. N	Lon. W	Source	Mw	Depth km	Strike deg	Dip deg	Rake deg	M ₀ 10 ¹⁷ N ^m
Mar. 25, 1993	13:34:35.4	45.04	122.61	Harvard	5.6	15	51	44	32	3.15
				Oregon	5.5	13	56	63	45	2.48
				R&L	5.6	22	310	75	173	3.40
				This Study ¹	5.5	15	359	50	79	2.30
				This Study ²	5.6	15	352	62	80	3.01
Sept. 21, 1993	03:28:55.4	42.31	122.01	Harvard	6.0	15	170	31	-76	10.85
				NEIC	5.9	11	164	25	-71	10.10
				Oregon	6.0	9	172	45	-75	11.40
				R&L	6.0	8	343	46	-83	11.00
				This Study ¹	5.8	11	4	73	-83	6.09
Sept. 21, 1993	05:45:33.7	42.35	122.02	This Study ²	5.8	11	194	12	-87	6.41
				Harvard	5.9	15	182	34	-85	10.07
				Oregon	6.0	9	172	48	-89	11.30
				R&L	6.0	8	1	46	-83	11.00
				Harvard	5.4	15	139	41	-104	1.60
Dec. 4, 1993	22:15:19.5	42.30	122.01	Oregon	5.5	6	162	43	-79	1.85
				This Study ¹	5.3	8	134	52	-104	1.04
				This Study ²	5.3	8	123	55	-104	0.93
				Harvard	5.8	15	4	40	-79	5.58
Feb. 3, 1994	09:05:04.2	42.76	110.98	NEIC	5.8	8	45	42	-63	2.90
				Oregon	6.0	12	2	18	-87	10.70
				R&L	5.7	4	356	32	-93	4.20
				This Study ¹	8	96	81	-96		
				This Study ²	5.8	8	101	82	-99	6.34
Sept. 12, 1994	12:23:43.2	38.82	119.65	ERI	---	10	40	74	-31	7.48
				Harvard	5.9	15	42	74	-13	8.41
				NEIC	6.0	14	135	63	-176	14.00
				This Study ¹	5.8	10	43	68	-3	5.50
				This Study ²	5.8	10	42	62	-4	5.05
Sept. 12, 1994	23:57:09.8	38.76	119.74	This Study ¹	5.1	10	161	31	-80	4.75
				This Study ²	5.1	10	164	27	-76	4.23
				This Study ¹	4.4	10	14	65	-13	0.05
Sept. 13, 1994	06:01:23.0	38.15	107.98	This Study ¹	4.4	10	14	65	-13	0.05
				This Study ²	4.3	10	38	4	-39	0.03

ERI: Earthquake Research Institute; Harvard: Harvard University (CMT); NEIC: National Earthquake Information Center; Oregon: Oregon State University; R&L: Ritsema and Lay (1995); This Study¹: BASIN crustal model; This Study²: CUS crustal model.

Table 10
Central United States (*CUS*) crustal model

Layer	Thickness km	V_p km/s	V_s km/s	Density g/cm ³	Q_α	Q_β
1	1	5.00	2.90	2.5	600	300
2	10	6.10	3.52	2.7	600	300
3	9	6.40	3.70	2.9	600	300
4	20	6.70	3.87	3.0	1000	500
5	Half-space	8.15	4.70	3.4	1000	500

Table 11
Basin and Range (*BASIN*) crustal model proposed by
Patton and Taylor (1984)

Layer	Thickness km	V_p km/s	V_s km/s	Density g/cm ³	Q_α	Q_β
1	19	6.0	3.47	2.7	600	300
2	12	6.7	3.87	2.9	1000	500
3	Half-space	8.0	4.62	3.4	1000	500

Table 12
Stations included in the inversion of the March 25, 1993, Scotts Mills earthquake

Station	Epicaltral Distance, km	Azimuth, deg	Component	Time-window, s Begin End
<i>WDC</i>	494	179	<i>R, T, Z</i>	-5 300
<i>CMB</i>	799	166	<i>R, T, Z</i>	-5 350
<i>SAO</i>	923	174	<i>R, T, Z</i>	-5 400
<i>ISA</i>	1098	160	<i>R, T, Z</i>	-5 400

R, T, Z are the radial, transversal, and vertical component, respectively

Table 13
Stations included in the inversion of the September 21, 1993 (03:28:55.4),
Klamath Falls earthquake

Station	Epicentral	Azimuth,	Component	Time-window, s	
	Distance, km	deg		Begin	End
<i>WDC</i>	198	193	<i>R, T, Z</i>	-5	150
<i>COR</i>	273	338	<i>R, T, Z</i>	-5	150
<i>CMB</i>	495	163	<i>R, T, Z</i>	-5	200
<i>SAO</i>	618	175	<i>R, T, Z</i>	-5	200
<i>ISA</i>	798	156	<i>R, T, Z</i>	-5	220
<i>DUG</i>	805	104	<i>Z</i>	-5	250

R, T, Z are the radial, transversal, and vertical component, respectively

Table 14
Stations included in the inversion of the
December 4, 1993, Klamath Falls earthquake

Station	Epicentral	Azimuth,	Component	Time-window, s	
	Distance, km	deg		Begin	End
<i>WDC</i>	197	193	<i>Z</i>	-5	150
<i>COR</i>	278	336	<i>R, T, Z</i>	-5	150
<i>CMB</i>	489	163	<i>R, T, Z</i>	-5	200
<i>SAO</i>	617	175	<i>Z</i>	-5	250
<i>ISA</i>	798	156	<i>R, T, Z</i>	-5	250
<i>DUG</i>	804	104	<i>Z</i>	-5	300

R, T, Z are the radial, transversal, and vertical component, respectively

Table 15
Stations included in the inversion of the
February 3, 1994, Wyoming earthquake

Station	Epicentral Distance, km	Azimuth, deg	Component	Time-window, s	
				Begin	End
<i>GOL</i>	580	124	<i>R, T, Z</i>	-5	250
<i>NEW</i>	777	324	<i>R, T, Z</i>	-5	250
<i>ALQ</i>	951	154	<i>R, T, Z</i>	-5	250
<i>CMB</i>	955	240	<i>R, T, Z</i>	-5	250

R, T, Z are the radial, transversal, and vertical component, respectively

Table 16
Stations included in the inversion of the
September 12, 1994, California-Nevada mainshock

Station	Epicentral Distance, km	Azimuth, deg	Component	Time-window, s	
				Begin	End
<i>CMB</i>	111	218	<i>R, T, Z</i>	-5	175
<i>SAO</i>	278	216	<i>R, T, Z</i>	-5	175
<i>WDC</i>	322	309	<i>R, T, Z</i>	-5	175
<i>ISA</i>	367	164	<i>R, T, Z</i>	-5	175
<i>DUG</i>	600	73	<i>Z</i>	-5	200
<i>GOL</i>	1233	81	<i>R, T, Z</i>	-5	400
<i>ALQ</i>	1244	106	<i>R, T, Z</i>	-5	400

R, T, Z are the radial, transversal, and vertical component, respectively

Table 17
Stations included in the inversion of the
September 12, 1994, California-Nevada earthquake (aftershock)

Station	Epicentral	Azimuth,	Component	Time-window, s	
	Distance, km	deg		Begin	End
<i>CMB</i>	111	216	<i>R, T, Z</i>	-5	175
<i>SAO</i>	278	215	<i>R, T, Z</i>	-5	175
<i>WDC</i>	311	309	<i>R, T, Z</i>	-5	175
<i>DUG</i>	611	74	<i>Z</i>	-5	200
<i>GOL</i>	1233	81	<i>R, T, Z</i>	-5	400
<i>ALQ</i>	1256	106	<i>R, T, Z</i>	-5	400

R, T, Z are the radial, transversal, and vertical component, respectively

Table 18
Stations included in the inversion of the September 13, 1994,
Colorado earthquake

Station	Epicentral	Azimuth,	Component	Time-window, s	
	Distance, km	deg		Begin	End
<i>GOL</i>	278	53	<i>R, T, Z</i>	-5	100
<i>ALQ</i>	389	159	<i>R, Z</i>	-5	150
<i>DUG</i>	467	299	<i>Z</i>	-5	175

R, T, Z are the radial, transversal, and vertical component, respectively

Figure Captions

- Figure 1.** Interaction of the Caribbean plate and its neighboring plates (Atlantic, Cocos, Nazca, North America, and South America). The arrows indicate the directions of relative plate motions. The digital stations deployed at regional distances ($<12^\circ$) from western Venezuela are shown as solid triangles within open circles. Currently, all these stations are in operation, except *CAR* (Venezuela).
- Figure 2.** Major active fault systems in western Venezuela (after Singer *et al.*, 1992; Soulas, 1986; Soulas *et al.*, 1987). The seismicity ($m_b \geq 5.0$) occurred during the last three decades reported by the National Earthquake Information Center (*NEIC*) is shown as circles ($m_b \leq 5.3$) and squares ($m_b > 5.3$). The open symbols represent shallow depth seismicity ($h < 70$ km) and the solid figures indicate intermediate depth events ($h \geq 70$ km). The arrows denote the directions of relative motions of the faults.
- Figure 3.** Map of the epicentral area (star) and focal mechanisms (lower hemisphere projections) determined previously for the September 21, 1993 (03:28:55.4), Klamath Falls earthquake. The *CMT* is the Centroid Moment Tensor solution of Dziewonski *et al.*, 1994b. The *NEIC* is the moment tensor solution of Sipkin and Needham, 1994. The *OSU* is the Oregon State University solution of Braunmiller *et al.*, 1995. The *R&L* is the solution obtained by Ritsema and Lay (1995). The solid and open small circles on the focal mechanisms indicate the positions of the *P* and *T* axes on the focal sphere. Inset shows the *CMT* solution on a focal sphere, indicating the azimuth of the stations (open circles) involved in the *P_{nl}* signals forward modeling. The stations used in this study are indicated as solid triangles. Not shown are stations *DUG* and *PAS*.
- Figure 4.** Comparison between the theoretical (dashed lines) and observed (solid lines) vertical (top), radial (middle), and transverse (bottom) component seismograms for the September 21, 1993 (03:28:55.4), Klamath Falls earthquake recorded at the station *WDC* (azimuth= 193° ; $\Delta=198$ km), using the following crustal structures: A) one layer over a half-space; B) crustal model according to Saikia and Burdick (1991). The values of Q_β are from

Lin (1989); C) crustal structures for the path from the hypocenter to every station. The values of Q_{β} are from Lin (1989); D) The values of Q_{β} are from Al-Khatib and Mitchell (1991); and E) the same values of (D), except for a low Q_{β} in the half-space. For each

Figure 5. Waveform fit (dashed lines) to observed (solid lines) vertical (top), radial (middle), and transverse (bottom) component waveforms of the September 21, 1993 (03:28:55.4), Klamath Falls earthquake recorded at the station *COR* (azimuth=338°; Δ =273 km), using the same crustal structures indicated in Fig. 4.

Figure 6. Comparison between the synthetic (dashed lines) and observed (solid lines) vertical (top), radial (middle), and transverse (bottom) component seismograms for the September 21, 1993 (03:28:55.4), Klamath Falls earthquake recorded at the station *CMB* (azimuth=163°; Δ =495 km), using the same crustal structures indicated in Fig. 4.

Figure 7. Waveform fit (dashed lines) to observed (solid lines) vertical (top), radial (middle), and transverse (bottom) component waveforms for the September 21, 1993 (03:28:55.4), Klamath Falls earthquake recorded at the station *SAO* (azimuth=175°; Δ =618 km), using the same crustal structures indicated in Fig. 4.

Figure 8. Comparison between the theoretical (dashed lines) and observed (solid lines) vertical (top), radial (middle), and transverse (bottom) component seismograms for the September 21, 1993 (03:28:55.4), Klamath Falls earthquake recorded at the station *ISA* (azimuth=156°; Δ =798 km), using the same crustal structures indicated in Fig. 4.

Figure 9. Comparison between the synthetic (dashed lines) and observed (solid lines) vertical (top), radial (middle), and transverse (bottom) component seismograms for the September 21, 1993 (03:28:55.4), Klamath Falls earthquake recorded at the station *DUG* (azimuth=104°; Δ =805 km), using the same crustal structures indicated in Fig. 4.

Figure 10. Waveform fit (dashed lines) to observed (solid lines) vertical (top), radial (middle), and transverse (bottom) component waveforms for the September 21, 1993 (03:28:55.4), Klamath Falls earthquake recorded at the station *PAS* (azimuth=159°; Δ =967 km), using the same crustal structures indicated in Fig. 4.

Figure 11. Comparison between the calculated (dashed lines) and observed (solid lines) vertical (top), radial (middle), and transverse (bottom) component seismograms for the July 22, 1993, Colombia-Venezuela border earthquake recorded at the station *SJG* (azimuth=23°; $\Delta=1396$ km), using the modified crustal model of Saikia and Burdick (1991)

Figure 12. Map of epicentral locations (stars) of earthquakes in western United States analyzed through the moment tensor inversion, using regional seismograms. The solid triangles indicate the seismological stations that were utilized in this study.

Figure 13. Epicenter location (star) and focal mechanisms (lower-hemisphere projections) determined in this study and by previous workers of the March 25, 1993, Scotts Mills earthquake. *CMT* is the Harvard University solution. *OSU* is the Oregon State University focal mechanism. *R&L* is the solution obtained by Ritsema and Lay (1995). *CUS* and *BASIN* are the fault plane solutions obtained in this study using the Central United States (Table 10) and the Basin and Range (Table 11) crustal models, respectively. The solid and open small circles on the focal mechanisms indicate the positions of the *P* and *T* axes on the focal sphere, respectively. The stations *COR* and *WDC* are exhibited as solid triangles. The other stations are out of the figure. Inset shows the *CUS* solution on a focal sphere, indicating the azimuth of the stations (open circles) involved in the moment tensor inversion.

Figure 14. Results of the moment tensor inversion using regional seismograms of the March 25, 1993, Scotts Mills earthquake. The crustal structure utilized is the *CUS* model shown in Table 10. The predicted (dashed lines) and observed (solid lines) seismograms are indicated for each component/station included in the inversion.

Figure 15. Results of the moment tensor inversion using regional seismograms of the March 25, 1993, Scotts Mills earthquake. The crustal structure utilized is the *BASIN* model indicated in Table 11. The theoretical (dashed lines) and observed (solid lines) waveforms are indicated for each station/component included in the inversion.

Figure 16. Map of the epicentral location (star) and focal mechanisms (lower-hemisphere projections) determined in this study and by previous workers of the September 21, 1993

(03:28:55.4), Klamath Falls earthquake. *CMT* is the Harvard University solution. *NEIC* is the National Earthquake Information Center mechanism. *OSU* is the Oregon State University focal mechanism. *R&L* is the solution obtained by Ritsema and Lay (1995). *CUS* and *BASIN* are the fault plane solutions obtained in this study using the Central United States (Table 10) and the Basin and Range (Table 11) models, respectively. The solid and open small circles on the focal mechanisms indicate the positions of the *P* and *T* axes on the focal sphere, respectively. The stations *COR* and *WDC* are exhibited as solid triangles. The other stations are out of the figure. Inset shows the *CUS* solution on a focal sphere, indicating the azimuth of the stations (open circles) included in the moment tensor inversion.

Figure 17. Epicenter location (star) and focal mechanisms (lower-hemisphere projections) of the September 21, 1993 (05:45:34.0), Klamath Falls earthquake. This event is the second mainshock of the seismic sequence that occurred during that day near Klamath Falls, Oregon. *CMT* is the Harvard University solution. *OSU* is the Oregon State University focal mechanism. *R&L* is the solution obtained by Ritsema and Lay (1995). The solid and open small circles on the focal mechanisms indicate the positions of the *P* and *T* axes on the focal sphere, respectively. The stations *COR* and *WDC* are exhibited as solid triangles. The other stations are out of the figure.

Figure 18. Results of the moment tensor inversion of the September 21, 1993 (03:28:55.4), Klamath Falls earthquake using the *CUS* model. The synthetic (dashed) and observed (solid) seismograms are indicated for each station/component included in the inversion.

Figure 18a. Results of the moment tensor inversion of the September 21, 1993 (03:28:55.4), Klamath Falls earthquake using the *CUS* model (*Cont.*).

Figure 19. Comparison between the predicted (dashed lines) and observed (solid lines) seismograms obtained from the moment tensor inversion of the September 21, 1993 (03:28:55.4), Klamath Falls earthquake, using the *BASIN* model. The waveforms are indicated for each station/component involved in the inversion.

Figure 19a. Comparison between the predicted (dashed lines) and observed (solid lines) seismograms obtained from the moment tensor inversion of the September 21, 1993 (03:28:55.4), Klamath Falls earthquake, using the *BASIN* model (*Cont.*).

Figure 20. Map of epicentral location (star) and focal mechanisms (lower-hemisphere projections) of the December 4, 1993, Klamath Falls earthquake. *CMT* is the Harvard University solution. *OSU* is the Oregon State University focal mechanism. *CUS* and *BASIN* are the fault plane solutions obtained in this study using the Central United States (Table 10) and the Basin and Range (Table 11) models, respectively. The solid and open small circles on the focal mechanisms indicate the positions of the *P* and *T* axes on the focal sphere, respectively. The stations *COR* and *WDC* are exhibited as solid triangles. The other stations are out of the figure. Inset shows the *CUS* solution on a focal sphere, indicating the azimuth of the stations (open circles) involved in the moment tensor inversion.

Figure 21. Comparison between the predicted (dashed lines) and observed (solid lines) seismograms obtained from the moment tensor inversion of the December 4, 1993, Klamath Falls earthquake using the *CUS* model. The waveforms are indicated for each station/component included in the inversion.

Figure 22. Comparison between the predicted (dashed lines) and observed (solid lines) seismograms obtained from the moment tensor inversion of the December 4, 1993, Klamath Falls earthquake using the *BASIN* model. The waveforms are indicated for each station/component included in the inversion.

Figure 23. Epicenter location (star) and focal mechanisms (lower-hemisphere projections) of the February 3, 1994, Wyoming earthquake. *CMT* is the Harvard University solution. *OSU* is the Oregon State University focal mechanism. *NEIC* is the National Earthquake Information Center mechanism. *R&L* is the solution obtained by Ritsema and Lay (1995). *CUS* and *BASIN* are the fault plane solutions obtained in this study using the Central United States (Table 10) and the Basin and Range (Table 11) models, respectively. The solid and open small circles on the focal mechanisms indicate the positions of the *P* and *T* axes on the focal sphere, respectively. The station *DUG* is exhibited as solid triangle. The other stations

are out of the figure. Inset shows the *CUS* solution on a focal sphere, indicating the azimuth of the stations (open circles) involved in the moment tensor inversion.

Figure 24. Results of the moment tensor inversion of the February 3, 1994, Wyoming earthquake using the *CUS* model. The synthetic (dashed lines) and observed (solid lines) seismograms are shown for each station/component included in the inversion.

Figure 25. Results of the moment tensor inversion of the February 3, 1994, Wyoming earthquake using the *BASIN* model. The theoretical (dashed lines) and observed (solid lines) seismograms are indicated for each station/component involved in the inversion.

Figure 26. Map of epicentral location and focal mechanisms (lower-hemisphere projections) of the September 12, 1994, California-Nevada mainshock. *CMT* is the Harvard University solution. *OSU* is the Oregon State University focal mechanism. *ERI* is the Earthquake Research Institute solution. *CUS* and *BASIN* are the fault plane solutions obtained in this study using the Central United States (Table 10) and the Basin and Range (Table 11) models, respectively. The solid and open small circles on the focal mechanisms indicate the positions of the *P* and *T* axes on the focal sphere, respectively. The stations *CMB*, *ISA*, and *SAO* are exhibited as solid triangles. The other stations are out of the figure. Inset shows the *CUS* solution on a focal sphere, indicating the azimuth of the stations (open circles) involved in the moment tensor inversion.

Figure 27. Epicenter location and focal mechanisms (lower-hemisphere projections) of the September 12, 1994, California-Nevada aftershock. *CUS* and *BASIN* are the fault plane solutions obtained in this study using the Central United States (Table 10) and the Basin and Range (Table 11) models, respectively. The solid and open small circles on the focal mechanisms indicate the positions of the *P* and *T* axes on the focal sphere, respectively. The stations *CMB*, *ISA*, and *SAO* are exhibited as solid triangles. The other stations are out of the figure. Inset shows the *CUS* solution on a focal sphere, indicating the azimuth of the stations (open circles) involved in the moment tensor inversion.

Figure 28. Comparison between the predicted (dashed lines) and observed (solid lines) seismograms obtained from the moment tensor inversion of the December 4, 1993,

Klamath Falls earthquake using the *CUS* model. The waveforms are indicated for each station/component included in the inversion.

Figure 28a. Comparison between the predicted (dashed lines) and observed (solid lines) seismograms obtained from the moment tensor inversion of the December 4, 1993, Klamath Falls earthquake using the *CUS* model (Cont.).

Figure 29. Comparison between the predicted (dashed lines) and observed (solid lines) seismograms obtained from the moment tensor inversion of the December 4, 1993, Klamath Falls earthquake using the *BASIN* model. The waveforms are indicated for each station/component included in the inversion.

Figure 29a. Comparison between the predicted (dashed lines) and observed (solid lines) seismograms obtained from the moment tensor inversion of the December 4, 1993, Klamath Falls earthquake using the *BASIN* model (Cont.).

Figure 30. Results of the moment tensor inversion of the September 12, 1994, California-Nevada earthquake (aftershock) using regional seismograms and the *CUS* model. The synthetic (dashed lines) and observed (solid lines) seismograms are indicated for each station/component included in the inversion.

Figure 30a. Results of the moment tensor inversion of the September 12, 1994, California-Nevada earthquake (aftershock) using the *CUS* model (Cont.).

Figure 31. Results of the moment tensor inversion of the September 12, 1994, California-Nevada earthquake (aftershock) using the *BASIN* model. The predicted (dashed lines) and observed (solid lines) seismograms are indicated for each station/component included in the inversion.

Figure 31a. Results of the moment tensor inversion of the September 12, 1994, California-Nevada earthquake (aftershock) using the *BASIN* model (Cont.).

Figure 32. Map of epicentral location (star) and focal mechanisms (lower-hemisphere projections) of the September 13, 1994, Colorado earthquake. *CUS* and *BASIN* are the fault plane solutions obtained in this study using the Central United States (Table 10) and the Basin and Range (Table 11) models, respectively. The solid and open small circles on the

focal mechanisms indicate the positions of the P and T axes on the focal sphere, respectively. The station GOL is shown as solid triangle. The other stations are out of the figure. Inset shows the CUS solution on a focal sphere, indicating the azimuth of the stations (open circles) included in the moment tensor inversion.

Figure 33. Comparison between the predicted (dashed lines) and observed (solid lines) seismograms obtained from the moment tensor inversion of September 13, 1994, Colorado earthquake using the CUS model. The waveforms are indicated for each station/component included in the inversion.

Figure 34. Comparison between the predicted (dashed lines) and observed (solid lines) seismograms obtained from the moment tensor inversion of September 13, 1994, Colorado earthquake using the $BASIN$ model. The waveforms are indicated for each station/component included in the inversion.

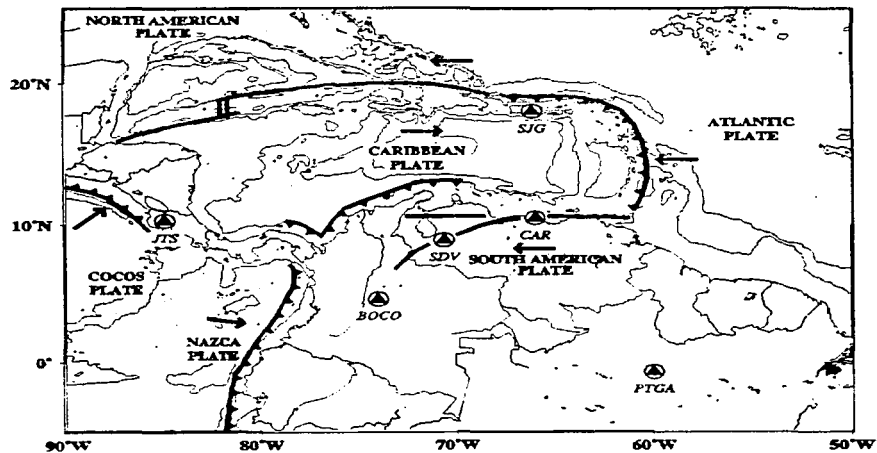


Figure 1

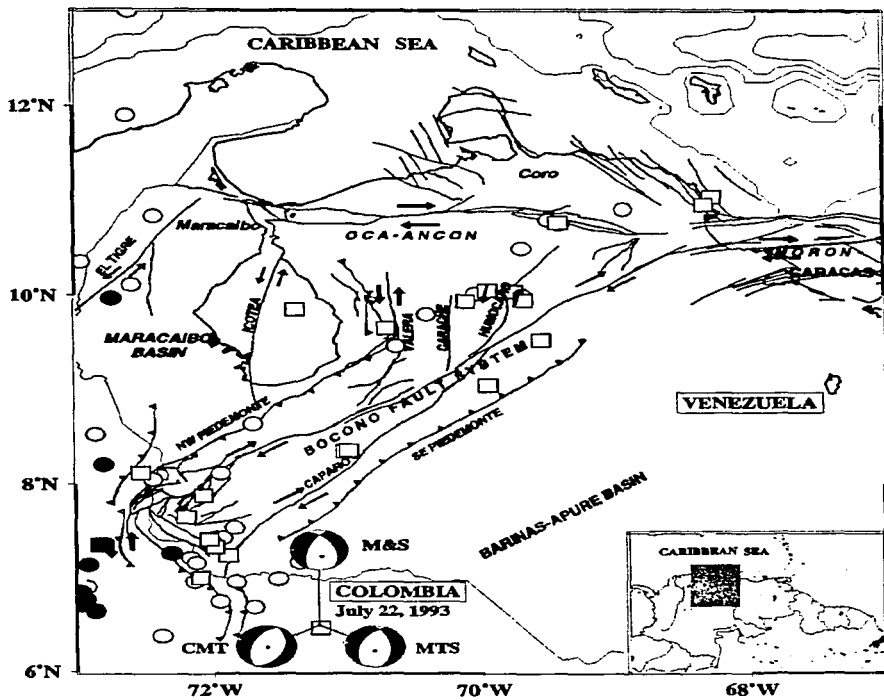


Figure 2

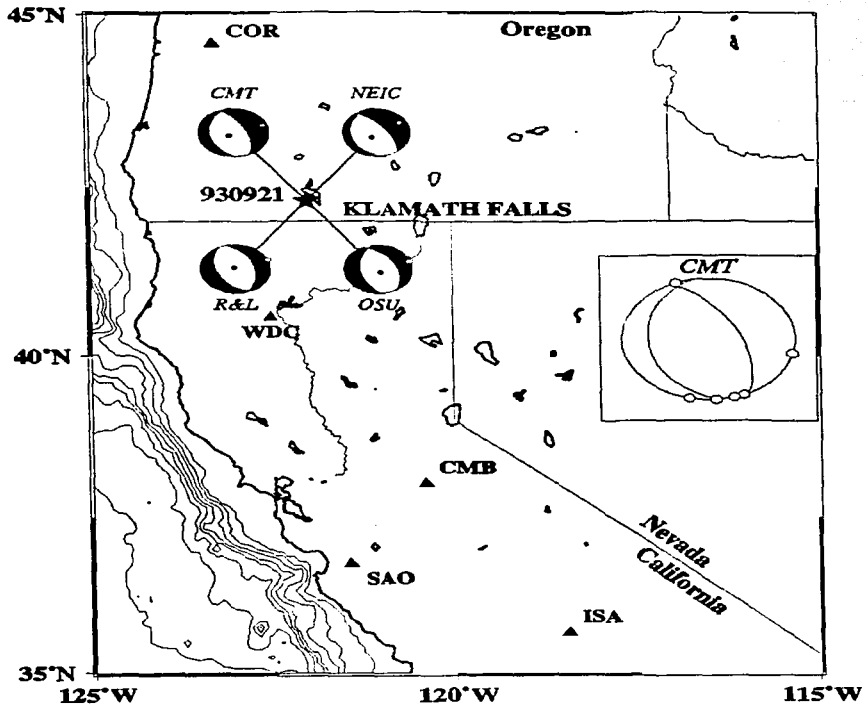


Figure 3

Station WDC

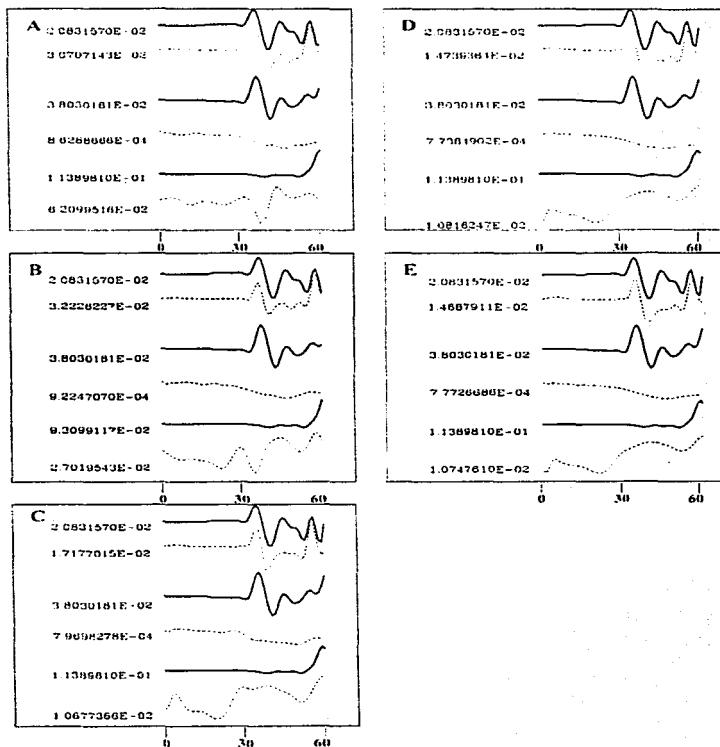


Figure 4

Station COR

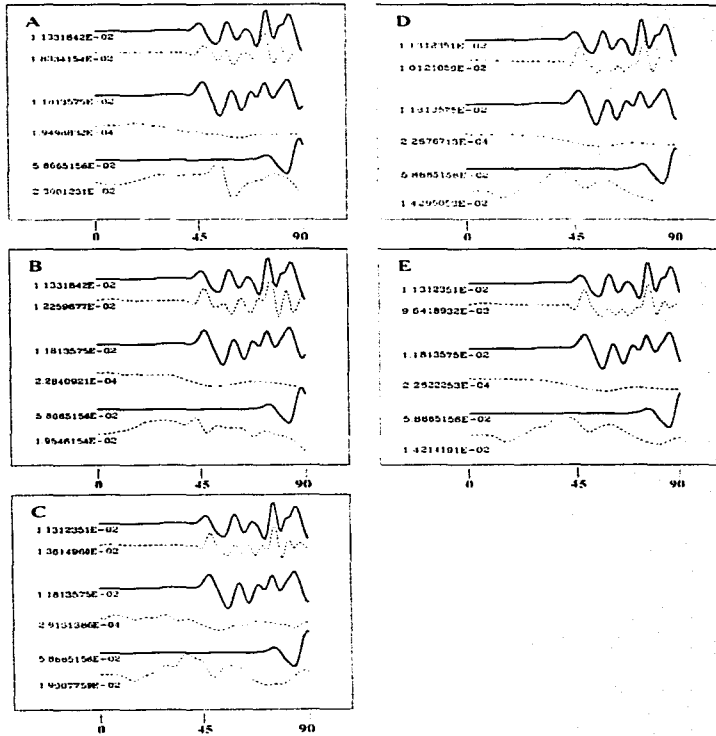


Figure 5

Station CMB

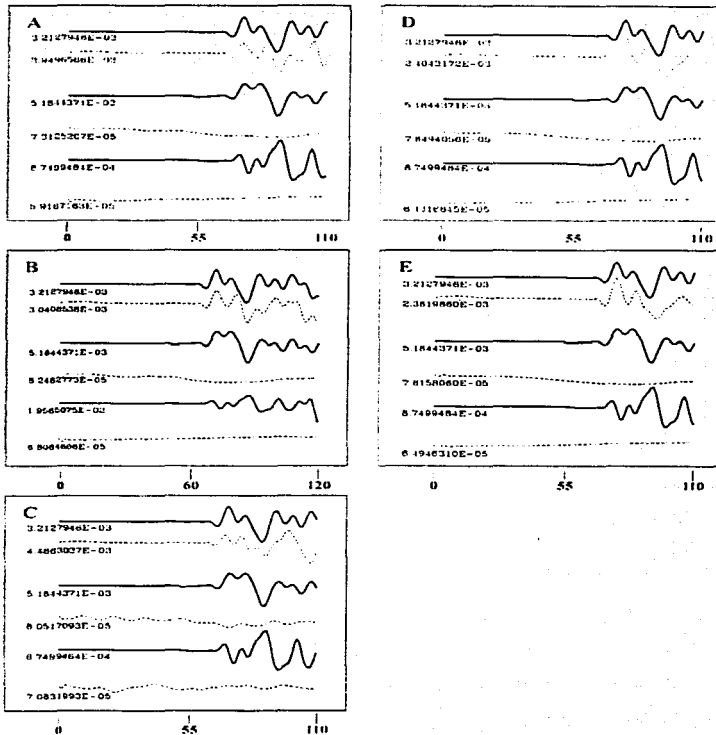


Figure 6

Station SAO

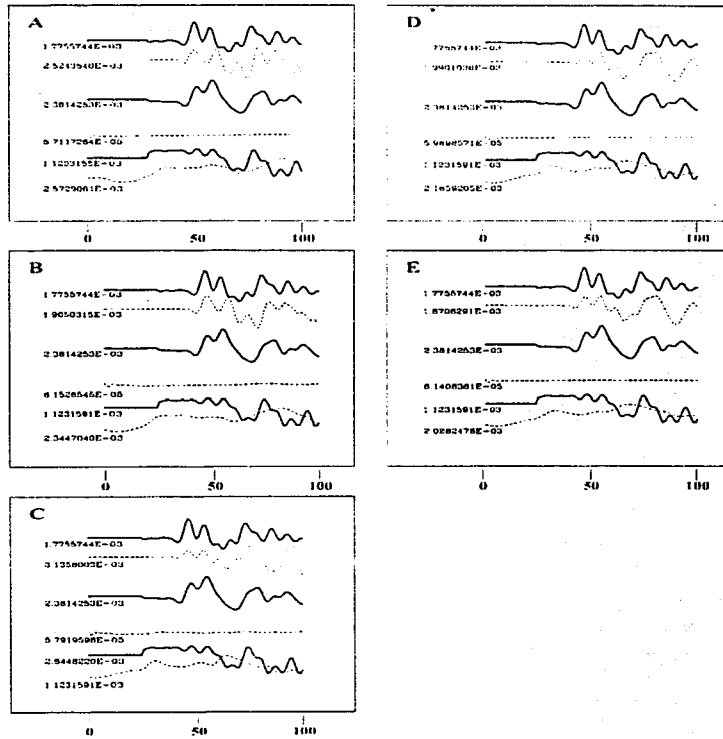


Figure 7

Station ISA

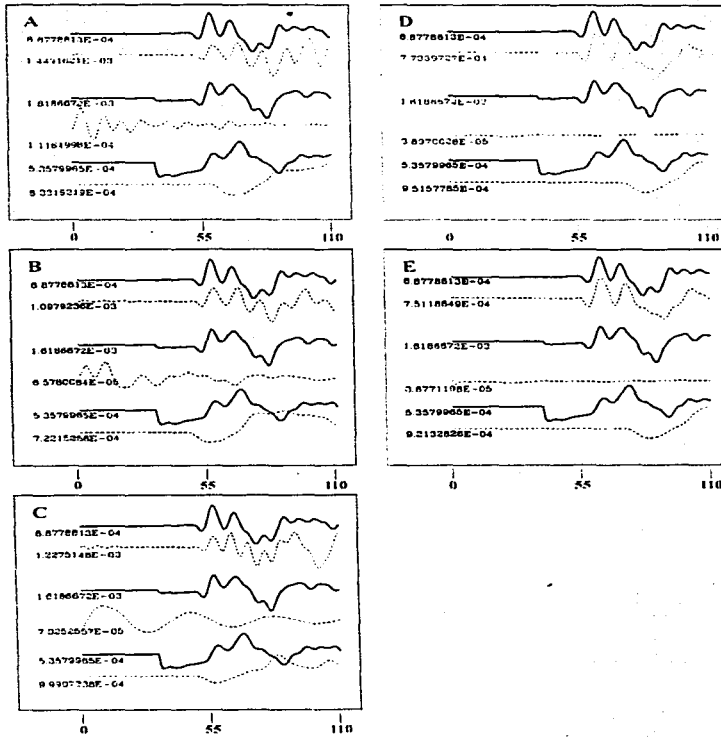


Figure 8

Station DUG

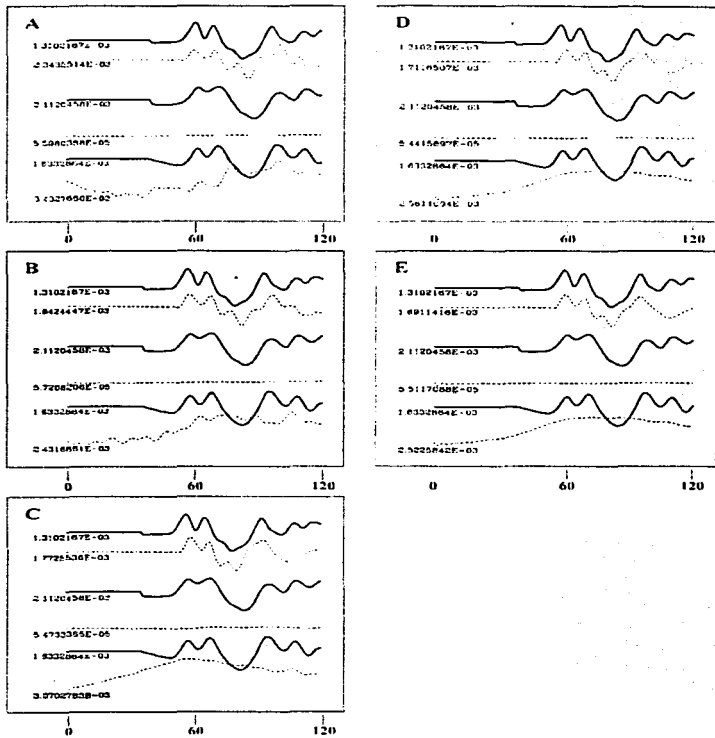


Figure 9

Station PAS

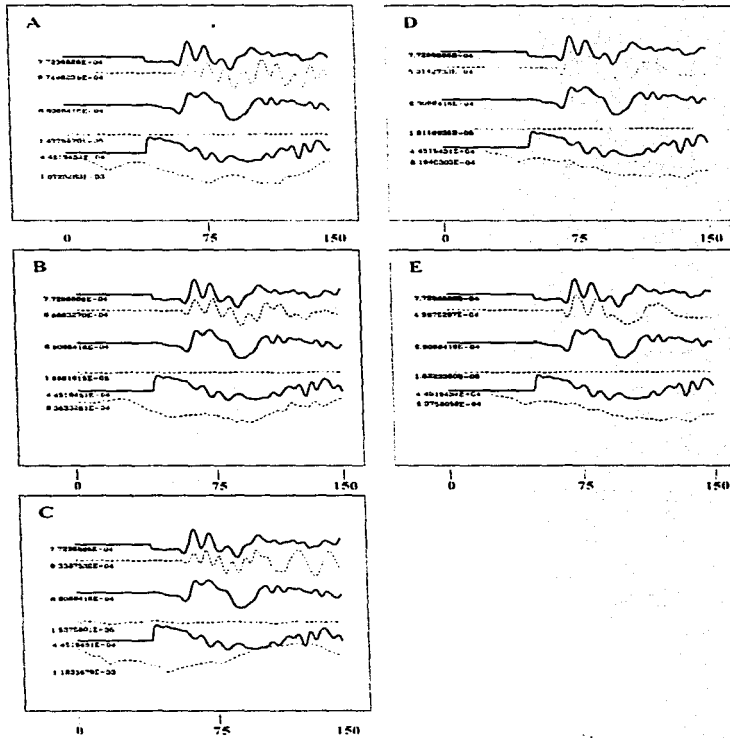


Figure 10

Station SJG

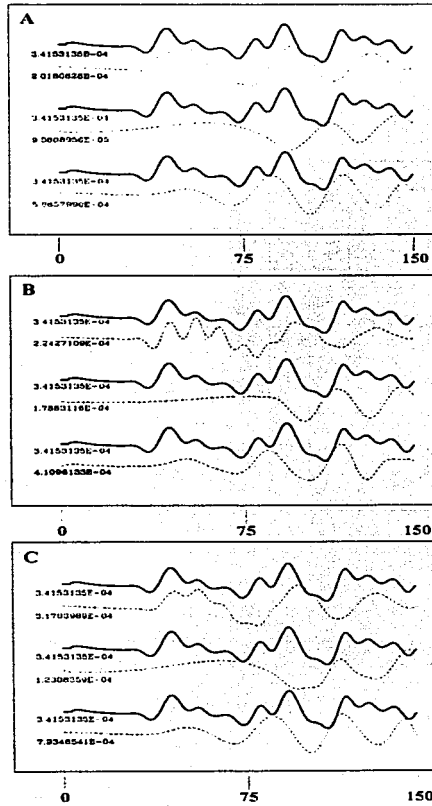


Figure 11

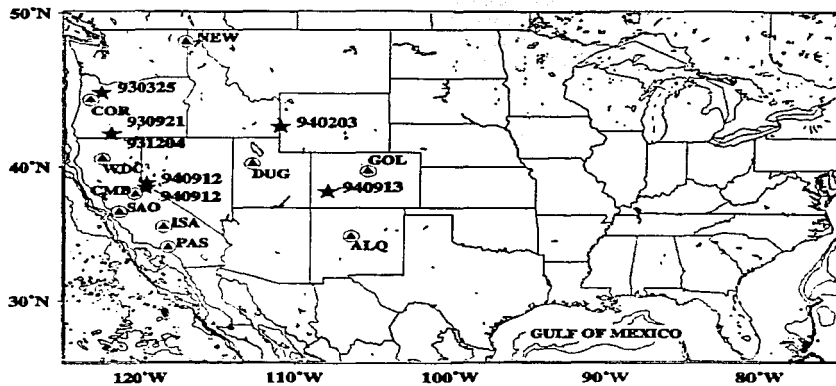


Figure 12

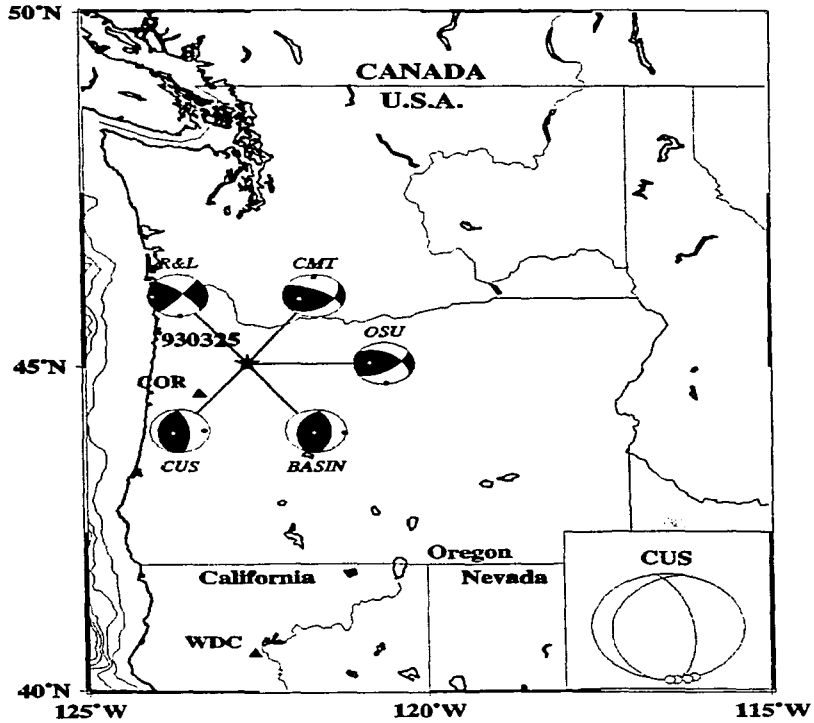


Figure 13

March 25, 1993 - CUS model.

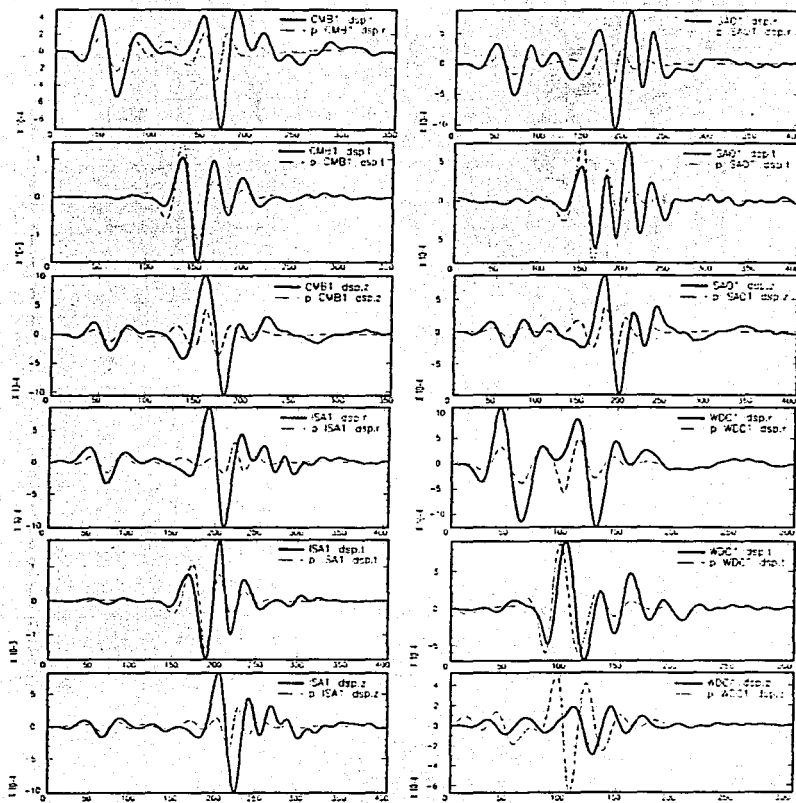


Figure 14

March 25, 1993 - BASIN model

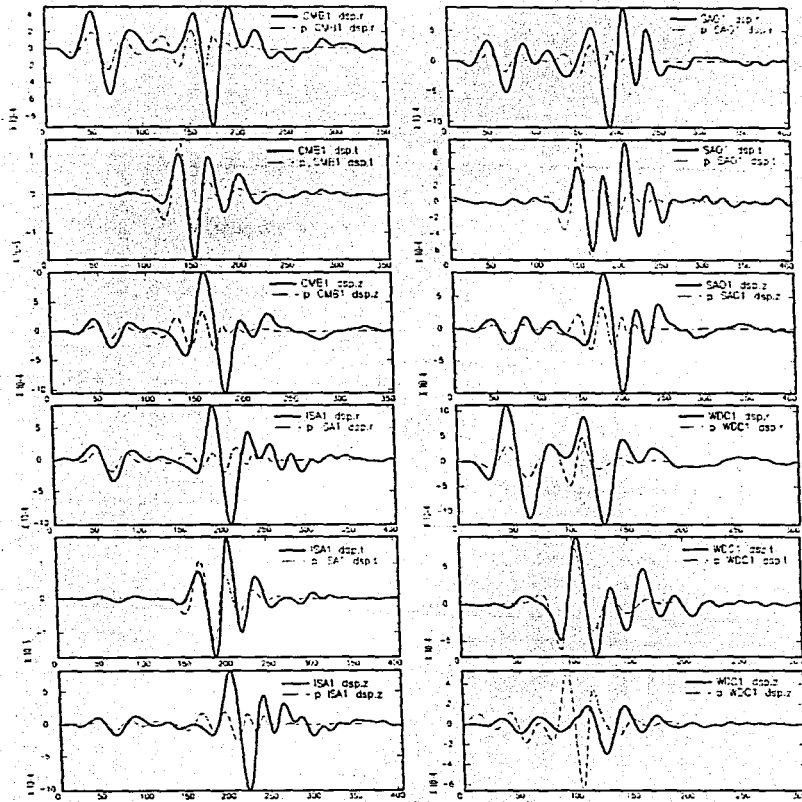


Figure 15

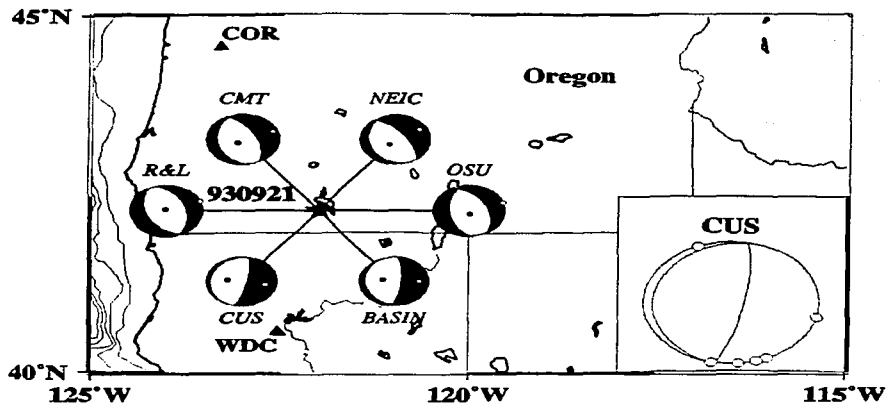


Figure 16

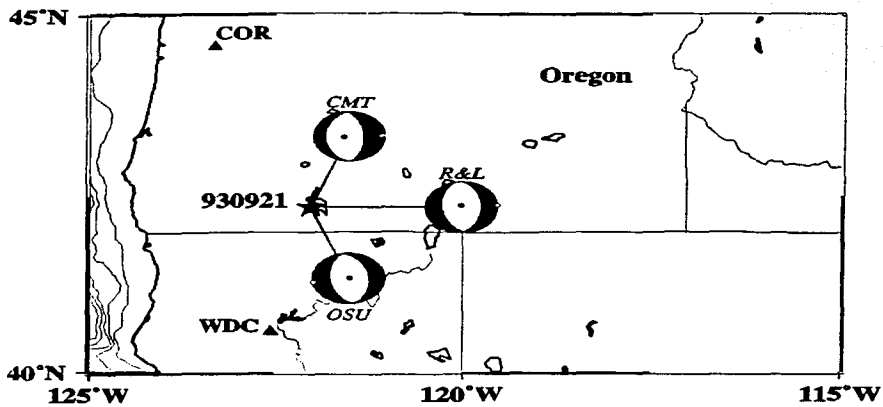


Figure 17

September 21, 1993 - CUS model

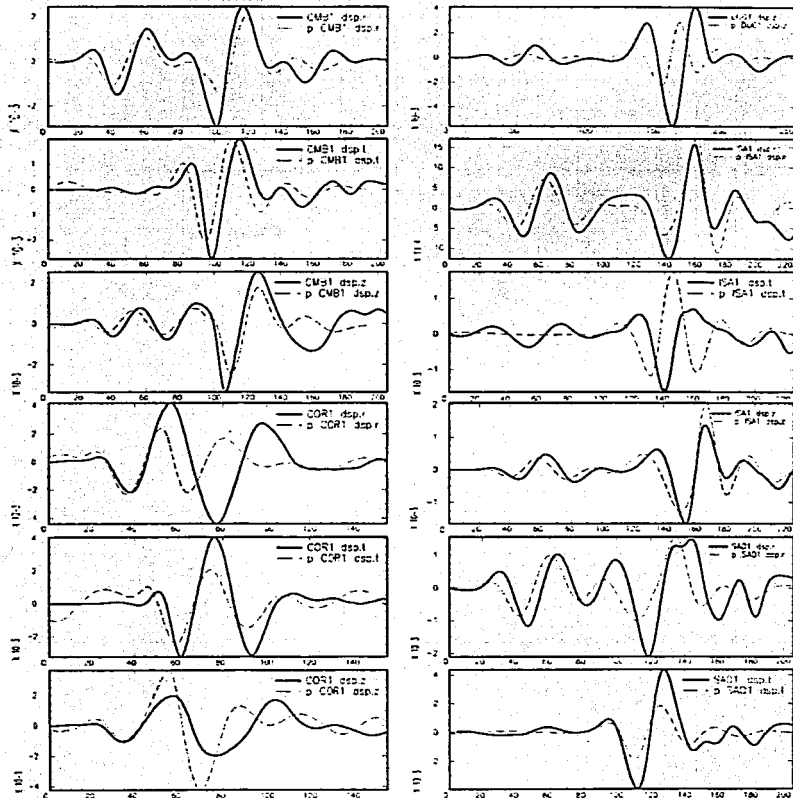


Figure 18

September 21, 1993 - CUS model (Cont.)

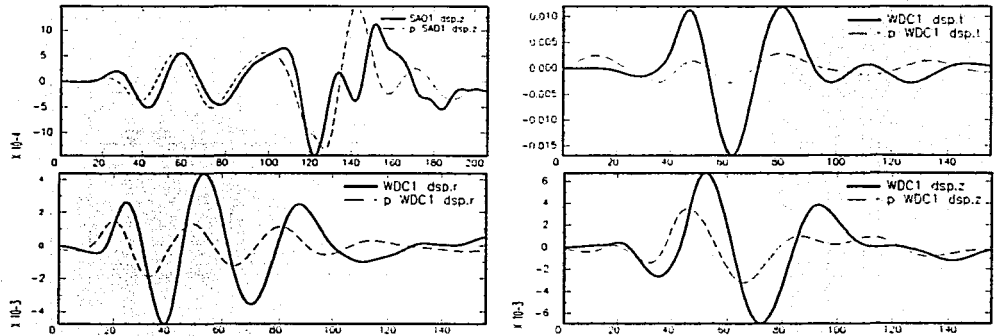


Figure 18 (Cont.)

September 21, 1993 - BASIN model

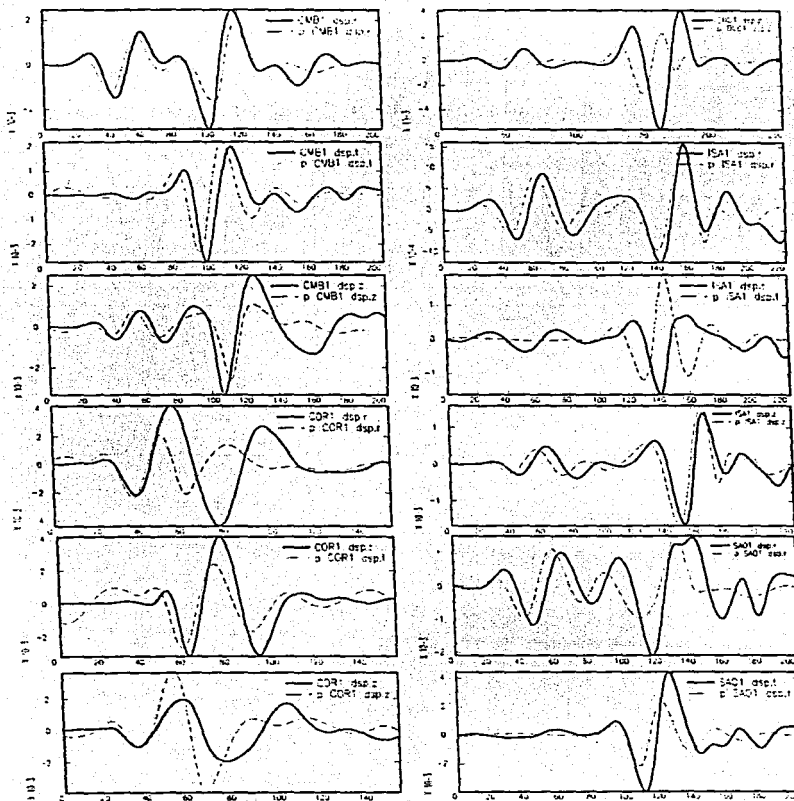


Figure 19

September 21, 1993 - BASIN model

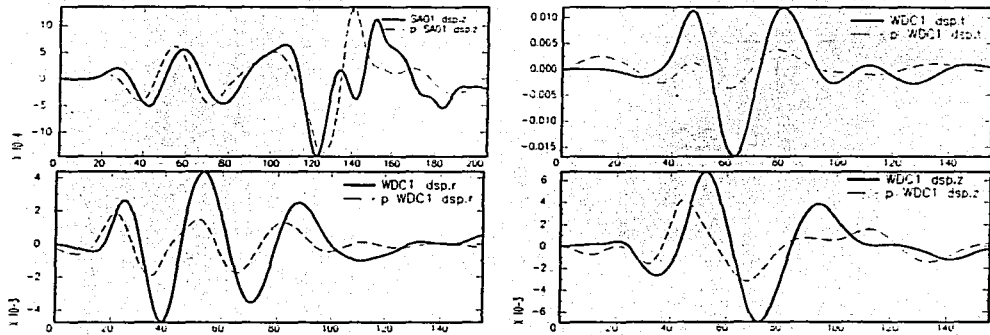


Figure 19 (Cont.)

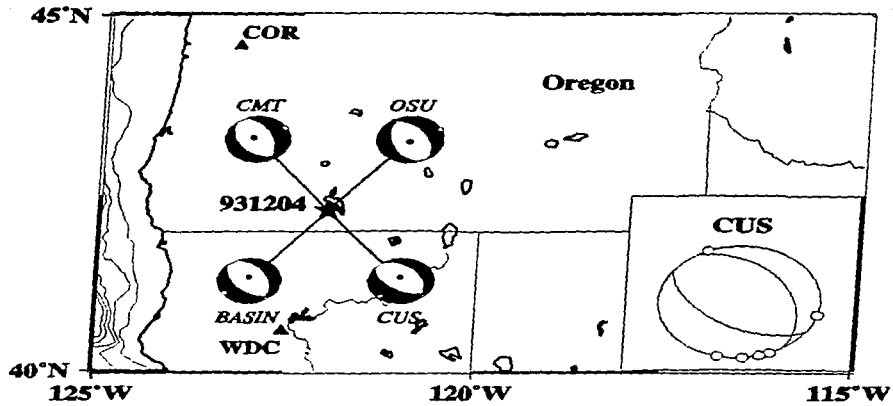


Figure 20

December 4, 1993 - CUS model

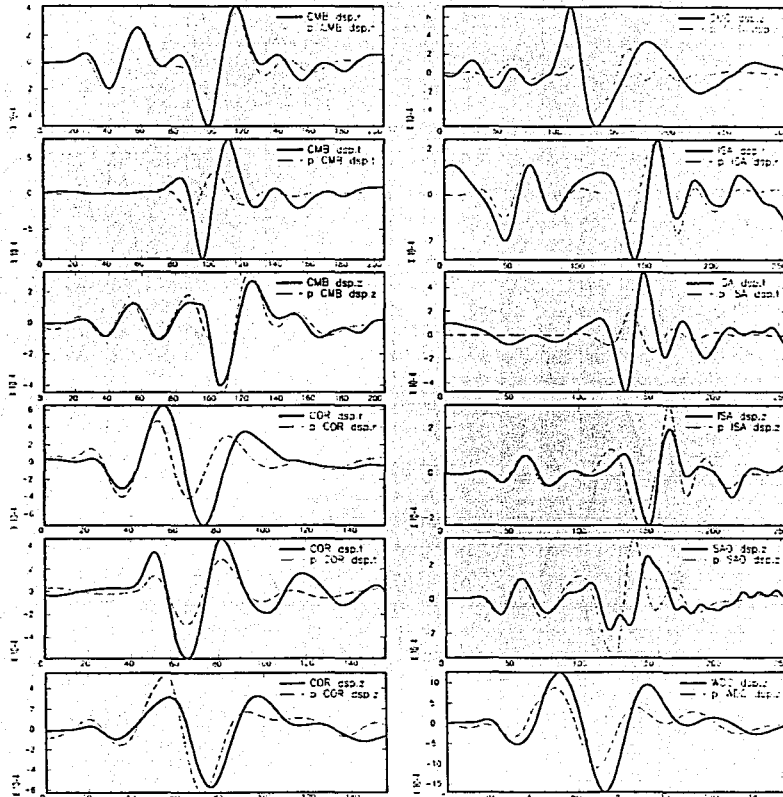


Figure 21

December 4, 1993 - BASIN model

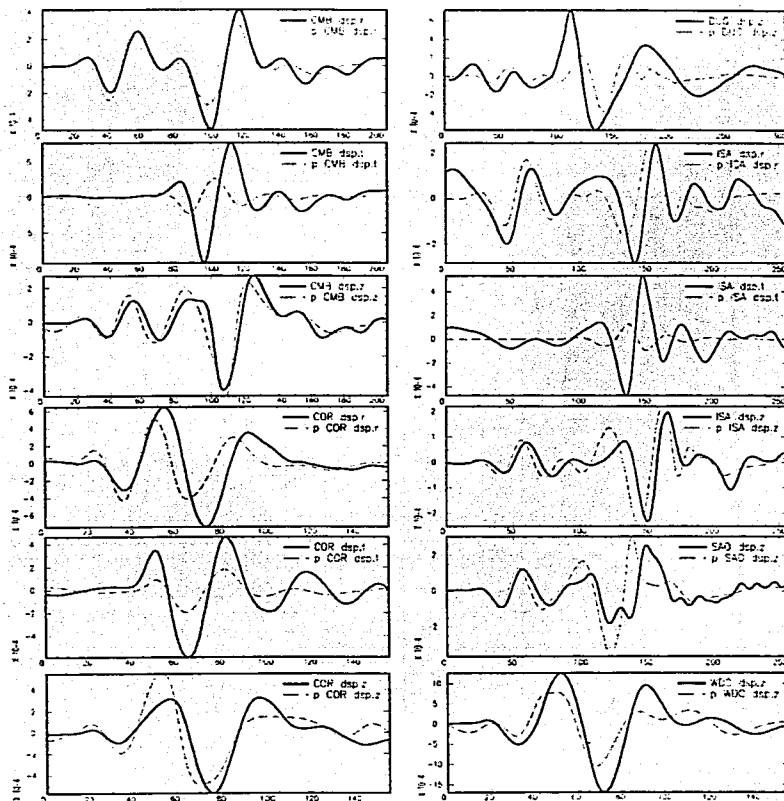


Figure 22

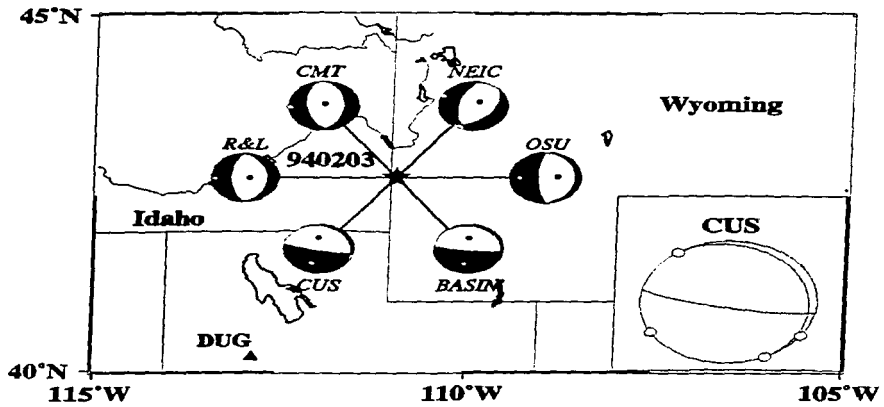


Figure 23

February 3, 1994 - CUS model

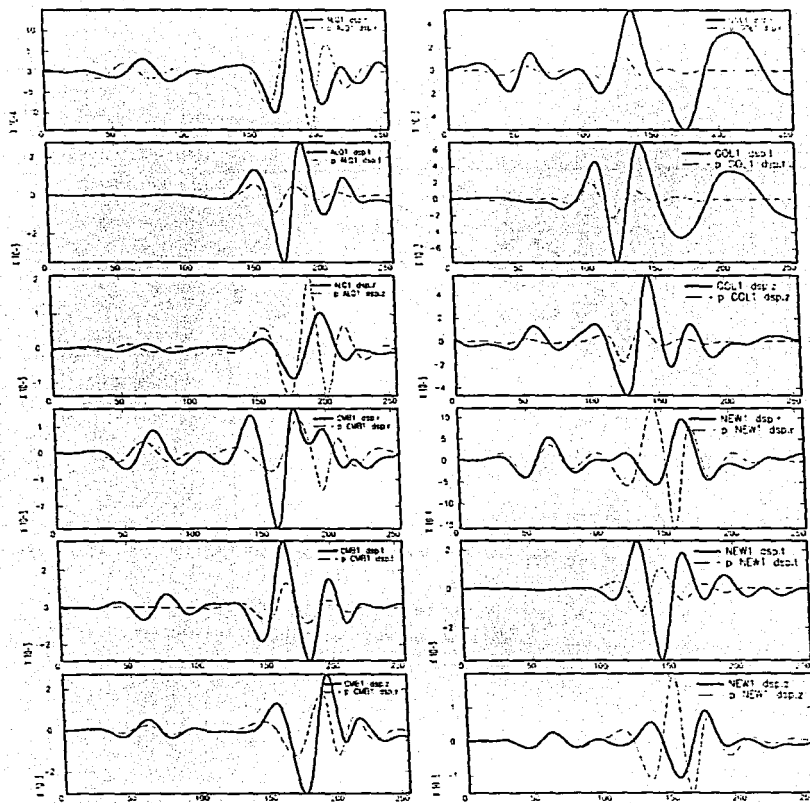


Figure 24

February 3, 1994 - BASIN model

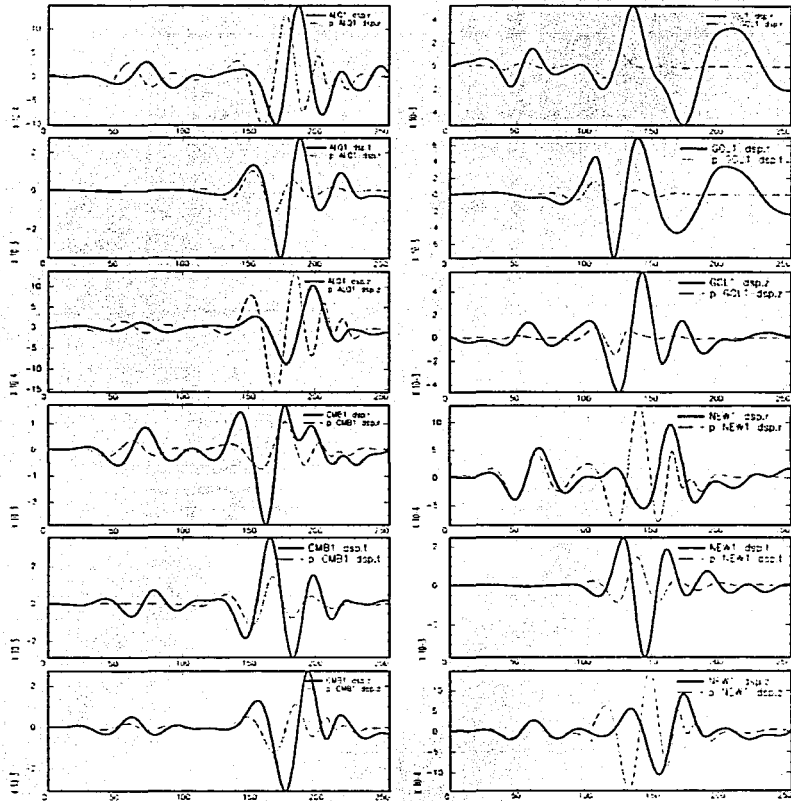


Figure 25

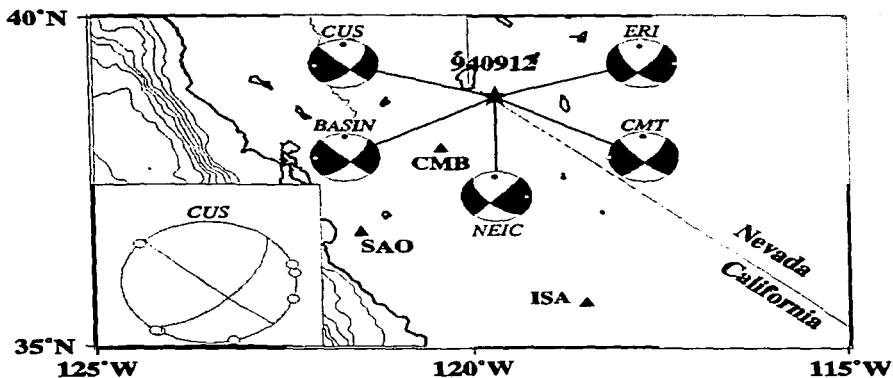


Figure 26

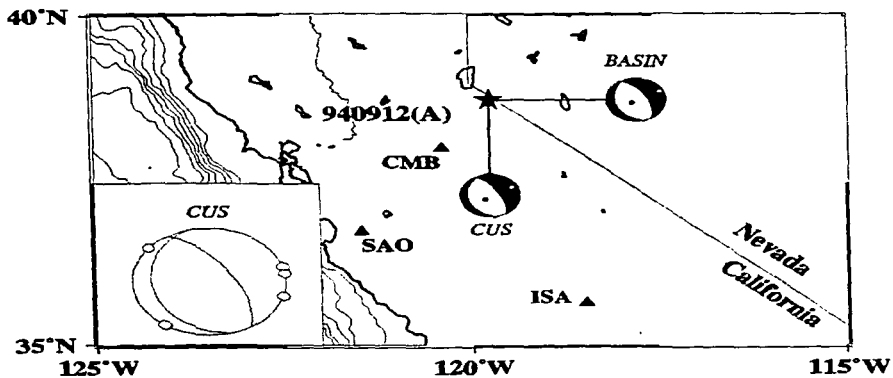


Figure 27

September 12, 1994 - CUS model

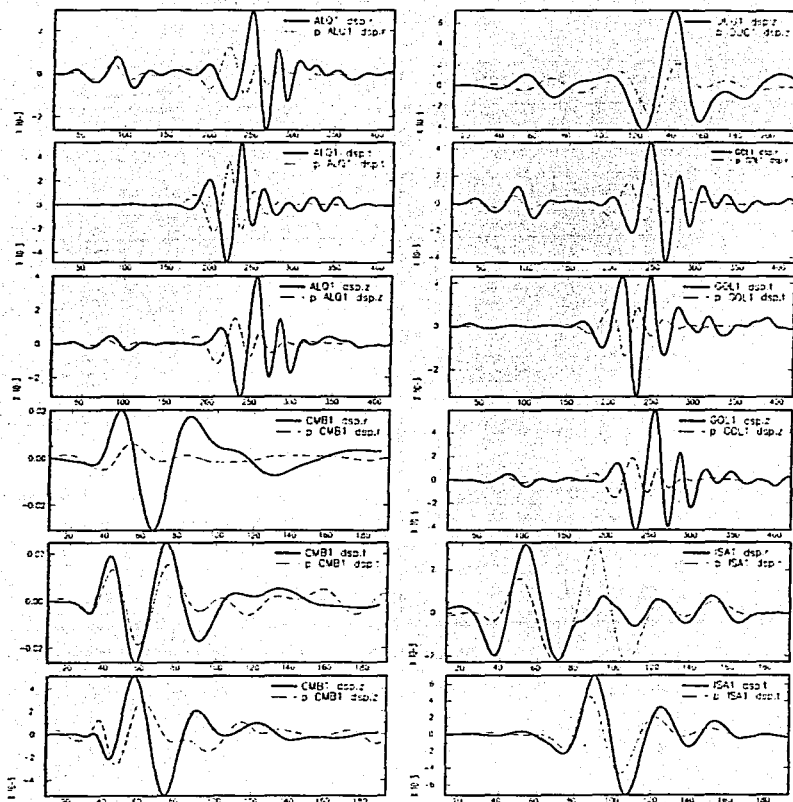


Figure 28

September 12, 1994 - CUS model

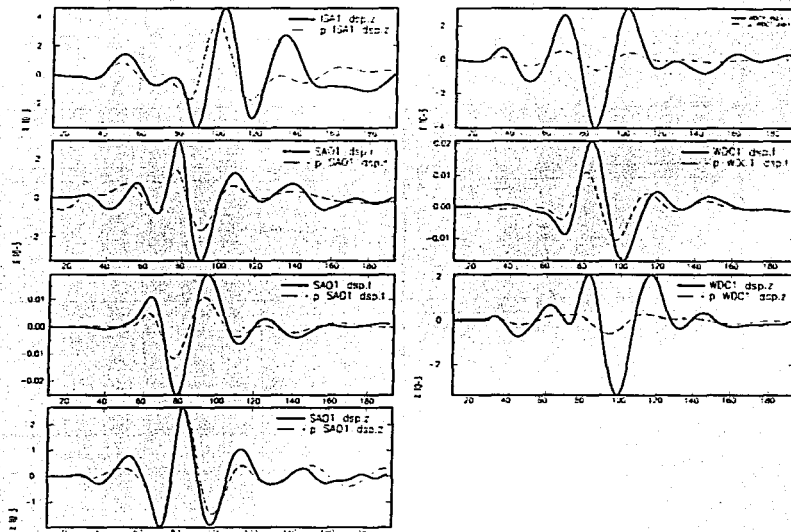


Figure 28 (Cont.).

September 12, 1994 - BASIN model

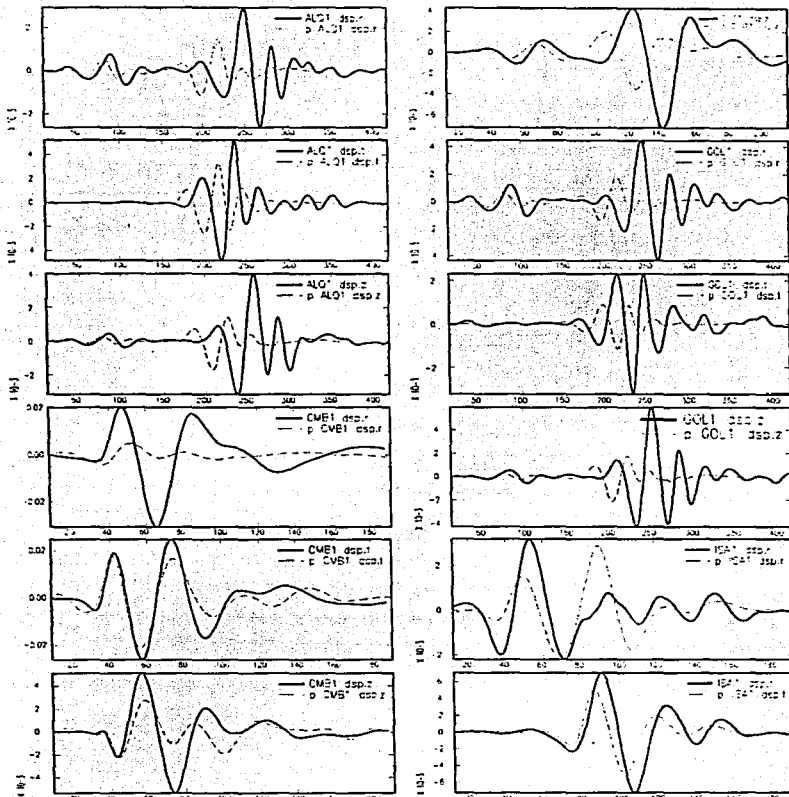


Figure 29

September 12, 1994 - BASIN model

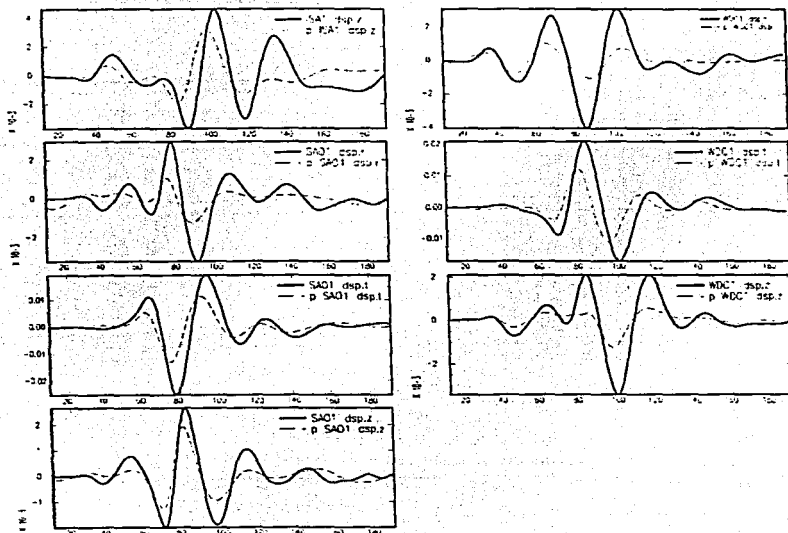


Figure 29 (Cont.)

September 12, 1994 - CUS model (aftershock)

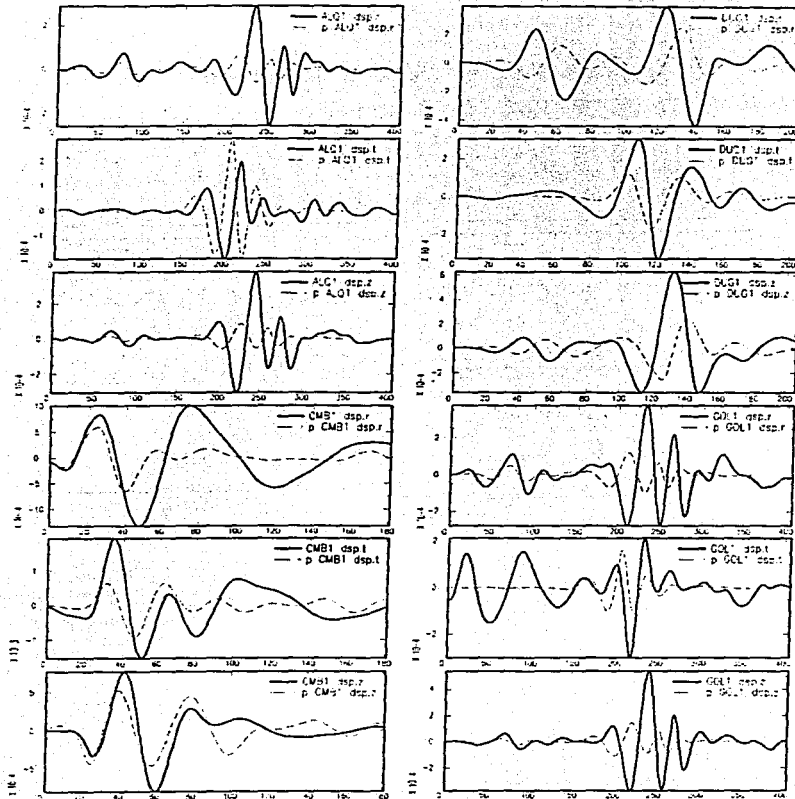


Figure 30

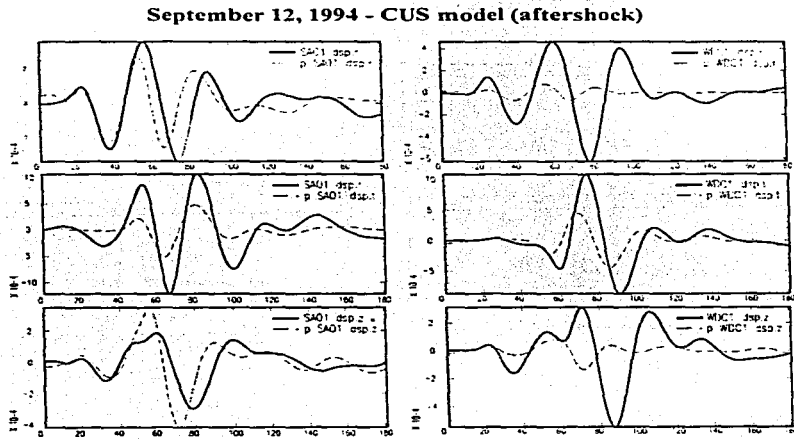


Figure 30 (Cont.)

September 12, 1994 - BASIN model (aftershock)

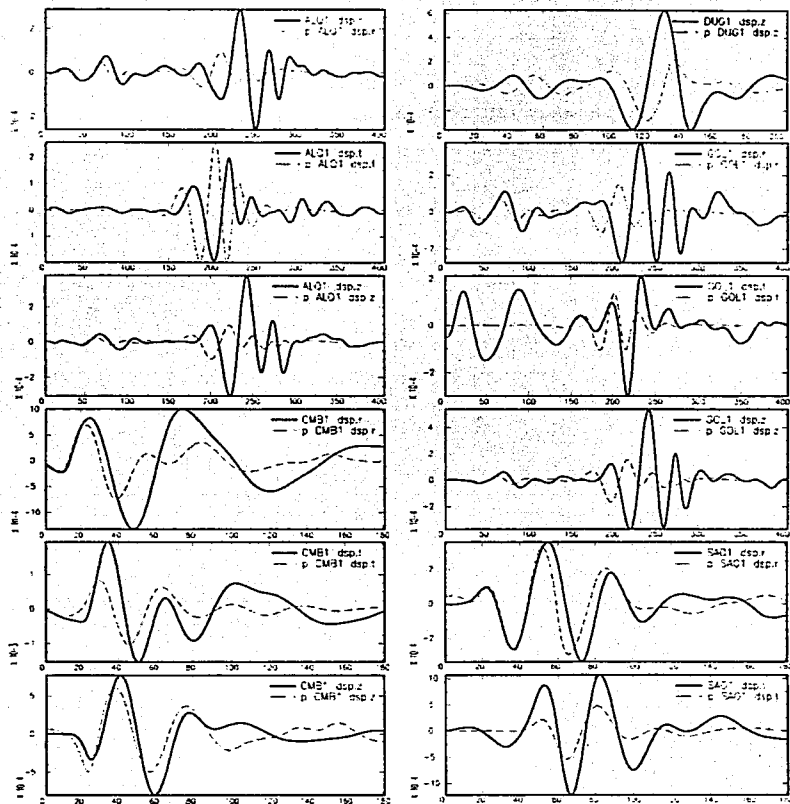


Figure 31

September 12, 1994 - BASIN model (aftershock)

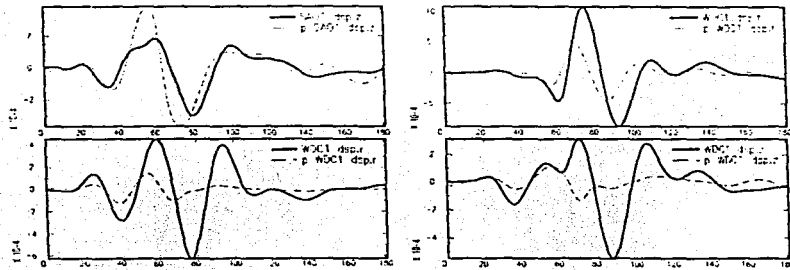


Figure 31 (Cont.)

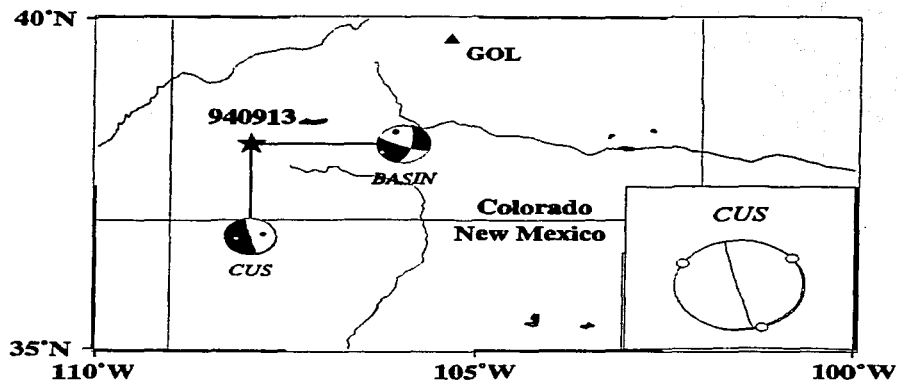


Figure 32

September 13, 1994 - CUS model

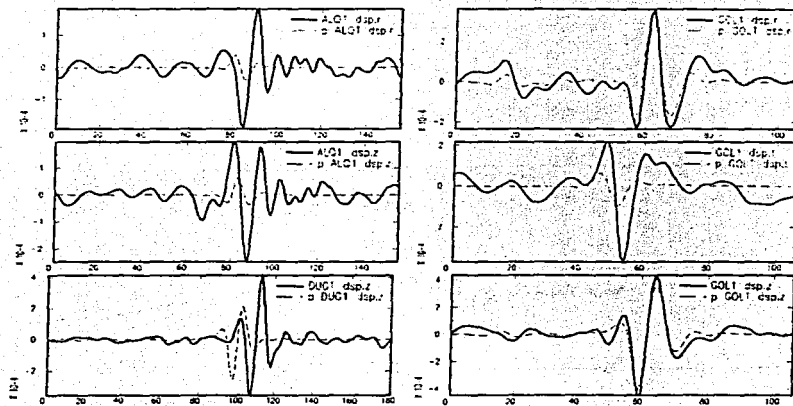


Figure 33

September 13, 1994 - BASIN model

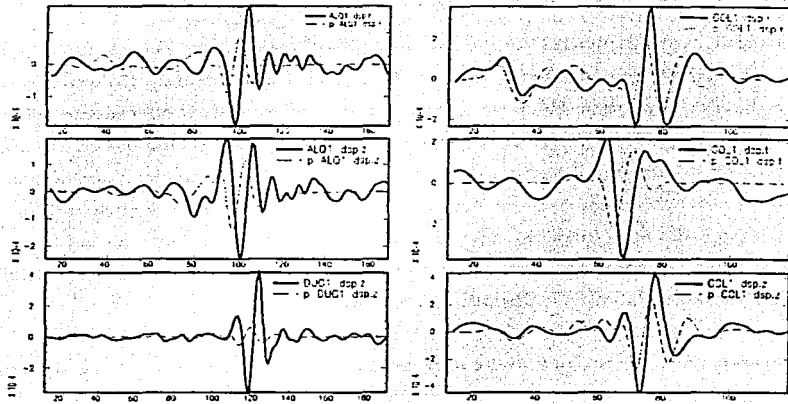


Figure 34

VI. Conclusiones

El estudio de la sismicidad superficial ($m_b \geq 5.4$) ocurrida en el occidente de Venezuela y de la sismicidad de profundidad intermedia ($m_b > 4.2$) generada al norte de Colombia y occidente de Venezuela durante el período 1964-1994, ha permitido mejorar el conocimiento sobre el régimen tectónico de la región y proponer un modelo que explica la cinemática de los diferentes fallamientos existentes en la zona. Además, la reciente instalación de nuevas estaciones sismológicas de banda ancha en la región del Caribe, Centro América y norte de Sur América, ha abierto las posibilidades para la puesta en marcha de una herramienta que permita la determinación de los parámetros focales de sismos de magnitud intermedia, mediante la inversión del tensor de momento sísmico utilizando sismogramas regionales.

Subducción de la placa del Caribe al norte de Colombia y noroccidente de Venezuela

El análisis de la sismicidad de profundidad intermedia al norte de Colombia y occidente de Venezuela, muestra la presencia de una placa litosférica subducida por más de 400 km de longitud por debajo de la costa suroeste del Caribe. La geometría de esta placa se definió en el rango de 60 a 180 km de profundidad, mediante la evaluación de los parámetros focales de los sismos con magnitud $m_b \geq 4.2$ ocurridos al norte de Colombia y noroccidente de Venezuela durante el período 1964-94. Las líneas de igual profundidad muestran una placa con dirección aproximada *NNE-SSW* y que buza hacia el este con una pendiente promedio de 25° - 32° , en ese rango de profundidades. La orientación de los ejes *T* en los mecanismos focales, indican fallamientos tensionales y generalmente están alineados paralelos al gradiente de la placa subducida, inferido a partir de la sismicidad.

En una primera aproximación, la baja tasa de sismicidad superficial y la ausencia de sismos de subducción a lo largo de la costa norte y noroeste de Colombia, sugieren que la subducción de la placa del Caribe no está ocurriendo actualmente. Sin embargo, medidas geodésicas recientes

han demostrado una tasa de convergencia relativa entre la placa del Caribe y el Bloque Norte de los Andes de 1 a 2 cm/año. Quizás, la ausencia de sismicidad superficial en el norte de Colombia se deba a que la subducción es muy lenta (<1 cm/año) y está tomando lugar por debajo de un prisma acrecionario de hasta 10 km de espesor, compuesto de sedimentos con alta presión de poros. Ahora, si se asume una tasa de subducción de 2 cm/año, la ocurrencia de sismos hasta profundidades de hasta 200 km en esta región, sugiere que la subducción de la litósfera Caribeña por debajo de Sur América puede haber tomado lugar desde hace 10 millones de años.

Los resultados de los mecanismos focales y orientación de los ejes T de eventos fuera y cerca del Nido de Bucaramanga, sugieren que esta concentración de sismicidad ocurre en la misma placa litosférica donde se originan los otros sismos de profundidad intermedia al norte de Colombia y occidente de Venezuela.

Orientación regional del campo de esfuerzos

El ambiente tectónico complejo en el noroeste de Sur América ha motivado que la dirección del campo de esfuerzos compresivo en esta zona haya sido un punto de discusión por los últimos 20 años. Varios autores han concluido que la dirección del campo de esfuerzos compresivo está orientado este-oeste debido a la subducción de la placa de Nazca por debajo de la placa Suramericana. Sin embargo, otros autores han reportado una dirección principal del campo de esfuerzos compresivos $NW-SE$ inducido por la subducción de la placa del Caribe por debajo de la placa Suramericana al norte de Colombia y noroccidente de Venezuela. Ambas direcciones del campo de esfuerzos sugeridas concuerdan en general con el campo de esfuerzos esperado para inducir el movimiento relativo dextral entre las placas Caribe y Sur América.

Los mecanismos focales obtenidos en este estudio claramente sugieren dos diferentes direcciones del campo de esfuerzos compresivo en el occidente de Venezuela. Los sismos localizados al suroeste de Venezuela, indican un campo de esfuerzos compresivo orientado $E-W$. Sin embargo, los mecanismos focales de los sismos en el noroeste de Venezuela,

aproximadamente al norte de la latitud 10°N . muestran una rotación de los ejes P desde el $NE-SE$ hasta $NNE-SSW$.

Estas dos conjuntos de direcciones del campo de esfuerzos compresivo bien definidos que actúan en el occidente de Venezuela ha motivado una comparación entre las tasas de deformación en las zonas norte y sur del área estudiada.

Zona de deformación altamente fallada y deformada

La correlación entre los mecanismos focales determinados en este estudio y las fallas activas muestran que la liberación de energía sísmica en el occidente de Venezuela no ocurre en un sistema de fallas único, tal como en Boconó o en Oca-Ancón; sino que la sismicidad se genera en fallas con diferentes orientaciones, distribuidas sobre un gran volumen sísmogénico. El cálculo de la deformación volumétrica de esta región considerada como un solo bloque mediante la utilización del tensor de momento sísmico, muestra una tasa de deformación compresiva de 5.6×10^{-10} año $^{-1}$ orientada casi N-S ($N4^{\circ}\text{E}$). Al separar la región en dos sectores al norte y sur de la latitud 10°N , los principales valores de la tasa de deformación fueron 1.6×10^{-9} año $^{-1}$ en la dirección $N5^{\circ}\text{E}$ y 1.7×10^{-9} año $^{-1}$ orientado $-N99^{\circ}\text{E}$, respectivamente.

Estos resultados muestran que cuando la región se dividió en dos secciones, la tasa de deformación compresiva tuvo un comportamiento similar a las orientaciones promedios de los ejes P . En la parte norte, la tasa de deformación compresiva orientada casi norte-sur se debe probablemente a la subducción de la placa del Caribe por debajo de Sur América; mientras que la tasa de deformación compresiva orientada en dirección este-oeste en la parte sur está posiblemente asociada a la convergencia entre las placas Nazca y Sur América. Sin embargo, en todo el volumen deformado, la tasa de deformación compresiva está orientada norte-sur.

Otro factor que demuestra la presencia de una zona altamente deformada y fallada es la ocurrencia de eventos sísmicos complejos de magnitud moderada, originados por fuentes múltiples. Además de la ocurrencia del sismo de El Tocuyo en 1812 y el de Caracas en 1967, existe una secuencia sísmica compleja originada en Boca del Tocuyo, noroccidente de Venezuela.

durante los meses de abril y mayo de 1989. El evento principal del 30 de abril y la réplica mayor del 4 de mayo se originaron mediante fuente múltiples que produjeron trenes de ondas muy largos que indujeron la licuación de los suelos en el área epicentral. Esta intensa licuación causada por los dos eventos parece ser consecuencia de la presencia de sedimentos saturados no consolidados, acelerados por la larga y sostenida duración del movimiento del terreno inducido por procesos de ruptura múltiple.

Modelo tectónico

Tal como ha sido mencionado anteriormente, en el occidente de Venezuela existen sistemas de fallas principales y secundarios, orientados en diferentes direcciones, que subsisten dentro de un mismo régimen tectónico. La evaluación neotectónica de la mayoría de estas fallas, aunado a la determinación de los mecanismos focales y a la direcciones de los principales ejes de esfuerzos, han permitido proponer un modelo cinemático conocido con el nombre de mecanismo "bookshelf" o "domino". En este caso, al actuar los sistemas de fallas de Boconó y Oca-Ancón en forma individual o como pareja de esfuerzos con desplazamiento lateral derecho, las fallas *NNE-SSW* que separan los bloques experimentan un deslizamiento lateral izquierdo y se produce una rotación de los bloques en sentido horario. Este mecanismo bookshelf se ha observado también en fallas individuales en el occidente de Venezuela, pero a una menor escala, tal como es el caso de las fallas de Valera e Icoetea.

Definición del borde suroeste de la placa del Caribe

Los resultados obtenidos de la evaluación sismotectónica de la región muestran evidencias que pudiesen relacionar la frontera entre las placas Caribe y Sur América con el sistema de fallas de Boconó y con el Cinturón Deformado del Caribe Sur. Por lo tanto, se pudiese estar presente ante una frontera de placas definida por toda una zona de deformación, comprendida entre los Andes Venezolanos y el Cinturón Deformado del Caribe Sur. Este argumento pareciera resolver

la vieja incertidumbre sobre el porqué no puede restringirse un polo de rotación para las placas Caribe y Sur América, utilizando datos a lo largo del sistema de fallas de Boconó.

En un esfuerzo para estimar la velocidad relativa entre las placas Caribe y Sur América con base en el tensor de momento sísmico, se asumió que los sismos estudiados ocurrieron a lo largo del sistema de fallas de Boconó. El movimiento relativo resultante es de 2.12×10^{-3} cm/año, lo cual es tres órdenes de magnitud menor que la velocidad esperada.

Modelación e inversión de sismogramas regionales

La presencia de una tectónica regional compleja y de una sismicidad superficial con magnitud $m_b \geq 5.4$ dispersa en el occidente de Venezuela, motivó un intento de evaluar el comportamiento de la sismicidad superficial con magnitud $m_b < 5.4$ utilizando sismogramas regionales. A tal efecto, se analizaron dos metodologías que permitiesen obtener los mecanismos focales de esos eventos más pequeños y de esta manera reunir mayor información para validar y/o reforzar las conclusiones alcanzadas y los modelos propuestos. Lamentablemente la escasez de información en las estaciones sismológicas ubicadas a distancias regionales del occidente de Venezuela, no permitió cubrir ese objetivo. Sin embargo, en su lugar se analizaron varios eventos ocurridos en el occidente de Estados Unidos, los cuales nos permitieron ensamblar un procedimiento que servirá en un futuro cercano, con la reciente instalación de nuevas estaciones banda-ancha a nivel regional, cumplir con la meta propuesta.

Los resultados obtenidos con los sismos analizados son satisfactorios, si se considera que el procedimiento utilizado se implantó para desarrollarse de una manera automática, sin que se produzca una realineación de los sismogramas sintéticos y observados. Esto implicó, la utilización de un modelo de corteza único para las diferentes trayectorias de los rayos y para la determinación de los tiempos teóricos de llegada de las ondas para el inicio de la inversión.